Microscopy of Cells on Nanostructured Substrates

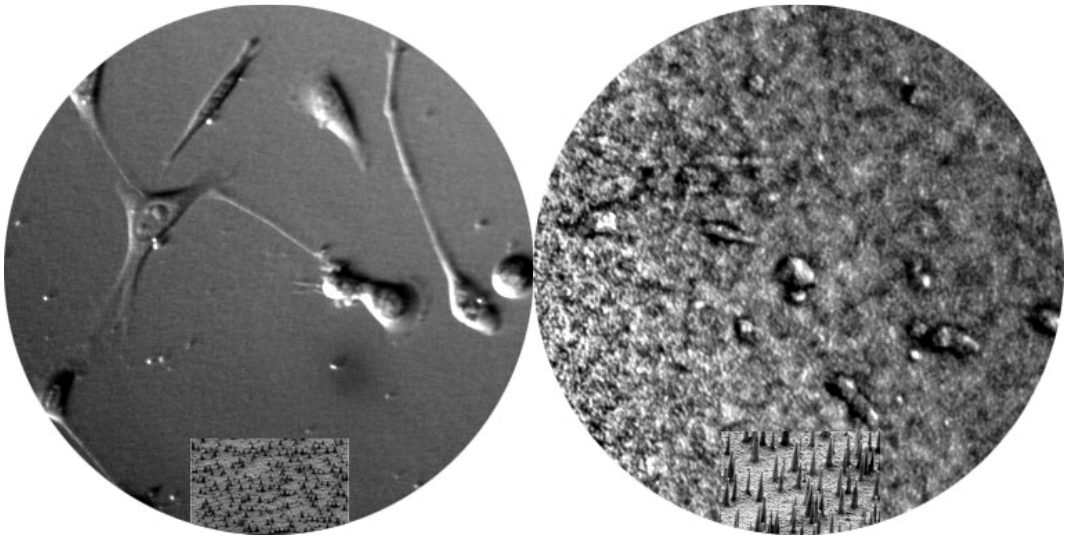

Martin Toft Madsen
s042445

M.Sc. Thesis

Supervisor: Kristian Mølhave

Kgs. Lyngby, November 2nd, 2009

DTU Nanotech
Department of Micro- and Nanotechnology

Preface

This master thesis corresponds to 35 ECTS (European Credit Transfer System) points and has been written as a partial fulfilment of the requirements for obtaining a Master of Science in Engineering (MSc.E.) degree at the Technical University of Denmark (DTU). The project has been carried out from March 2009 to November 2009 at the Department of Micro- and Nanotechnology (Nanotech) at DTU.

The project was elaborated in the Molecular Windows Group and has been supervised by:

Kristian Mølhave,
Associate Professor, Head of the Molecular Windows Group at DTU Nanotech
Main supervisor

Joanna Malgorzata Lopacinska,
PhD Student at DTU Nanotech
Co-supervisor

Cristian Grădinaru,
PhD Student at DTU Nanotech
Co-supervisor

Kgs. Lyngby, Denmark
November 2nd, 2009

Martin Toft Madsen

Abstract

In this experimental project a survey of living cells on different nanostructured substrates has been made by use of time-lapse microscopy. The correlation between the size and shape of nanostructured substrates and the behaviour of the cells adhering and living on these substrates has been studied.

A temperature-controlled stage fitting in a microscope and regulated by a feedback loop on a connected computer has been successfully made and tested. Furthermore a cell culture chamber (CCC) that fit inside the temperature-controlled stage and in which the cells could live on different fabricated nanostructures, was also successfully created and tested.

Nanostructured substrates were produced using e-beam lithography (EBL) on PMMA and black Si samples from a former project were also available for the study. Time-lapse movies of living fibroblast cells were successfully obtained on both types of nanostructures and on baseline substrates, and a clear dependence was found between the characteristics of the nanostructured black Si substrates and the motility of the fibroblast cells living on it. Black Si with spikes with a height of 1.2 µm, a diameter of 200 nm, and a density of 9 μm^{-2}, was found to kill fibroblast cells, while black Si with spikes with a height of approximately 6 µm, a diameter of 1.2 µm, and a density of 0.1 μm^{-2} allowed for survival of the fibroblast cells, although the cell motility was dramatically decreased compared to flat Si. Black Si substrates with spikes with a height of approximately 300 nm, a diameter of 100 nm, and a density of 9 μm^{-2} and 21 μm^{-2}, respectively, were found to dramatically increase the motility of the fibroblast cells compared to flat Si. No obvious difference was found between the behaviour of the fibroblast cells living on the EBL PMMA patterns consisting of dots with a diameter of 30-50 nm, a depth of 80-100 nm, and a pitch of 50 nm and 200 nm, respectively, compared to flat PMMA.

Table of Contents

Preface ..... **i**
Abstract ..... **iii**
Table of Contents ..... **v**
Acknowledgements ..... **vii**
1 Introduction **1**
1.1 State of the Art 1
1.2 This Project 1
2 Introduction to the Cell and its Motility **3**
3 The Temperature Stage **5**
3.1 The Temperature Stage Setup 5
3.2 Temperature Precision 7
3.3 The Thermistors 7
3.4 The Thermistor Circuit Setup 8
3.5 Thermistor Self-Heating 9
3.6 DAQ Measurement Resolution and Resistor Tolerance 9
3.7 The LabVIEW Program 10
3.8 Testing the Temperature Stage 11
3.9 Calculations on Requirements for Heating the Medium in the Tubings 12
3.10 Testing Cell Behaviour at Different Temperatures 15
4 Culturing the Cells **16**
4.1 The Cell Culture Chamber 16
4.2 Designing the CCC 17
4.3 Preparation for Cell Experiments 21
4.4 Starting the Experiment 22
4.5 The Microscope 23
5 The Nanostructured Substrates **24**
5.1 Black Si 24
5.2 Creating Black Si 24
5.3 Black Si Samples 25
6 Observations on Cell Behaviour **29**
6.1 Recording the Time-Lapse Movies 29
6.2 Cell Behaviour 29
7 Modelling Cell Behaviour **37**
7.1 The Ornstein-Uhlenbeck Process 37
7.2 Analysing the Time-Lapse Movies 38
7.3 Interpreting the Motility Data 38
8 Making Nanostructured Substrates using Electron Beam Lithography **47**
8.1 Introduction to Electron Beam Lithography 47
8.2 Making the Nanostructured Surfaces 48
8.3 Surface Characterization 49
8.4 Electron Beam Structures for Cells 51
8.5 Observations on Cell Behaviour on Electron Beam Structures 52
8.6 Modelling Cell Behaviour 54
9 Conclusion **55**
9.1 Future Work 56

10 References **57**
Appendix A - Library of Black Si Surfaces **59**
Appendix B - Black Si Substrates from Rasmus Davidsen **74**
Appendix C - Graphs Modelling Cell Behaviour **77**
Appendix D - Step-by-Step Guide for Time-Lapse Microscopy of Cells **114**

Acknowledgements

I would like to thank the entire Molecular Windows Group, who has supported me throughout this study, especially my supervisor Kristian Mølhave for his patience and inspiration, Joanna Malgorzata Lopacinska for the help in the cell culture lab and the help with carrying out the experiments, and Cristian Grădinaru for the help with the sometime late-hour data analysis. I would also like to thank Thomas Kjøller Nellemann for both proofreading this thesis and working with me in the 3-week course that lead to this project. Lastly, I would like to thank my parents for their proofreading and comments on this thesis.

1 Introduction

This thesis will study the interaction between cells and nanostructured substrates. This is studied to get an understanding of how cellular behaviour depends on the topography of the underlying substrate. Such knowledge could help in the engineering of better biomaterials enhancing things like cell migration and adhesion on such materials. This could further help in the development of medical applications such as implantable devices, surgery, and drug delivery, as these things are interacting directly with cells, and hence the materials of these need to contribute with a healthy environment for the cells.

1.1 State of the Art

Research on cell interactions with nanostructured substrates is a new field, since until recently it has not been possible to make well-controlled surface structures in the nanometre range. There are an almost infinite number of combinations of cell type, growth conditions, and nanostructured substrates to study, and the exact mechanisms of the cell interacting with such substrates is not yet fully explained. However, several studies have looked at cells interacting with different kinds of nanostructures. It has been found that TiO_2 nanotubes with a diameter of less than 30 nm enhance the cellular activities of mesenchymal stem cells compared to smooth TiO_2, while cell adhesion and spreading were severely impared on TiO_2 nanotubes with a diameter larger than 50 nm, resulting in dramatically reduced activity and high cell death (Park, Bauer et al. 2007). Primary bovine aortic endothelial cells (BAECs) have also been found to show enhanced mobility on TiO_2 nanotubes with a diameter of approximately 100 nm compared to flat Ti, and it is speculated that the ~10 nm spacing between the nanotubes allowing fluid spaces, and hence enabling continued supply of natural blood underneath the attached cell, to contribute to a healthier environment for the cells (Brammer, Oh et al. 2008). Furthermore SaOS2 cells have shown a strickingly extended morphology on carbon nanotubes (CNT) 5-20 nm in diameter and 20-40 µm in length compared to flat polycarbonate (PC) (Aoki, Yokoyama, et al. 2006). On a somewhat larger scale, a very recent study has shown that fibroblast cells alter both shape and migration speed when adhering to an anisotropic micro- and nanopattern array of poly(urethane acrylate) (PUA) (Kim, Han et al. 2009).

1.2 This Project

Preliminary results showed good adhesion and extended morphology for the eukaryotic fibroblast NIH3T3 cell on black Si, which is similar in material and topography size range to the TiO_2 nanotubes, but can be produced in larger areas relatively cheap and fast, and at the same time allow for tuning of the topography features. HeLa cells died on the same substrate; hence the fibroblast cells will be used in this study to make a survey of the behaviour of cells on nanostructured substrates trying to get an idea of how these cells interact with and behave on these specific structures. Cell behaviour on surfaces produced using electron beam lithography will also be studied, since such surfaces can be produced with utmost precision. This method of creating nanostructures, though, is at the same time limited by the very slow and expensive production process. Due to in-house experience with modelling motility of living cells, this particular part of cell behaviour will be analysed through

the use of a mathematical model, which has not yet been done on cells on nanostructured substrates.

To study cell behaviour and make the motility experiments a temperature-controlled stage using a PID controller and a cell culture chamber was made to fit in an optical microscope. The microscope is connected to a computer that would continuously obtain images with a fixed interval resulting in time-lapse movies of living cells on the nanostructured substrates.

This thesis will start out with a short introduction to the cell and its motility. Subsequently a description is made of how the temperature-controlled stage was created and tested. The creation and testing of the cell culture chamber (CCC) will then be described along with the procedure of getting the cell experiments started. Afterwards a description of the production and the characterization of the nano-structured substrates will be made. Then, the obtained time-lapse movies will be analysed in two different ways. At first, general observations on the cell behaviour on both baseline substrates and on the nanostructures will be made. Afterwards the motility data from the time-lapse movies will be analyzed and fitted to a mathematical model describing cell migration.

Since the results on cell behaviour on surfaces produced with the electron beam lithography was scarce the description of these structures along with the results obtained are described in a single chapter at the end of the report.

Lastly, a conclusion on the findings will be made, and further studies will be proposed.

2 Introduction to the Cell and its Motility

The cell is the basic structural and functional unit of all known living organisms. Each cell can reproduce by cell division, build cell components, transform energy by taking up nutrients (the so-called metabolism) and respond to external stimuli such as a change in temperature, pH, or level of nutrient. Furthermore, each cell is enclosed by a cell membrane consisting of a lipid bilayer containing embedded proteins.

There are two types of cells, prokaryotic and eukaryotic cells. This study is using the eukaryotic fibroblast as cell type. An eukaryotic cell is defined by the presence of a nucleus, and fungi, plants, and animal and human cells are examples of eukaryotic cells. Inside the cell the cytoskeleton is the cell scaffold. It helps the cell keep its shape, as well as helps when the cell is taking up external material (endocytosis) and while separating daughter cells (cytokinesis) after cell division. Most important for this study, though, is the cytoskeleton's ability to move parts of the cell in the cell's process of growth and motility.

In addition to the cytoskeleton and the nucleus that contain the DNA, numerous other sub-cellular components called organelles exist inside the eukaryotic cell. The nucleus is also one such organelle. Other organelles include mitochondria, which are the organelles responsible for the cell's energy currency adenosine triphosphate (ATP), vesicles, which transport or digest the cell's product and waste, the Golgi apparatus, which processes and packages macromolecules, and lysosomes, which digest excess organelles, food particles and engulfed bacteria and viruses. Some of these things can sometimes be seen in the microscope images of the cells.

The size of a eukaryotic cell is on the order of 10-100 µm in diameter. For a thorough study of cell motility, an understanding of the focal adhesion sites is necessary. When a cell moves protrusion of the leading part of the cell occurs. This part is called lamellipodia or filopodia depending on its shape and structure. Lamellipodia is a wide structure, while filopodia is a narrower structure. New focal adhesion sites are created in these parts, while retraction takes place in the rear part of the cell. The cytoskeleton then contracts to make the cell move. There is no absolute size or pitch for these adhesion sites, but they are of course smaller than the cell itself.

The cell can interact with a substrate in different ways depending on the type of substrate. This is seen in Figure 1. Round, elongated, and polygonal shapes are seen. Round cells usually indicate poor adhesion, while the other shapes mean better adhesion for the cells on the substrate, indicating the substrate supports cell motility better.

The fibroblast cell is a stem cell, which means that it can renew itself by division and differentiate into a diverse range of specialized cell types.

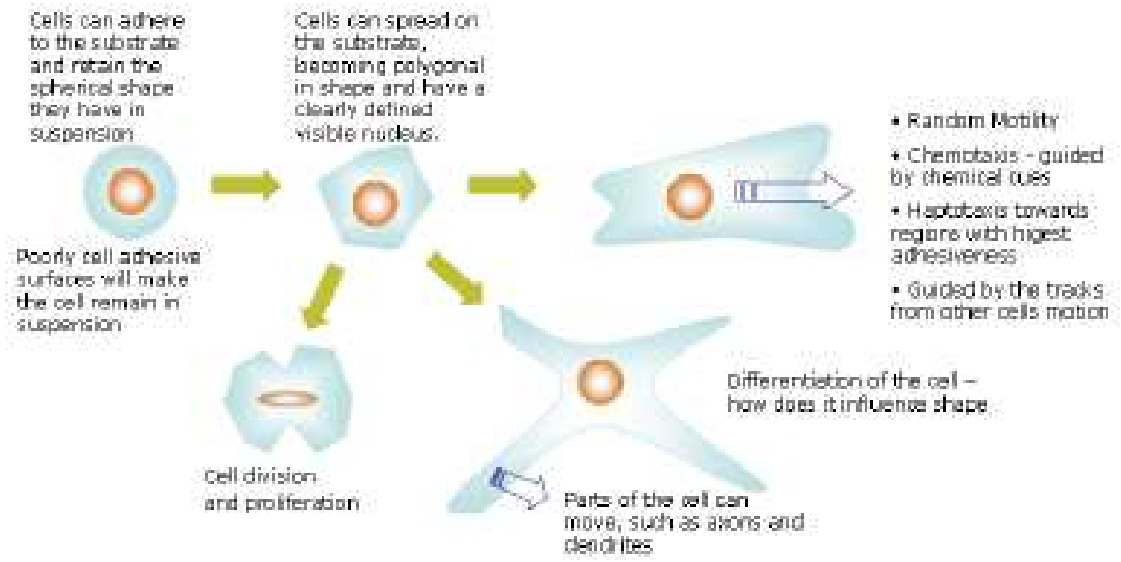

Figure 1. Different kinds of cell-substrate interactions (Grădinaru, Lopacinska, et al. 2009).

3 The Temperature Stage

Temperature influences cell behaviour and is therefore an important parameter to keep constant. One of the goals of this study was therefore to build a temperature-controlled stage to mount in the microscope, wherein the cells would have a constant temperature of 37.0±0.2 °C. As the stage with the living cells in it was placed in a room with normal room temperature fluctuating at about 25 °C, the stage would need to be insulated and heated.

In this section the setup of the temperature stage will be explained. It will be discussed which measures were taken to keep the temperature at 37.0 °C and how well this was achieved.

3.1 The Temperature Stage Setup

To achieve the goal of getting a stable temperature at 37.0 °C a computer-controlled temperature stage was made using a PID (proportional-integral-derivative) controller, though not using any derivative measurements. The stage included 2 negative temperature coefficient (NTC) thermistors to measure the temperature and 8 resistors used as distributed heaters to obtain the needed homogeneous temperature. These were all connected to a LabJack (model U3-HV), which is a USB-based data acquisition device (DAQ) that provides both analogue and digital electrical inputs and outputs. The setup is schematically shown in Figure 2 and the inside of the stage is shown in Figure 3.

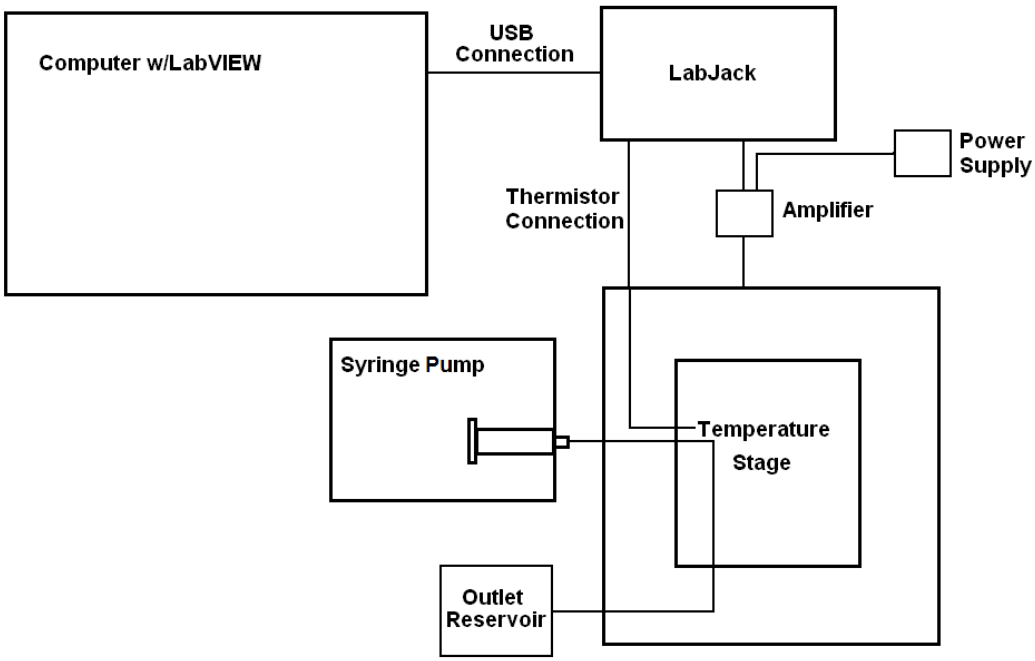

Figure 2. Temperature stage setup with the connected computer, syringe pump, and DAQ.

A LabVIEW program was made to control the ports on the DAQ via the USB connection on the computer. This program made sure that if the temperature was below

37.0 °C a certain temperature-dependent voltage was created across the 8 heat resistors to raise the temperature of the temperature stage.

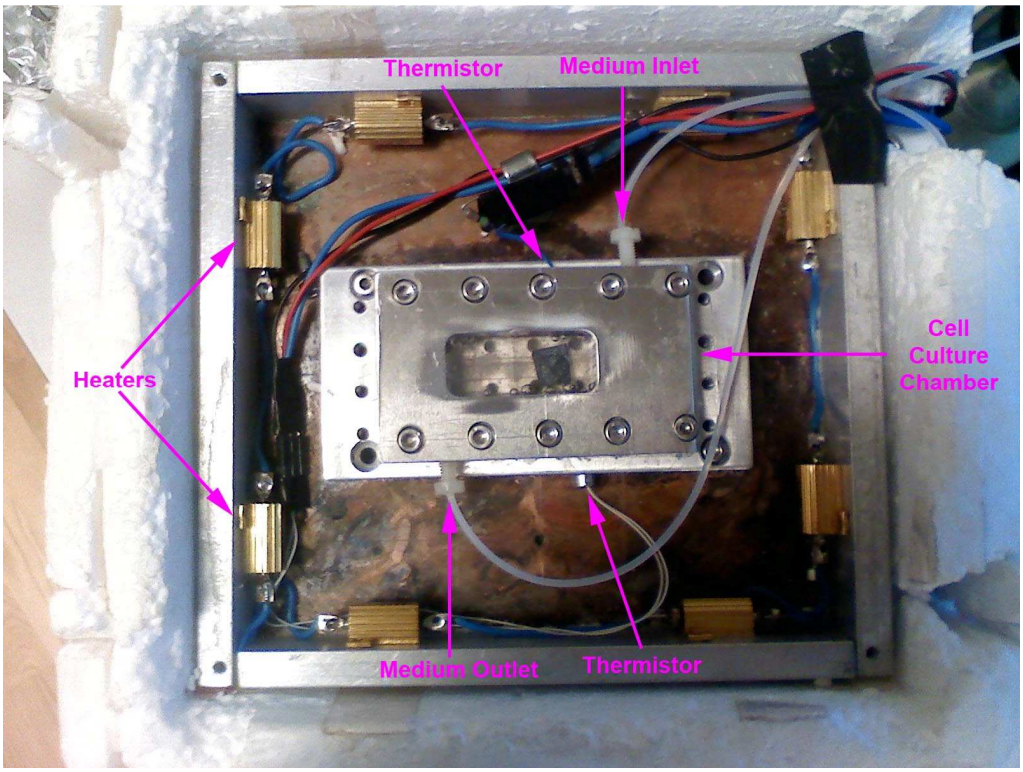

Figure 3. The inside of the temperature stage with the cell culture chamber in the middle.

The required power to keep the required temperature can be calculated by means of Fourier's Law;

$$\frac{\Delta Q}{\Delta t} = -k \cdot A \cdot \frac{\Delta T}{\Delta x} \qquad \textbf{Eq. 1}$$

In this experiment expanded polystyrene was used as the insulating material encapsulating a top and bottom plate of copper used to make sure the stage had a large thermal mass and a homogeneous heat distribution. An Al block, which has a large thermal conductivity, was mounted inside the stage to raise the cell culture chamber. This was done so the placement of the substrates with the cells inside the stage would fit the working distance of 19 mm of the microscope objective used to monitor the cells.

The stage encapsulated in the polystyrene measured approximately 140 x 150 x 30 mm^3, and the thickness of the expanded polystyrene itself was approximately 13 mm. On the sides two layers of expanded polystyrene was used for insulating, making up a total thickness of 26 mm. Taking the room temperature to be 25 °C and knowing that the conductivity of expanded polystyrene is 0.03 W/(m·°C), a rough estimate for the heat dissipation of the system can now be calculated to be approximately 1.4 W by means of Fourier's Law, which was used as a starting point when making the temperature controller.

3.2 Temperature Precision

To obtain the most precise temperature measurements several experiments were carried out. Thermistors, as used in the final setup, were compared to thermocouples. These readings did not correlate, and over the span of days or weeks, the temperature measurements could differ by more than 1 °C.

A thermocouple is a junction between two different metals, which depending on temperature will create small voltages due to the thermoelectric effect. Due to these small voltages, typically in the µV-range, a lot of amplification is needed for the used DAQ to measure them. Furthermore, thermocouples only allow readings of temperature differences, requiring knowledge about the temperature at the so-called cold junction, which in this case is the DAQ, introducing another source of error. These two facts along with the knowledge that thermistors are very accurate, since they are used for measuring the temperature in modern laser systems, lead to the conclusion that the thermocouples are not precise enough to measure with a precision of 0.2 °C. This is the reason why thermistors were used for temperature measurements.

3.3 The Thermistors

Thermistors are passive semiconductor devices. Their resistance varies with temperature, and the thermistors used in these experiments decreased resistance with increasing temperatures, hence the name negative temperature coefficient thermistor, or just NTC. The effect comes from the fact that as temperature rises electrons are promoted into the conduction band of the semiconductor.

Thermistors were used to measure the temperature in two different places in the stage. One thermistor (NTC1) was mounted in the Al block just underneath the cell culture chamber, while the other one (NTC2) was mounted inside the cell culture chamber only a few millimetres from the cells. The PID controller was using the mean temperature from the last 10 s obtained from NTC1 as this was the most stable reading with least risk of heating the stage too much or too little.

The relation between temperature and resistance, however, was not linear. A look-up table showing the resistance of NTC1 from -40.00 °C to 125.00 °C with 1 °C intervals was used to calibrate it by fitting an equation to the look-up table. Putting this temperature-resistance equation into the LabVIEW program, it was then able to calculate the temperature based on the measured resistance.

Usually the logarithmic Steinhart-Hart equation is used to calculate the resistance of a thermistor, but it was not possible to fit this equation to the look-up table with any of several computer programs tried. Instead, a simpler logarithmic equation of the form $T = ln(R)+T_0$ was used to fit the points between 20.00 °C and 45.00 °C making sure that the equation matched the look-up table exactly at 37.0 °C as seen in Figure 5.

To calibrate NTC2, which had no exact specifications supplied, both thermistors were placed inside the Al block in the temperature stage. The temperature was now set to 36.0 °C, 37.0 °C, and 38.0 °C, respectively, according to NTC1, and NTC2 was then calibrated using these measurements. The measurements were then fitted to Eq. 3.

$$R = R_0 \cdot (1 + C)^{T_0 - T} \Rightarrow \qquad \textbf{Eq. 2}$$

$$T = T_0 - \frac{\ln(R / R_0)}{\ln(1 + C)} \qquad \textbf{Eq. 3}$$

Here

T	[°C]	is the temperature,
R	[Ω]	is the resistance
R_0	[Ω]	is the resistance at T_0, and
C	[*unitless*]	is the relative change in resistance per °C.

Of course, this calibration along with the accurate fitting only at exactly 37.0 °C for NTC1 meant that the temperature calculated would not be quite accurate when not at 37.0 °C. However, a minor difference of maybe 1 °C at a temperature of 25 °C would not make a difference, as the important thing in this aspect would be whether the temperature was above or below 37.0 °C and by approximately how much in order for the PID controller to heat the stage accordingly. As the temperature approached 37.0 °C the temperature measured would get closer and closer to the real value.

3.4 The Thermistor Circuit Setup

Since the DAQ device was measuring voltage differences and not resistances, a small voltage-dividing circuit was applied to each. Figure 4 shows the circuit. A resistor with a known resistance was connected in serial with the thermistor. The voltage difference across the thermistor and the resistor was set to 5 V by the DAQ device and both this voltage and the voltage across the thermistor U_{NTC} was measured. The thermistor was connected to ground to minimize measurement errors, and the resistor was also placed inside the temperature stage to minimize its resistance drift.

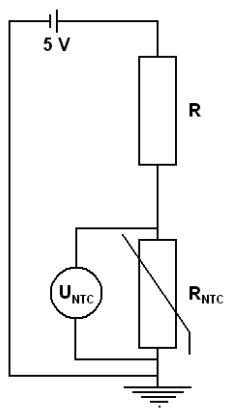

Figure 4. Thermistor circuit setup.

Knowing the resistance R of the resistor and the fact that the voltage difference across the resistor was simply the difference between U_{NTC} and 5 V, the current could be calculated by means of Ohm's law. Since the resistor was connected in serial with the thermistor the current across the two was the same. Knowing this and the voltage across the thermistor the resistance of the thermistor can easily be calculated:

$$R_{NTC} = \frac{U_{NTC}}{I} = \frac{U_{NTC} \cdot R}{5\,\text{V} - U_{NTC}} \qquad \textbf{Eq. 4}$$

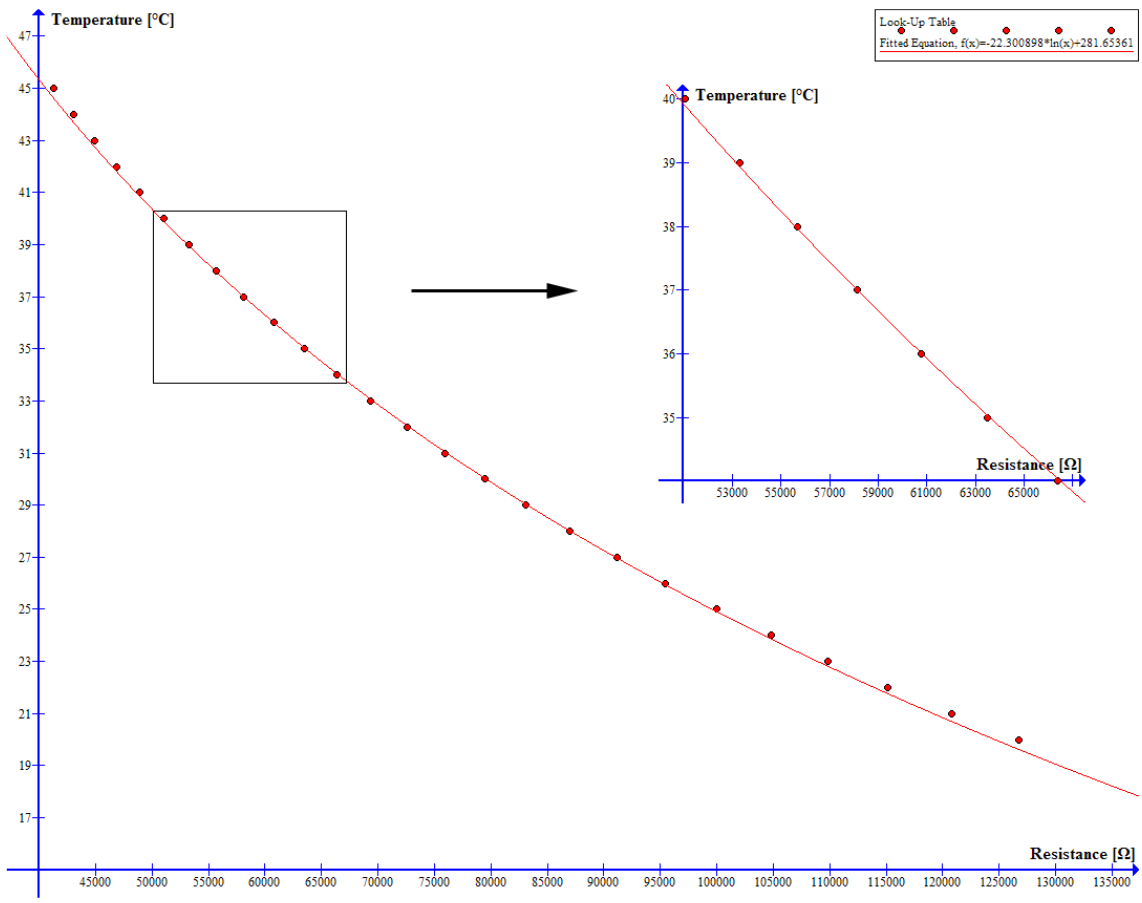

Figure 5. Graph showing the fitted equation and the look-up table data point.

3.5 Thermistor Self-Heating

Due to self-heating effect (Joule heating) of the thermistor, the measured temperature will be slightly higher than the actual temperature. To reduce this effect, a small current must be used. In this study no more than 3 V was supplied to the thermistors which generated a current of approximately 50 µA through the thermistors. The heating of the thermistors was then on the order of 0.1 mW. The dissipation constant for NTC1 was specified at 1 mW/°C if placed in still air at 25 °C. The self-heating should then not account for more than about 0.1 °C. A similar dissipation is assumed to hold for the other thermistor.

3.6 DAQ Measurement Resolution and Resistor Tolerance

According to the user's guide the ports used on the LabJack had a measurement range of 0-3.6 V with a 12-bit resolution, which means that every measurement had an uncertainty of 0.44 mV. Converting this precision into a temperature precision in the setup yields an uncertainty of 0.01 °C. During the measurements, though, it seemed like the discrete voltage levels measured by the LabJack were separated by 5 mV, which means the uncertainty was 0.06 °C, or in other words that the temperature would change about 0.12 °C when jumping between these discrete measured voltages.

The resistors used had a tolerance of 1%. Converting this tolerance into a temperature precision in the thermistor circuit used in this study gives an uncertainty of 0.2 °C. However, the resistances of the resistors used were measured, and they were placed at

a stable temperature inside the temperature stage, so the uncertainty stemming from these will likely be lower.

3.7 The LabVIEW Program

The heating resistors in the temperature stage were connected to the analogue inputs on the DAQ measurement device (LabJack) that fed the signals to a computer via a USB connection. A LabVIEW program with a graphical user interface (GUI) was made to receive and treat this signal. A screenshot of the GUI can be seen in Figure 6. The program shows the temperature measured from all the connected thermistors. However, as mentioned, the resolution of the voltage measurements meant that the raw temperature measurements were in discrete values 0.1 °C apart. To make the measurements more precise the last 20 raw measurements were averaged as this would make use of the uncertainty causing a measurement to often vary between two different values. The raw measurements were made once per program cycle, and the cycle time could be set in the program. During this study it was set to 0.5 s, which means that the temperature was averaged over the last 10 s.

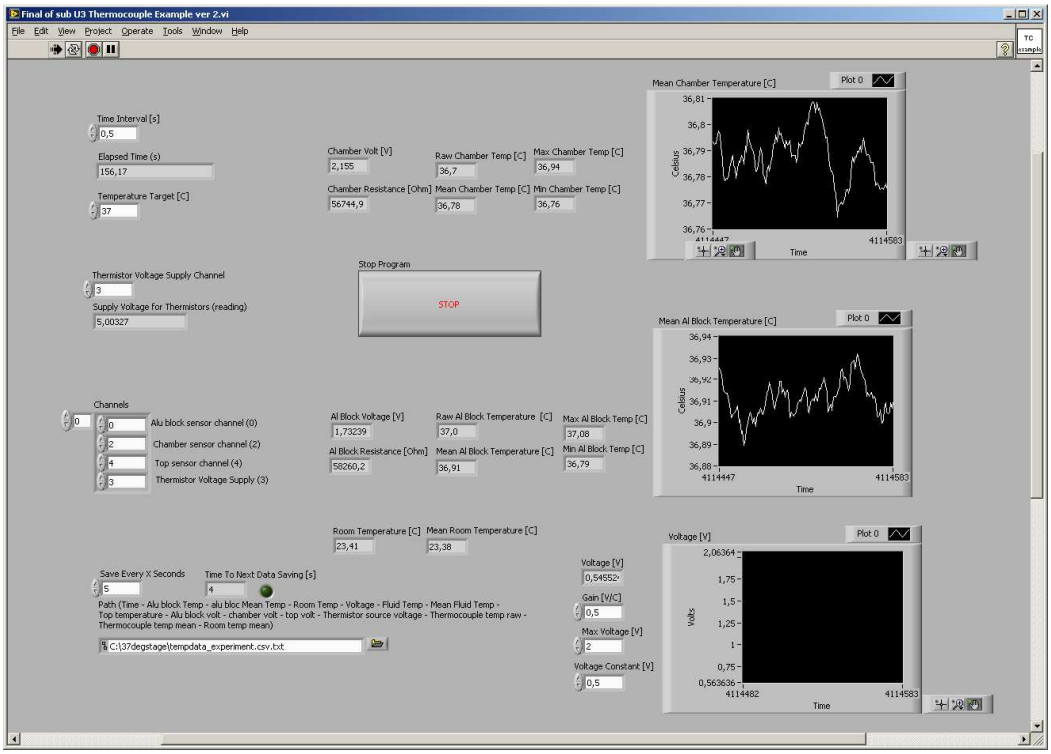

Figure 6. Screenshot of the custom-made LabVIEW program.

The 1.4 W heat dissipation found earlier was used as a starting point in the LabVIEW program when deciding how much power should be dissipated by the heaters in the stage. The LabVIEW program controlled the voltage which the LabJack sent through the 8 series connected resistors used as heaters. Each resistor had a resistance of 1 Ω, so the voltage across them should then according to Joule's first law be set to

$$P = R \cdot I^2 = \frac{U^2}{R} \Rightarrow$$

$$U = \sqrt{P \cdot R} = \sqrt{1.4\ \mathrm{W} \cdot 8\ \Omega} = 3.4\ \mathrm{V}$$

Between the LabJack and the stage with the 8 resistors was a power amplifier amplifying the voltage 10 times, hence only 0.34 V should be set as the base voltage in the LabVIEW program for keeping the temperature stage at 37.0 °C.

However, when performing test runs on the setup it was seen that a higher voltage was needed to keep the temperature at 37.0 °C. A voltage of 0.5 V seemed to give good results and the extra 0.16 V needed can be explained by the hole in the top part of the expanded polysterene used to gain visible access to the stage when obtaining time-lapse movies of the living cells.

As the surroundings were not static the temperature was controlled by a simple feedback loop in the program. Once in every cycle the program would measure the temperature of the Al block in the stage. As opposed to the temperature in the cell culture chamber itself, which was made of more insulating polycarbonate, the Al block would react faster to temperature changes allowing for better heating control. The temperature measured would then be subtracted from the setpoint and subsequently be multiplied by a constant that could be set in the program. This constant was typically set at 0.5 V/°C, which meant that an additional voltage of 0.5 V would be applied across the heating resistors for every 1 °C that the temperature was below 37.0 °C. This contribution was added to the 0.5 V needed to keep the stage at 37.0 °C. To avoid that the temperature overshoots 37.0 °C when heating the temperature stage a maximum voltage across the heating resistors could be set in the program. The value was set at 2.0 V, which means that a voltage of 2.0 V would be set across the resistors until the temperature reached 34.0 °C, after which the voltage would drop until it reached 0.5 V when the stage reached a temperature of 37.0 °C. These settings seemed to prevent any significant overshoot and at the same time give reasonably fast heating times (usually 10-15 min. from room temperature to 37.0 °C). If heated above 37.0 °C the 0.5 V/°C multiplication constant would make sure that the voltage would drop and reach 0 V if a temperature of 38.0 °C was ever reached in the chamber.

The LabVIEW program also created a log file, which would log the run time and the temperature measurements from the entire run. Both a maximum and a minimum temperature indicator for each thermistor were also located in the program making it easy to see if the temperature had reached critical values.

3.8 Testing the Temperature Stage

Several tests were made to make sure that the stage could keep the temperature steady for longer periods before experiments with cells were made. In Figure 7 a graph is seen showing the temperature of the Al block (NTC1), the chamber close to the cells (NTC2), and the room temperature (LabJack) from an actual cell experiment.

A small overshoot to 37.3 °C is then seen in the Al block for 3-4 min., before it stabilises at around 37.0 °C. The average temperature from 20 min. after heating has begun, when the temperature has reached a plateau, and until the end of the experiment 72 h later is 37.01±0.04 °C for the Al block. The maximum temperature in the Al block during the test was the 37.27 °C reached at the start, while the minimum temperature occurs at several small dips that, however, never drop below 36.75 °C.

Looking at the temperature in the chamber the overshoot is avoided and the maximum reached is 37.07 °C, while the minimum after initial heating is 36.65 °C. The average chamber temperature from 20 min. after heating has begun until the end is 36.81±0.07 °C. Even though the temperature in the chamber is a bit below 37.0 °C it was decided to keep the Al block at 37.0 °C to be sure not to overheat the cells.

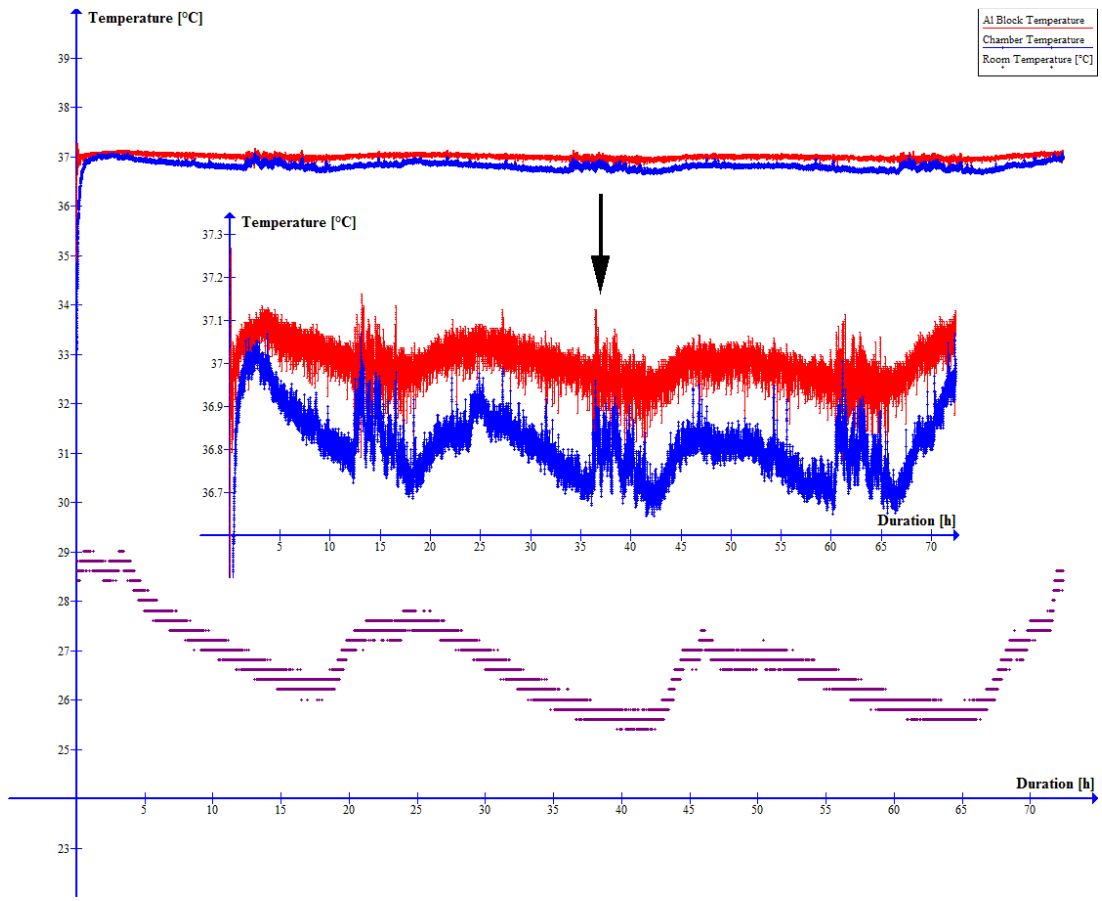

Figure 7. Graph showing a test of the temperature stage. The red (top) graph is the temperature inside the Al block in the stage, the blue one (just below) is the temperature inside the chamber right next to the cells, while the dotted purple one (bottom) is showing the room temperature.

3.9 Calculations on Requirements for Heating the Medium in the Tubings

It is not enough for the temperature stage to be exactly 37.0 °C as what actually matters is that the temperature of the fluid or cell culture medium in which the cells are is 37.0 °C. Therefore the fluid travelling from a syringe pump outside the temperature stage to the cells inside the stage needs to be heated from room temperature outside the stage to 37.0 °C inside the stage. This can be ensured by making sure that the fluid travels a certain distance and hence time through the tubing inside the temperature stage. To calculate how long the tubing inside the temperature stage must be from it enters the stage to its inlet in the cell culture chamber Newton's law of cooling can be used:

$$\frac{dQ}{dt} = h \cdot A \cdot (T_{env} - T_0) \qquad \textbf{Eq. 5}$$

Here

Q	[J]	is the thermal energy,
t	[s]	is the time,
h	[W/(m^2·°C)]	is the heat transfer coefficient,
A	[m^2]	is the surface area where the heat is being transferred,
T_0	[°C]	is the temperature of the object's surface, and
T_{env}	[°C]	is the temperature of the environment.

The heat transfer coefficient is that of the tubing with the medium inside. To find the combined heat transfer coefficient, it must first be found for each one.

The heat transfer coefficient for the tubing can be calculated by the use of the heat transfer coefficient of a pipe wall:

$$h_{tubing} = \frac{2k_{tubing}}{d_i \cdot \ln(d_o / d_i)} \qquad \textbf{Eq. 6}$$

where

k_{tubing}	[W/(m·°C)]	is the effective thermal conductivity of the tubing,
d_i	[m]	is the inner diameter of the tubing, and
d_o	[m]	is the outer diameter of the tubing.

The heat transfer coefficient of the medium inside the tubing will be approximated by the formula

$$h_{medium} \approx \frac{k_{water}}{r} \qquad \textbf{Eq. 7}$$

where

k	[W/(m·°C)]	is the effective thermal conductivity of water, and
r	[m]	is the inner radius of the tubing

Heat transfer coefficients add inversely, hence

$$\frac{1}{h_{system}} = \left(\frac{1}{h_{medium}} + \frac{1}{h_{tubing}}\right) = \left(\frac{r}{k_{water}} + \frac{d_i \cdot \ln(d_o / d_i)}{2k_{tubing}}\right) \qquad \textbf{Eq. 8}$$

Rewriting Eq. 5 gives

$$\frac{dQ}{dt} = h \cdot A \cdot (T_{env} - T_0) \Rightarrow \qquad \textbf{Eq. 9}$$

$$\frac{dT}{dt} = -\frac{h_{system} \cdot A}{m \cdot c} \cdot (T_0 - T_{env}) \qquad \textbf{Eq. 10}$$

where

T	[°C]	is the temperature of the medium,
m	[kg]	is the mass of the medium, and
c	[J/(kg·°C)]	is the specific heat capacity of the medium.

Using that the temperature surrounding the tubing is constantly 37 °C, Eq. 10 can be solved without regards to the medium inside actually moving. Solving it with the boundary conditions $T(0) = T_0$ and $T(t) = T_{env}$ for $t \rightarrow \infty$ gives

$$T(t) = T_{env} + (T_0 - T_{env}) \cdot \exp(-\frac{t}{t_0}) \qquad \textbf{Eq. 11}$$

where

$$t_0 = \frac{m \cdot c}{h_{system} \cdot A} \qquad \textbf{Eq. 12}$$

Replacing time t with tubing length l using the velocity of the medium inside the tubing v gives the final equation

$$T(l) = T_{env} + (T_0 - T_{env}) \cdot \exp(-\frac{l}{v \cdot t_0}) \qquad \textbf{Eq. 13}$$

A graph showing the medium temperature as a function of tubing length inside the stage can be seen in Figure 8. If the medium is 20 °C when it enters the temperature stage it will be 36.9 °C when it has travelled 1.3 mm with the PTFE tubings, which had an inner diameter of 0.8 mm and an outer diameter of 1.6 mm, and the medium flow rate of 5 µL/min. corresponding to v = 0.167 mm/s used, and assuming the medium had the same specific heat capacity and density as water, c = 4.18 J/(kg·°C) and $\rho = 1.00 \cdot 10^3$ kg/m^3. In other words, the tubings are so small that the medium inside them will be reaching the temperature outside them almost immediately.

To sum it up, it is important to make sure that the fluid gets the right temperature only a small distance before the inlet to the cell culture chamber with the substrates and the cells; the tubing placement until that point is not important from a temperature point of view. Since the fluid travels through a bubble trap inside the cell culture chamber before reaching the cells, it can even be argued that of importance is only that the cell culture chamber is kept at the right temperature. Even if the tubing gets close to the heating resistors at the edge of the stage that are more than 37.0 °C, the heat should be dissipated from the tubings and the medium before the medium reaches the cell culture chamber inlet as the heat transfer is just as fast from inside to outside the tubings as the other way around. Of course, this is only from a temperature point of view, as the medium could perhaps be damaged from the temporary heating, hence the inlet tubing was not placed close to these.

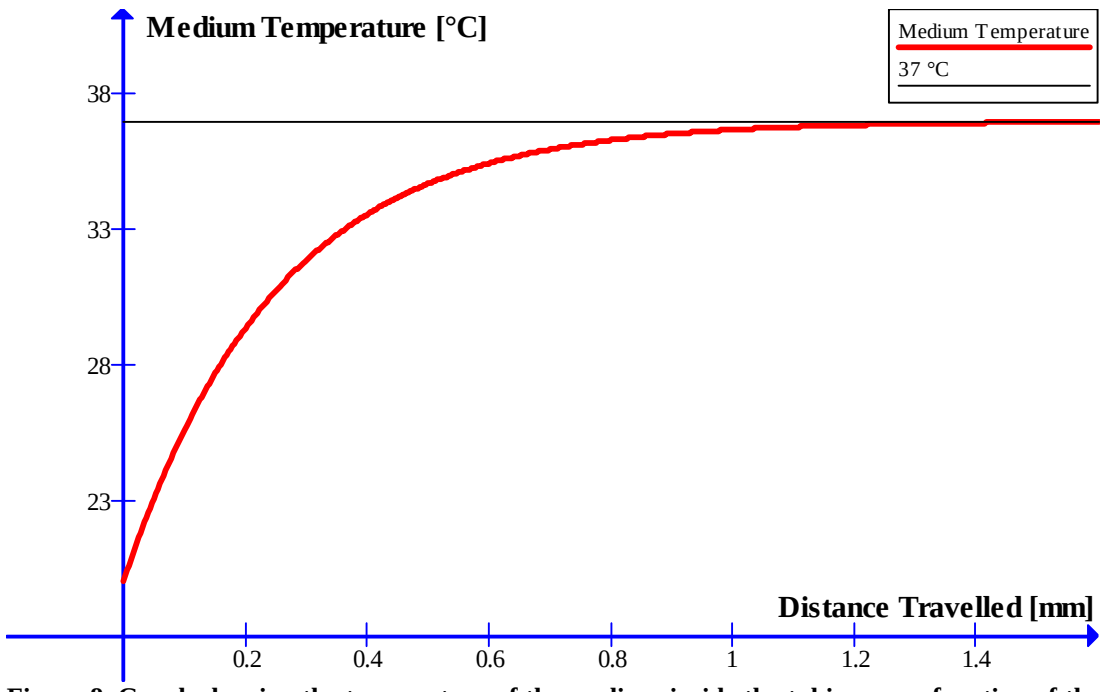

Figure 8. Graph showing the temperature of the medium inside the tubings as a function of the distance travelled inside the temperature stage.

3.10 Testing Cell Behaviour at Different Temperatures

A cell experiment with HeLa cells on glass and changing temperatures was made to get an idea of how the cells would behave at different temperatures. This was done before the decision to use fibroblast cells for the experiments on nanostructured substrates was made. The temperature experiment started at 35 °C on the first day, then 37 °C the next day, then 38 °C for one day, and finally 39 °C for one day.

Unfortunately the cell proliferation rate was so high already at 35 °C that the number of cells was so large just one day into the experiment that individual cell tracking and counting were impossible due to the cells forming an almost confluent monolayer. Since this was more of a trial experiment just to get an idea of the influence which temperature had on cell behaviour another experiment was not conducted.

It is still possible from the obtained movies, though, to get an idea of how the temperature affects the cells. At all four temperatures the cells seemed to proliferate similarly. The time it takes for each cell to divide was between 30 min. and 2 h at all temperatures, and judging qualitatively the proliferation rate seems about the same. At 39 °C, though, many of the cells die, indicating this temperature is too high for cell culturing.

From this short experiment it seems unlikely that a temperature difference of ±1 °C makes a significant difference. However, to rule out that any findings in this study are due to temperature differences, baseline substrates in the form of glass and flat Si is placed alongside the nanostructured substrates in each experiment as a way to make sure variables such as the temperature are constant.

4 Culturing the Cells

A proper cell culture chamber (CCC) and preparation of cells are needed when observing the behaviour of living cells. In this chapter it will be described how and why the CCC is designed as it is. Afterwards it will be described how to prepare the CCC for the cell experiments, and how to get the cells into it. Finally a short introduction to the microscope is made.

For future convenience, a step-by-step guide for starting experiments with microscopy of cells in the CCC made is found in Appendix D.

4.1 The Cell Culture Chamber

Several things need to be taken into account when designing and making a chamber suitable for culturing cells in both a temperature stage and in a microscope. These things include:

Size
The CCC has to fit in the temperature stage and the working distance of the objective on the microscope must also be considered.

Material
The material has to be biocompatible, water proof, and preferably readily available and easy to work with, i.e. durable but still easy to carve, drill and make threads in. It should also be able to withstand sterilization with either 70% ethanol or 0.5 M NaOH.

Bubbles
Bubbles can be a large problem in fluidic systems (Stangegaard 2005), so measures need to be taken to prevent these from influencing the experiments.

Inlet and outlet
Connections for the tubings supplying the cell culture medium need to be secure, easy to connect and tight in order not to leak during the experiments that run for days.

Opening and closing mechanism
In order to be able to place different substrates in the chamber a tight and reusable mechanism is needed for opening and closing the CCC.

Cell culture medium flow
The cell culture medium flow needs to supply the cells with nutrients, hormones, O_2 and CO_2, regulate pH and keep all those things at a constant level. However, it must not interfere with their movement or disturb them in any other way (Stangegaard 2005).

4.2 Designing the CCC

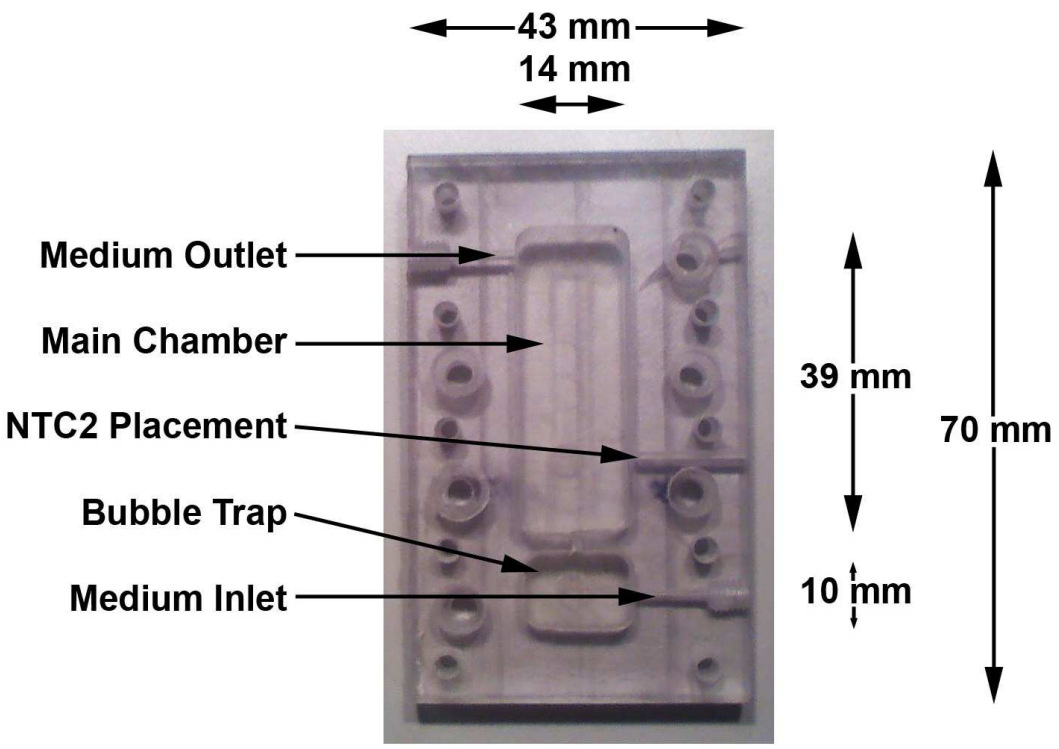

Figure 9. The cell culture chamber (CCC) made in polycarbonate.

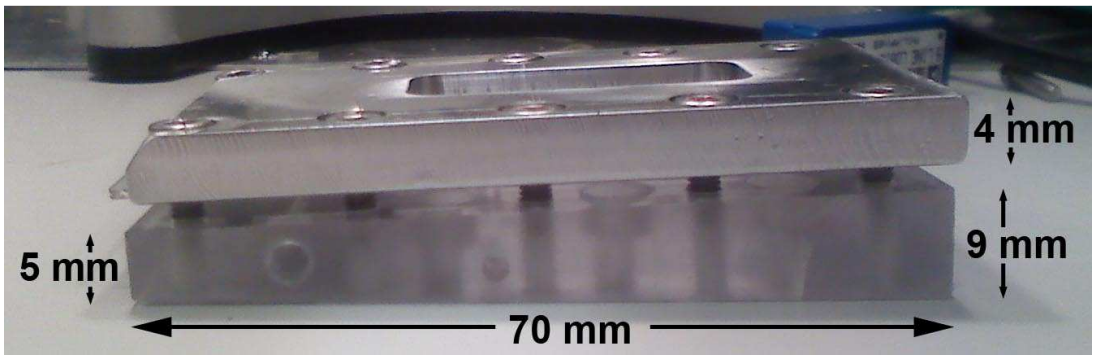

Figure 10. The cell culture chamber (CCC) with the Al lid.

A description of the progress of making the CCC taking into account the points outlined above follows.

The CCC was made from polycarbonate as this is easily available, waterproof, easy to work with and of course biocompatible.

The Bubble Trap

Bubbles can both kill cells and prevent pictures of the cells in the chamber. This was a major concern, so it was used as a starting point for designing the chamber. To reduce the problem three different design elements have been incorporated. The first one is the inclusion of a bubble trap placed just before the main chamber, wherein the cells

are cultured. The bubble trap is basically just a small chamber where the medium outlet is in the bottom, hereby trapping bubbles before they enter the main chamber.

Inclined and Hydrophilic Top Surface

The next thing for preventing problems with bubbles was the creation of an inclined surface causing bubbles to drift to the higher end of the chamber reducing the risk for bubbles in the rest of the chamber. When inclining the surface one needs to be aware of the refraction of the light that will occur between the cells and the objective of the microscope. As this could pose a problem with large inclination, different inclinations were tested with the 10x zoom objective (the one used when observing the cells) to see when refraction would cause a problem. An angle of 4° seemed to be the largest inclination possible without significant loss of picture quality.

To improve the effect of the inclined surface the material of the top cover needed to be as hydrophilic as possible. Taking into account that the top cover also had to be waterproof, transparent, and biocompatible, glass seemed to be the best choice, as other alternatives as PMMA and polycarbonate are more hydrophobic even with hydrophilic coatings. Therefore a microscope glass slide was used as top cover, as these are readily available.

A PDMS mold that fitted around the main chamber and the bubble trap was made to make sure that the glass slide was tight and no medium was leaking out. In order to clamp the glass slide down onto the PDMS securing a firm and tight closure of the chamber an Al lid was made with a hole in the middle allowing visible access for the microscope to the substrates with the cells in the main chamber. Five screws on each side of the glass slide secured the Al lid and made sure that the pressure on the glass was evenly spread. Earlier tests with a top part made from polycarbonate resulted in broken glass slides caused by the uneven pressure from the softer polycarbonate.

Microscope glass slides have a size of 76.2 x 25.4 mm^2 and this effectively limits the length and width of the CCC – this size is of course fine allowing room for several substrates placed in the CCC at once. The height is primarily limited by the 19 mm working distance of the 10x microscope objective and the possibility that a placement of the CCC too close to the top of the temperature stage could cause a heat loss resulting in difficulties keeping the CCC at a temperature of 37.0° C.

The final CCC measured 70 x 43 x 5-9 mm^3, while the main chamber for the cells measured 39 x 14 x 4-6 mm^3. More dimensions can be seen in Figure 9 and Figure 10.

Medium Flow

When the connection between the bubble trap and the main chamber, i.e. the inlet to the main chamber with the cells, was made, it was taken into account that the cell medium flow should not disturb the cells. I.e. if the inlet to the main chamber was too low, the medium flow would be at the same height as the cells exposing them to a shear stress. To minimize this effect the inlet was made 2 mm above the bottom of the chamber where substrates with cells would be placed.

Making a rough calculation on the flow rate in the chamber by just dividing the flow

rate of 5 µL/min. with the average cross-sectional area of the chamber gives a flow rate of approximately 10 µm/s. However, the flow is not uniform in the chamber and will probably be lower at the bottom part at the cells.

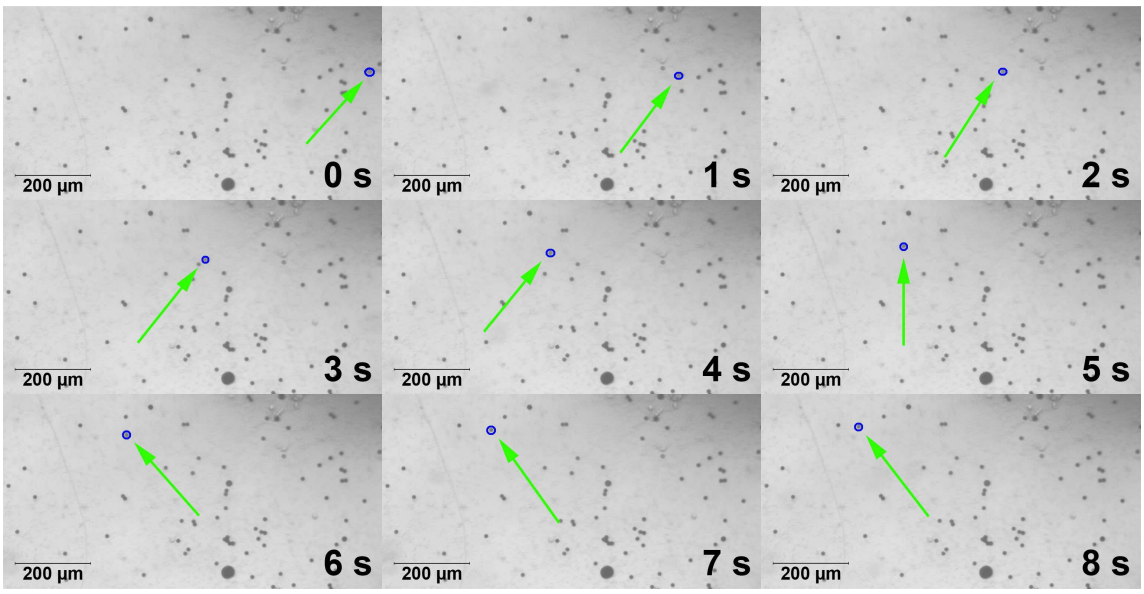

Figure 11. A 10 µm bead at the flow velocity measurements in the middle of the chamber. It starts out about 50 µm above the surface with a velocity of approximately 200 µm/s, but slows down as it gets closer to the substrate.

In order to find the flow at the cells flow measurements were made using beads with a diameter of 10 µm flowing about 50 µm above the substrates judged by the focus of the microscope. As the flow rate of 5 µL/min. used for the cell experiments was too low to make the beads move before settling and sticking to the surface, a flow rate of 1000 µL/min. was applied. This showed the velocity of the beads close to the inlet to be about 250 µm/s, 200 µm/s in the middle of the chamber, and about 150 µm/s at the outlet. The declining flow rate closer to the outlet can be explained by the inclined surface making the cross-sectional area of the chamber smaller at the inlet. This is supported by the fact that the flow rate change is indeed approximately inversely proportional with the change in the cross-sectional area of the chamber. Assuming the flow velocity scales linearly, the flow velocity 50 µm above the substrates is 0.75-1.25 µm/s at 5 µL/min. depending on the place in the chamber.

The flow experienced by the cells will most likely be even lower, as the flow velocity seems to decrease closer to the substrate. This can be seen in Figure 11, where the velocity of a 10 µm bead in the middle of the chamber decreases the closer it gets to the substrate below. In the first second it travels 189 µm about 50 µm above the substrate, but in its fourth second it only travels 92 µm and is about 20-30 µm above the substrate. From 7 s to 8 s the distance travelled is down to 31 µm when the bead is approximately 10 µm above the substrate.

To show that even the flow rate 50 µm above the substrate is sufficiently low, a comparison to Brownian motion of a signaling molecule, which typically has a mass of about m = 10 kDa, will be made. Assuming density of water such a molecule will have a Stokes radius of approximately r = 1.6 nm. Furthermore assuming a low

Reynolds number the Einstein-Smoluchowski relation can be written as follows and used to find the diffusion coefficient:

$$D = \frac{k_B T}{6\pi \cdot \eta \cdot r} \qquad \textbf{Eq. 14}$$

Here

D	[m^2/s]	is the diffusion coefficient,
k_B	[J/K]	is Boltzmann's constant ($1.381 \cdot 10^{-23}$ J/K),
T	[K]	is the absolute temperature of the fluid,
η	[Pa·s]	is viscosity of the fluid, and
r	[m]	is the Stokes radius of the particle.

If the viscosity is assumed equal to that of water, a Stokes radius of r = 1.6 nm gives the diffusion coefficient D = 161 µm^2/s. Looking at a length scale comparable to the cell L = 10 µm and using the diffusion length $L = 2\sqrt{Dt}$, it will take a signalling molecule 0.16 s to travel this distance due to diffusion, whereas it will take 8-13 s due to the flow. The flow should therefore not interfere with the cells.

Now it is seen that the flow is sufficiently low not to influence the cells, but it should also be large enough to keep nutrients, pH, O_2, etc. at a constant level. In cell experiments with rapidly growing cell types in culture flasks the medium should be replaced every 3-4 days (Masters 2000). With the 5 µL/min. flow rate in this study the medium inside the chamber was replaced in about 14 h. In other words, the medium flow was high enough to replace the old medium with new medium.

Inlet and Outlet Connections

About three quarters of the inlet and outlet were threaded with an M4 thread. A custom-made hollow plastic M4 screw with a tube inside could then easily be fastened securing stable and tight connections. At the end of the tube was a small rubber ring, sealing the connection between the end of the tube and the end of the threaded inlet and outlet, respectively.

Figure 12. The custom-made M4 screw connector.

Polytetrafluoroethylene (PTFE) tubings with an inner diameter of 0.8 mm and an outer diameter of 1.6 mm were used for the medium flow to and from the CCC, as the other common tubings made of silicone could introduce bubbles due to the gas permeability of silicone.

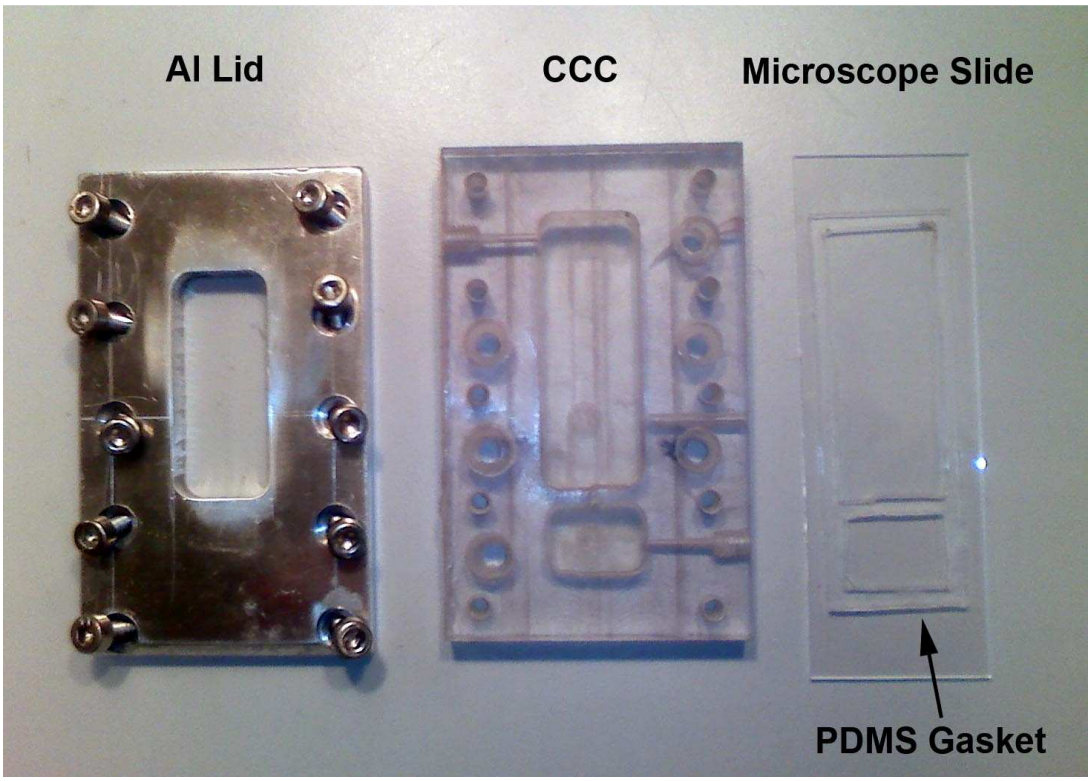

Figure 13. All four parts of the CCC.

4.3 Preparation for Cell Experiments

It is of the utmost importance that everything is sterile before culturing of cells start in the CCC. Therefore everything that could possibly come into contact with either the cells or the cell medium must be sterile before any experiments can begin.

All parts of the CCC (main part of the CCC, the PDMS mold, the microscope glass slide, the top Al top part, the screws), the tubings, the substrates and also the Al block, which the CCC is screwed onto inside the temperature stage, and the Allen key used to tighten the screws are cleaned with 70% ethanol and sterile tissues while wearing gloves. Parts with PMMA were, however, cleaned with 0.5 M NaOH, as PMMA is damaged by ethanol. Afterwards all these parts are placed under a sterile laminar flow and all parts except the microscope glass slide and the Al top part are put together. The CCC, the substrates, and the tubings are then flushed with Phosphate-Buffered Saline (PBS) or Hank's buffer to get rid of ethanol residues, since these could kill the cells.

The substrates are placed on a small piece of a microscope glass slide using Teflon-based Fomblin grease to make them adhere to the glass. The Fomblin grease has been sterilized using an autoclave and has a degassing rate of 10^{-12} mbar, which means it will not get dissolved into the medium. The glass piece itself is a bit smaller than the bottom area of the main chamber and either small pieces of PDMS between the glass piece and the side of the main chamber or Fomblin grease is used to keep it from moving during the experiment. It is important to make sure that the substrates and the piece of glass are placed horizontally as a tilted substrate will make it hard to get microscope images with the whole image in focus. Furthermore, a tilted substrate

would scatter the light from the microscope away from the objective of the microscope instead of into it, making it harder to get well-lit images.

4.4 Starting the Experiment

When everything has been sterilized and put together, cells in medium are injected into the chamber under the sterile laminar flow. The composition of the medium used for the NIH3T3 fibroblast cells was:

- 500 µL Penicillin-Streptomycin solution
- 5 mL of Newborn Calf Serum
- Dulbecco's Modified Eagle Medium: Nutrient Mixture F-12 (DMEM/F12) + GlutaMAX to 50 mL

$50 \cdot 10^3$ cells are injected into the chamber, corresponding to about $10 \cdot 10^3$ cells/cm^2 inside the main chamber. Optimally this will result in about 120 cells for each time-lapse movie covering an area of 1000 x 750 µm^2 resulting in an average cell-cell distance of 73 µm. Usually, though, less than half of that was actually seen in the time-lapse movies, probably due to some of the cells being flushed out before adhering to the substrates, resulting in average cell-cell distances of more than 100 µm at the start of the experiments.

Two different methods were used to get cells into the chamber. Either a syringe holding the same amount of medium as the CCC (approximately 4 mL, assuming the volume of the tubings to be very small) with cells inside are connected to the inlet tubing, and the medium with the cells is injected. The other way is to inject the cells in about 1 mL of medium down into the chamber before closing it and afterwards close it and fill the chamber with medium without cells. The latter method can avoid cells getting stuck in the inlet tubing. Both methods have to be carried out with the utmost care to avoid creation of bubbles in the chamber. The chamber itself is held in a tilted position when filling it with medium, so that the outlet inside the chamber is at the highest point to avoid air getting trapped inside. After the injection of medium with cells an empty syringe is connected to the outlet tubing to prevent contamination.

The CCC is afterwards put inside the temperature stage, which is then mounted in the microscope. As little movement as possible of the CCC with the cells is preferred, however, this order of doing things is necessary, as the space under the microscope is very confined and does not allow for mounting of the CCC inside the temperature stage.

Everything is now set up for the cell motility experiment to start. Usually the computers controlling the microscope and the temperature stage are already running at this point as they are used a lot. Heating of the temperature stage beforehand can also reduce the chances of overheating the cells before the temperature settles at 37.0 °C.

After everything has been set up cells have to adhere to the substrates. This usually takes from a few hours to a day. During this time no medium flow is applied to avoid flushing out the cells from the CCC. When it is seen that the cells have adhered to the substrates, a flow of 5 µL/min. is started using a syringe pump. The inlet tubing sup-

plying the medium to the cells is then also covered with Al foil to avoid photo damage of the medium (Stangegaard 2005).

4.5 The Microscope

The microscope used was a Zeiss Axiotech. Reflected light microscopy was used, as very few of the substrates were transparent. It offered adjustment of brightness, which was set as low as possible to minimize the light hitting the cells in order to minimize the phototoxic effect (Stangegaard 2005). Brightfield and aperture diaphragm could also be adjusted, effectively regulating the angle of the incoming light on the cells. As cells are largely transparent, lighting from an angle could make the edge of the cells more visible.

The objective was a 10x Zeiss with a 19 mm working distance, which had a field of view of 1000 x 750 μm^2. The microscope was connected to a computer, which received the images in a resolution of 1024 x 768 pixels. The electronically-controlled movable stage in the microscope, which the temperature stage was mounted on, could move in all three dimensions with a precision of 0.1 µm.

5 The Nanostructured Substrates

This chapter describes how the nanostructured substrates were created. Characterization of these substrates will also be made in this section.

Both so-called black Si and electron beam lithography (EBL) structures were made, however, due to time-constraints the latter were not thoroughly characterized. For this reason an independent chapter will follow in the last part of this thesis to describe creation, characterization, and results obtained on these substrates.

5.1 Black Si

Black Si is a nanostructured surface made of Si, which resembles grass structures in the nano- or micrometer-range and is sometimes called nanograss. Some types of black Si have a very low reflectivity of visible light, hence the name. A huge advantage is that it is both relatively cheap and fast to make larger surfaces of black Si. For the purpose of testing cell behaviour on nanostructured substrates, black Si is an easy way to get many different structures, which each are large enough to house hundreds if not thousands of cells to monitor.

5.2 Creating Black Si

A process called deep reactive-ion etching (DRIE) is used to create black Si. The equipment used at DTU Nanotech is an ASE (Advanced Silicon Etcher) delivered by STS in the Danchip cleanroom facilities.

Figure 14 shows how black Si is made. A Si wafer is placed in a grounded chamber, while the wafer itself is electrically isolated from the rest of the chamber. An RF electromagnetic field is then applied to the wafer in order to create plasma by ionizing the gas molecules inside the chamber. The power used to create this field is called the coil power and can be adjusted. The electrons stripped from the ions hitting the wafer will cause it to build up a negative charge. The positive ions will drift towards the wafer and will either chemically react with it or cause sputtering. To further enhance this effect a voltage can be applied to the wafer. The power controlling this bias is called the platen power and can also be adjusted.

The gasses inside the chamber are SF_6, C_4F_8, and O_2, though C_4F_8 was not used to create the structures used in this study. The O_2 gas serves to passivate the Si surface by creating an oxide layer. In this way the chemical reaction between SF_6 and Si will only take place where the Si surface has just been sputtered. Because of this a very anisotropic etch is possible, as the ions are hitting and sputtering the Si surface vertically. Due to the sputtering the Si wafer will heat up, hence a He gas flow on the back of the wafer will cool it down during the process.

By regulating the etch time, the pressure inside the chamber, the gas ratios, and the power of the electromagnetic field, the properties of the developed black Si can be adjusted. A higher etch time will create higher structures, while a higher pressure will yield a more isotropic etch because of more scattering of the ions. The gas ratio will control the etch rate and how isotropic the etch is. More O_2 then SF_6 will passivate

more, hence making the etch slower but also more anisotropic, and vice versa.

It should be noted that the surface on both Si and black Si will be oxidized by the air, meaning the surface on both is actually SiO_2.

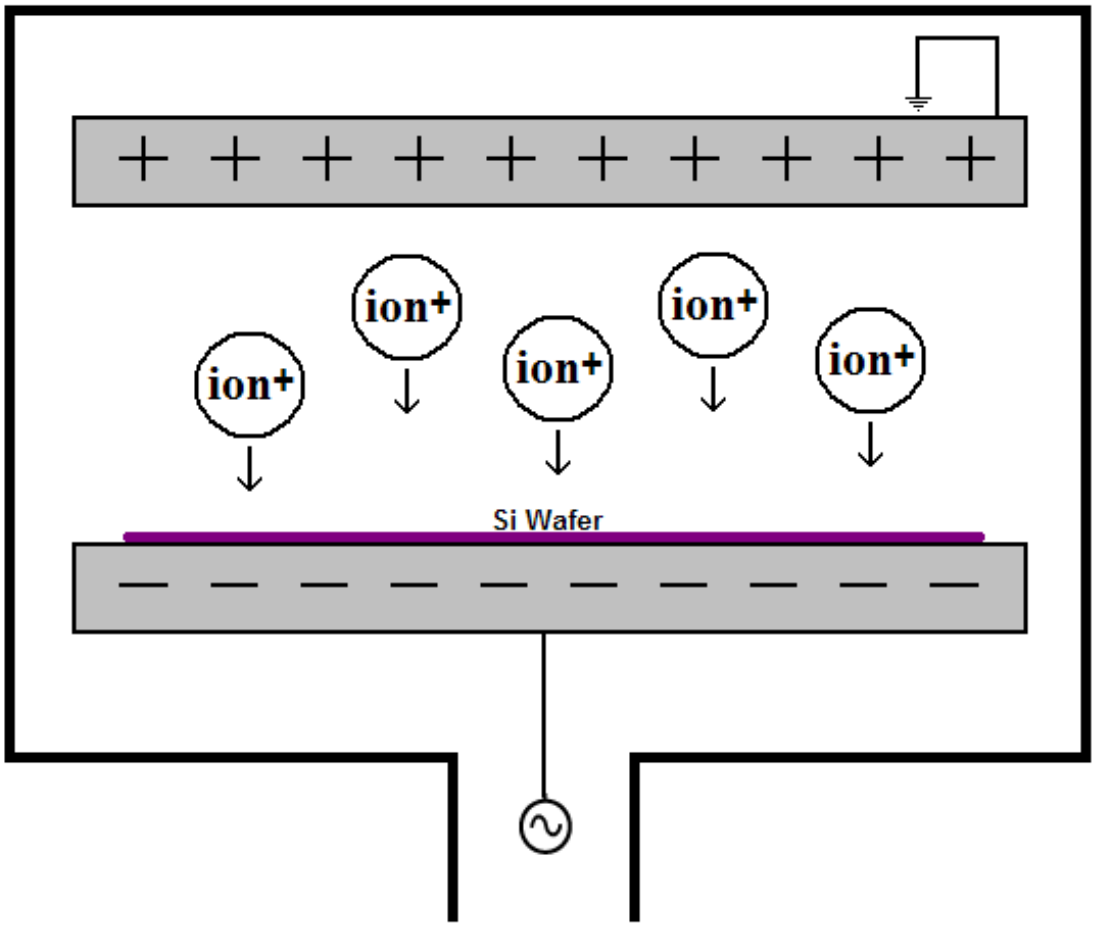

Figure 14. Sketch showing a reactive-ion etching process. Due to a RF electromagnetic field between the wafer and the chamber ions will be created that will hit and sputter the surface of the wafer.

5.3 Black Si Samples

The black Si samples used in this project have either been created in a former project, or have been supplied by Rasmus Davidsen, Bachelor student at DTU Nanotech. A complete library of available structures from the former project can be seen in Appendix A, where more pictures and process parameters for each sample are available. The process parameters to the black Si samples supplied by Rasmus Davidsen are unfortunately confidential at the moment, but more pictures of the samples can be seen in Appendix B.

Since black Si samples are easy and cheap to make, a wide array of different structures have been easily available. Samples exhibiting as different structures as possible have been chosen for time-lapse movies of cell to observe the behaviour on these. A non-processed Si sample has also been used for time-lapse of the cells to observe how

the cells behave on a flat Si substrate, to make it possible to attribute any peculiar findings on the black Si to their surface structures and not the material.

In total eight different black Si samples have been tested. In general they can be divided into two main groups. Four of them have sharp spikes, whereas the other four have more pyramid-like structures.

The four black Si samples with spikes can be seen in Figure 15 and Figure 16. The size of the spikes varies from a diameter of 100 nm and a height of 200-300 nm to a diameter of more than a 1 µm and a height of 6 µm. Compared to a cell diameter of approximately 10 µm, the smallest spikes are barely doorstep-like for the cells, whereas the largest spikes are in the size-range of the entire cell itself. These four samples can roughly be said to have large and dense spikes (15-17), small and dense spikes (16-05), large and sparse spikes (bs17c), and small and sparse (15-19).

The properties of the four black Si samples with spikes can be seen in Table 1.

Table 1. Properties of the Black Si Samples with Spikes.

Name	Spike Height [nm]	Spike Diameter [nm]	Spike Density [μm^{-2}]	Spike Pitch [µm]
15-17	1500	200	3	0.6
15-19	200-300	100	9	0.3
16-05	300-400	80-100	21	0.2
bs17c	6000	1200	0.1	3

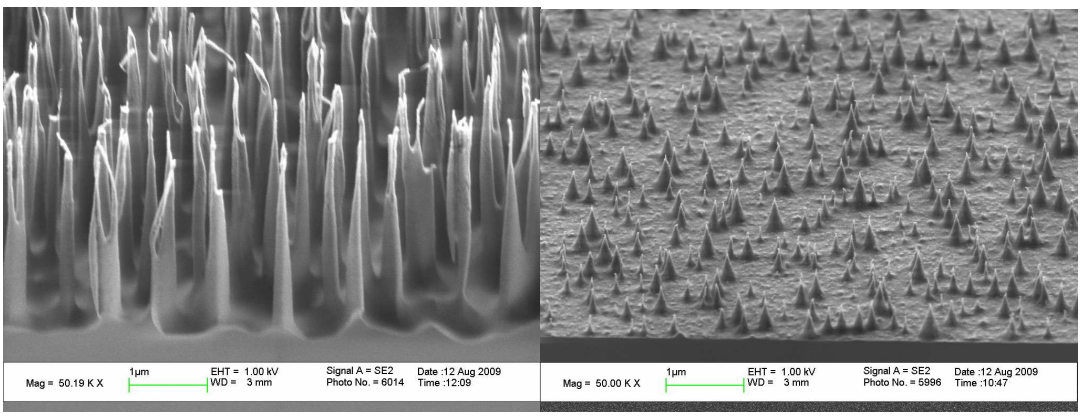

Figure 15. Scanning electron microscopy (SEM) images of Wafer 15-17 (left) and 15-19 (right).

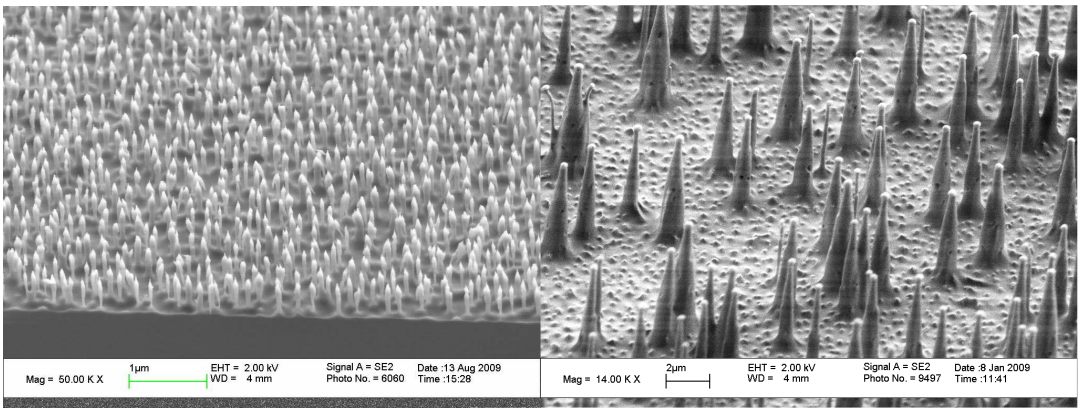

Figure 16. SEM images of Wafer 16-05 (left) and bs17c (right).

The four black Si samples with more pyramid-like structures can be seen in Figure 17 and Figure 18. These structures also vary quite a lot in size, the smallest ones having diameters and heights in the 100-200 nm-range, while the largest ones are in the µm-range.

The properties of the black Si samples with pyramid-like structures can be seen in Table 2.

Table 2. Properties of the Black Si Samples with Pyramid-Like Surfaces.

Name	Spike Height [nm]	Spike Diameter [nm]	Spike Density [μm^{-2}]	Spike Pitch [µm]
bs17m	1000-2000	1200-2400	0.2	2
bs17e	200-300	100	14	0.3
bs12c	300-400	200	10	0.3
bs12m	400	300-500	8	0.4

When working with such small structures, it should also be noted that both the cell culture medium and the cells themselves will make a thin coating on the substrate, which means the cells will not necessarily be exposed to the exact same substrate structures as is presented here.

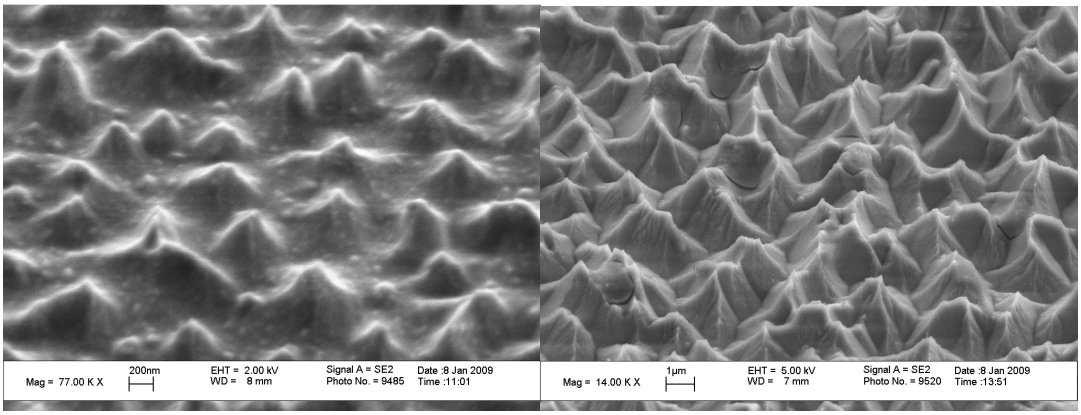

Figure 17. SEM images of bs17m (left) and bs17e (right).

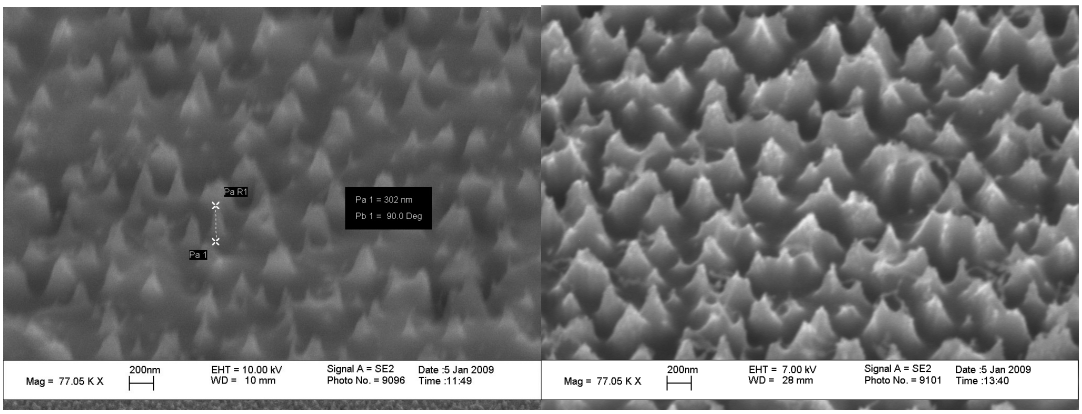

Figure 18. SEM images of bs12c (left) and bs12m (right).

6 Observations on Cell Behaviour

This section will start with a short explanation of how the time-lapse movies were obtained. Qualitative observations of the cell behaviour on the different substrates will subsequently be discussed. An overview of things like cell motility, morphology, polarization, proliferation and survival rates, and neighbourhood behaviour on the different substrates will be presented.

6.1 Recording the Time-Lapse Movies

A LabVIEW program developed by Kristian Mølhave, associate professor at DTU Nanotech, running on the computer connected to the microscope was used to obtain a time-lapse movie of the cells. The most important features of the program are:

• Adjusting time interval between obtaining images
- Shorter time intervals give more data, but also larger files and more time-consuming data processing. This can be changed to adapt to a specific cell type's motility.

• Stage movement allowing for time-lapse movies of different places/substrates
- Movies of several substrates and also several places on each substrate were obtained.
- Baseline measurements on glass were conducted in each experiment.
- Avoiding exposing the cells to light when not obtaining images.

• Auto focus to ensure proper focus even though the stage would drift

• Movies saved as AVI (video) and optionally also as BMP (image) files
- If the program crashed the AVI files could be corrupted.

6.2 Cell Behaviour

Both experiments (07092009 and 21092009), from which all time-lapse movies analyzed in this chapter are from, were started 3 days prior to the start of the analyzed time-lapse movies. The experiments were chosen by cell density and image quality, but the fact that the time passed since cell seeding was the same rules out this as an unknown parameter. After these 3 days the cells should be out of the lag period (Masters 2000) and in the phase where exponential growth is seen. Optimally the cells should be monitored continuously for a week or more after the seeding to determine both the lag period, the 'log phase' growth period and the 'plateau phase' in which the cells have become confluent with reduced growth, but the constrained availability of the microscope did unfortunately not allow this.

It should be noted that in one of the experiments (21092009) the fibroblast cells were labeled with a fluorescent dye (CellTracker CM-DiI), which should not affect cell behaviour. The appropriate filtering on the microscope to take advantage of the dye was unfortunately not available, which is why the dye does not appear in the microscope images. Furthermore, the flow rate was changed from 5 µL/min. to 4 µL/min. 6.3 h into the other experiment (07092009) due to a shortage of medium. This is unlikely to

have had any effect, especially as the experiment only lasted for another 1.1 h. To check if these two things had any effect, cells on the same substrate were compared across the experiments, and no differences were seen.

Survival Rate

A number indicating death and proliferation rate is found to get an idea of how suitable a given substrate is to the cells. One method used is to measure the time between the divisions of each cell. Since the number of cells dividing more than one time during a single movie was quite low in many cases, a different approach will be taken. Instead, the number of living cells is counted at the end and at the start of each movie to find the survival rate. If proliferation takes place this rate can be more than 100%. It is assumed that the same amount of cells will move in and out of the surveyed area during the experiment. As the obtained time-lapse movies are of different lengths, the survival rate will be converted into a survival rate per day noted in units of percentages per day using the formula

$$R = \left(\frac{C_{end}}{C_{start}}\right)^{\frac{24\,h}{t}} \qquad \textbf{Eq. 15}$$

Here R is the survival rate per day, C_{start} and C_{end} are the cell counts at the start and the end of the movie, respectively, and t [h] is the duration of the movie. All the measured numbers can be seen in Table 3 and Table 4 in the end of the chapter.

It should be noted that the number of cells in a particular movie does not necessarily reflect how suitable that particular substrate is for the cells. Different cell densities are often seen in different movies on the same substrate in the same experiment, most likely being influenced by the place they happen to fall down after injection. Hence this survival rate is used to measure how well they seem to survive once they have adhered to the substrate. Of course, the difference in cell densities will most likely influence the behaviour of the cells, but since it is not possible to accurately control this parameter in the setup, it will have to be considered as a source of error. Furthermore, it should be noted that the numbers are no exact measure of the suitability of the substrates for the cells. Cell division could be seen on all substrates, but of course this does not completely rule out the possibility of some of the cells still being in the lag period, hence proliferating at a far lower rate. A potentially longer lag period could be argued to stem from the structure of the given substrate, which would still give the number a connection with the substrate, albeit not in the exact same way. The numbers should therefore be seen as an addition to the observations written about each substrate in this section and not as a strictly correct mathematical model of cell behaviour in itself.

Cell Motility

The cell motility will be noted in this section, but only qualitatively. A more quantitative analysis of the motility will be made in the next chapter, where a mathematical model of cell motility will be discussed and the time-lapse movies analysed according to this model using both measured velocities and accelerations of the cells.

Cell Morphology

Cells can interact with the substrate in a number of different ways causing several different shapes as illustrated in Figure 1 in the introduction to the cell. Round, elongated, and polygonal shapes are seen, and the frequency of these shapes will be outlined. If not because of proliferation, a round shape indicates poor adhesion to the substrate, while the other shapes indicate better adhesion and hence also better support for cell motility. As the cells tend to change shape, mostly between the elongated and polygonal shapes, during a single time-lapse movie, exact numbers will not necessarily be given, as these could prove rather random.

General Observations

Before describing what was seen on each substrate, some general observations on the cells studied will be made. The cells seemed to adhere to each other to some extent, which was apparently independent on the substrate. Often a cell would migrate 10-20 µm to be able to adhere to another cell, or sometime tails from one cell would reach another cell up to 100 µm away. This was not always the case, though, since occasionally cells could be quite close to each other without touching each other at all. Cells adhering to each other would often suddenly retract and move away from each other. Daughter cells would often adhere to each other for several hours before retracting from each other. It did not seem, though, as if cells adhering to each other, daughter cells or not, would migrate in a certain way or pattern after retracting from each other.

The round cells did obviously not have any preferred direction of migration. The cells with elongated shapes, however, migrated in the direction of their elongation. A more or less clear wider front part with lamellipodia was formed when the elongated cells would migrate. This is shown in Figure 19A. The cells with polygonal shapes were rarely migrating and were mostly changing shape before doing so. When they eventually did migrate a wider front part with lamellipodia alike to the ones seen on the migrating elongated cells was seen as shown in Figure 19B.

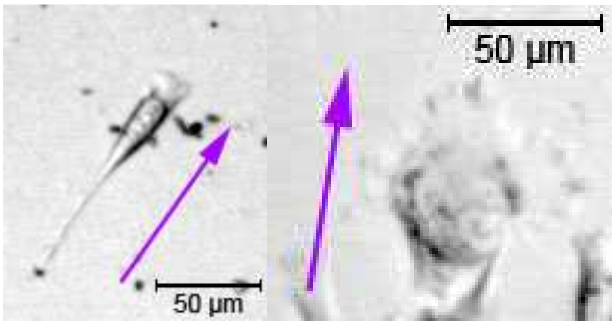

Figure 19A (left) & Figure 19B (right). Migrating elongated cell (left) and polygonal cell (right). The arrows show the directions of migration.

Glass

Glass was used as a baseline to see if any differences were seen between different experiments, which would indicate change in e.g. temperature, flow, or contamination. No obvious differences were seen, and the fibroblast cells did seem to adhere and migrate equally well in all the experiments. The cell adhesion was not quite as good as on the flat Si also studied, though. About half of the cells kept their round shape, indicating that the glass substrate was not really suitable for cell adhesion, while the other half were primarily forming elongated shapes. Only very few cells were seen forming

polygonal shapes. On the other hand, the motility of the cells seemed good, and no obvious differences could be seen in the velocities of the cells on the glass compared to the velocities of the cells on the flat Si substrate. An image showing the fibroblast cells on the glass substrate can be seen in Figure 20.

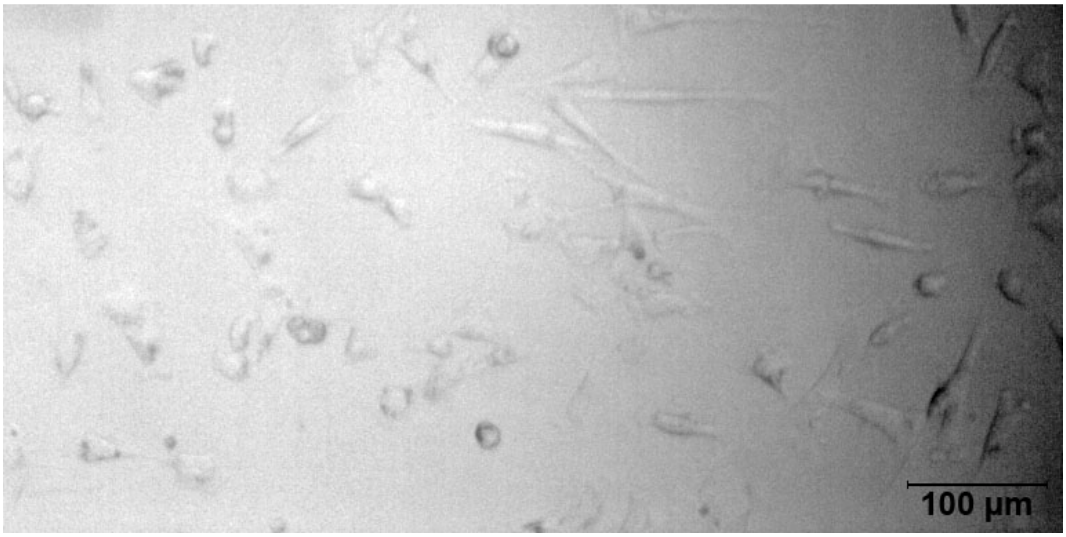

Figure 20. The glass substrate with cells as seen in the microscope.

Flat Si

The flat Si substrate seemed to suit the fibroblast cells well. They adhered to the substrate making only few round shapes, but many both elongated and polygonal shapes, a few of them with tails about 100 µm. The survival rate was measured to be 147% per day, meaning the cell count would be almost one and a half times more after 24 h indicating that the substrate was suitable for the cells. They also seemed to move around without any difficulties. An image showing the fibroblast cells on the flat Si substrate can be seen in Figure 21.

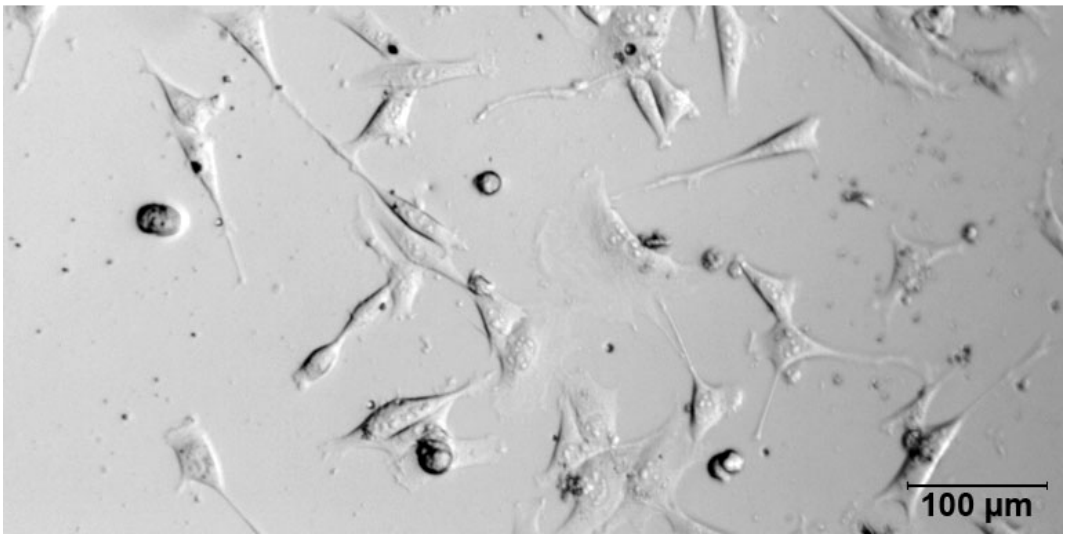

Figure 21. The flat Si substrate with cells as seen in the microscope.

15-17 Black Si

Cells did not appear under the microscope on the 15-17 black Si substrate. The substrate appeared very dark, as some types of black Si have a very high absorption of visible light. However, in spite of the bad lightning conditions, it would most likely still be possible to get a glimpse of cells if they were indeed adhering and living on the substrate. Taking into account that the 15-17 black Si substrate had spikes with a height of 1.5 µm and a density of 3 μm^{-2} it seems likely that the fibroblast cells are not able to adhere and survive on the substrate. It should be noted that only one movie using this substrates was recorded, because no cells could be seen anywhere on it prior to the start of obtaining the time-lapse movies. An image showing the 15-17 black Si substrate without cells can be seen in Figure 22 (left).

15-19 Black Si

As with the flat Si substrate the 15-19 black Si substrate seemed to suit the fibroblast cells. They adhered to the substrate and as with the flat Si substrate made both round, elongated, and polygonal shapes. A few more cells than on the flat Si appeared round. It also seems that a larger share of the cells formed long and thin tails reaching a length of up to 200 µm. The survival rate was measured to be 118% per day, a bit less than for flat Si. This, along with the higher fraction of rounds cells, indicates that the 15-19 black Si substrate is a bit more hostile for the fibroblast cells than the flat Si. The motility seemed to be about the same as for flat Si, though, with the cells moving around quite freely. An image showing the fibroblast cells on the 15-19 black Si substrate can be seen in Figure 22 (right).

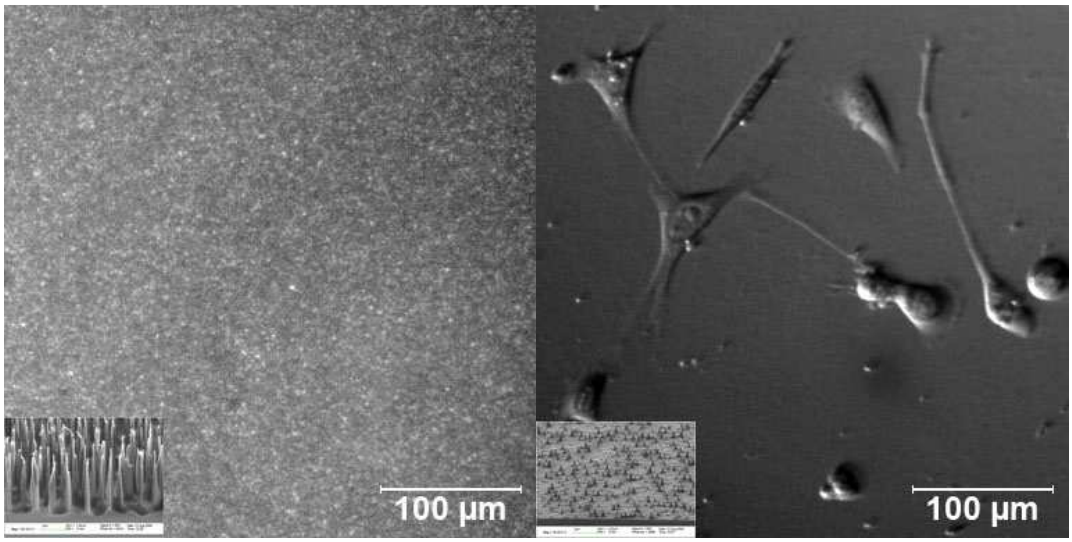

Figure 22. The substrates with cell as seen in the microscope. On 15-17 (left) no cells can be seen, whereas on 15-19 (right) the cells adhere. The small pictures in the lower left corners are SEM pictures of the substrates.

16-05 Black Si

About half of the cells had a round shape, indicating poorer adhesion to this structure than to flat Si. The other half, though, showed elongated or polygonal shapes and did seem to adhere quite well to the substrate. The motility of the cells did not seem ham-

pered, and the measured survival rate of 109% per day also indicates that the substrate is only a bit less suitable for the fibroblast cells than flat Si is. An image showing the cells on the 16-05 black Si substrate can be seen in Figure 23 (left).

Bs17c Black Si

The fibroblast cells seemed to adhere decently to the bs17c black Si substrate, showing mostly elongated and some round shapes. The cell size seemed smaller than on the flat Si substrate and very few polygonal shapes were seen where the cells spread out over a larger area. Moreover, the focus on the cells was quite far away from the focus on the substrate, which could indicate an increase in the height of the cells or the fact that the cell is adhering on top of the spikes of the substrate. Most interestingly, though, was the very limited motility which the cells seemed to have on this substrate. Most cells did not seem to move at all, or at least not more than the size of themselves (~10 µm) during an 18 h time-lapse movie. The survival rate was decent on both experiments conducted with this substrate, with survival rates per day being 100% and 114%, respectively. An explanation for these observations could be that the cells were simply unable to migrate on top of the 6 µm spikes on the substrate and that they were unable to form large polygonal shapes on such spikes. Further studies to see exactly how cell adhesion takes place on this substrate could be very interesting. An image showing the fibroblast cells on the bs17c black Si substrate can be seen in Figure 23 (right).

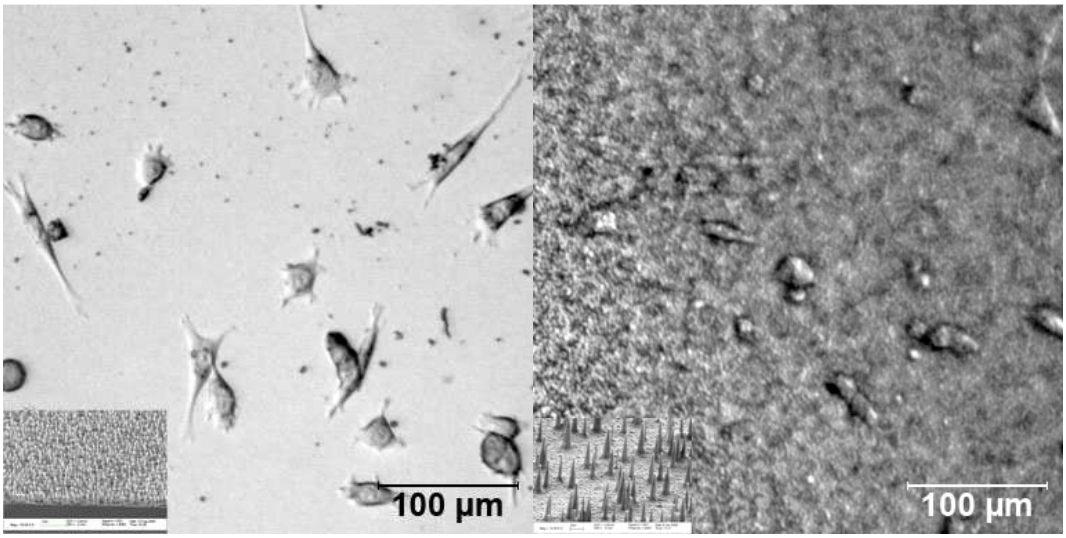

Figure 23. The substrates 16-05 (left) and bs17c (right) with cells as seen in the microscope. Notice the cells on bs17c are in focus while the substrate is not.

Bs17m Black Si

Cell adhesion seemed decent, but not great on the bs17m substrate. About half of the cells appeared round, with the rest forming primarily elongated shapes, though some polygonal shapes were seen. The cells also seemed a bit less motile than on flat Si, though they were clearly able to migrate on the substrate. The survival rate of 85% per day also indicates that the substrate is not as suitable for fibroblast cells as a flat Si substrate. An image showing the cells on the bs17m black Si substrate can be seen in Figure 24 (left).

Bs17e Black Si

The fibroblast cells could barely be seen on the bs17e substrate. It was possible to see that cells were adhering and migrating in the time-lapse movies, but anything more than that was impossible to make out. An image of what appeared under the microscope on the bs17e black Si substrate can be seen in Figure 24 (right).

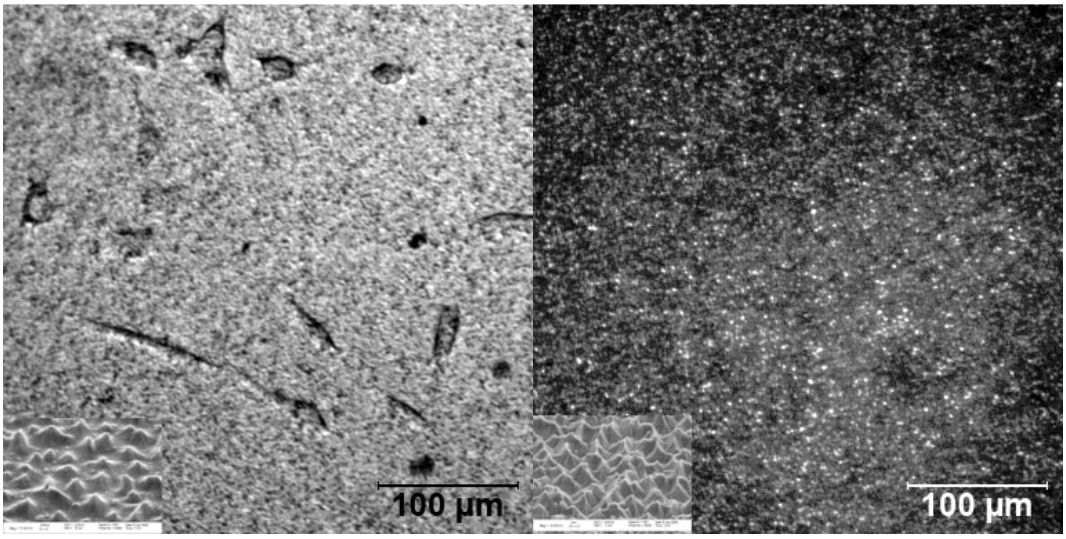

Figure 24. The substrates bs17m (left) and bs17e (right) with cells as seen in the microscope. It was almost impossible to see the cells on the bs17e substrate.

Bs12c Black Si

On the bs12c substrate about half of the observed cells appeared round indicating poor adhesion, while the rest were mainly elongated, although a few also made the larger polygonal shapes. The motility seemed about as high as on the flat Si, while the measured survival rate of 126% per day was only a bit lower than the number for the flat Si. An image showing the fibroblast cells on the bs12c black Si substrate can be seen in Figure 25 (left).

Bs12m Black Si

About one half of the cells appeared round on the bs12m substrate, with the rest showing elongated shapes. No polygonal shapes were seen, though it should be noted that cells were hard to spot on this substrate, making it possible that a few polygonal-shaped cells might have been adhering to the substrate. The motility seemed to be at about the same level as was the case with the flat Si, but the measured survival rate of 69% per day was much lower. An image showing the fibroblast cells on the bs12m black Si substrate can be seen in Figure 25 (right).

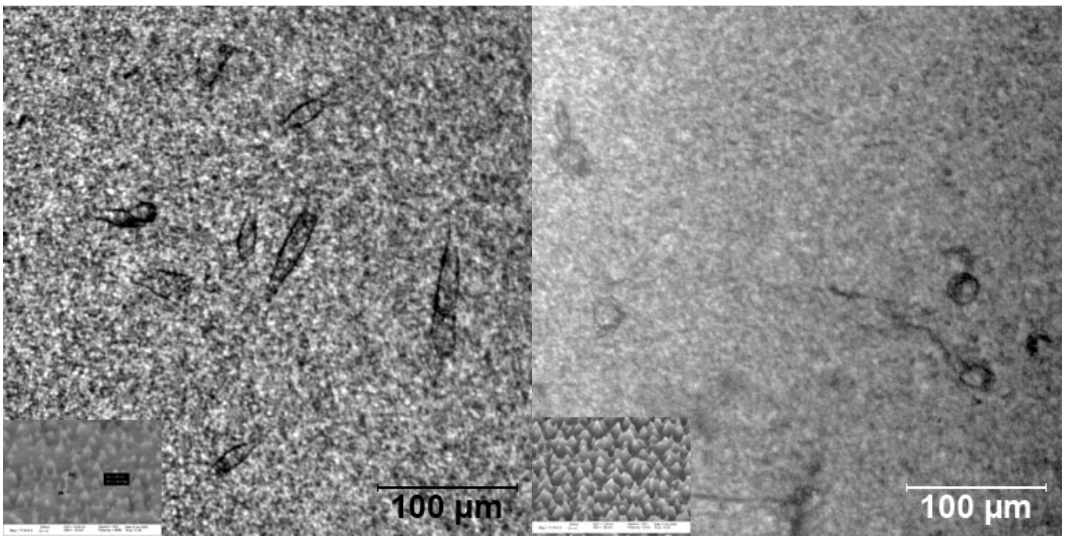

Figure 25. The substrates bs12c (left) and bs12m (right) with cells as seen in the microscope.

Table 3. Cell Counts and Survival Rates (Experiment 21092009).

Substrate	Number of Movies	Movie Duration [h]	Total Cell Count, Start	Total Cell Count, End	Survival Rate per Day
Si	2	17.93	69	92	147%
15-17	1	17.93	0	0	-
15-19	3	17.93	85	96	118%
16-05	4	17.93	188	200	109%
bs17c	3	17.93	47	52	114%
Glass at inlet	1	17.93	8	8	100%
Glass at outlet	1	17.93	4	4	100%

Table 4. Cell Counts and Survival Rates (Experiment 07092009).

Substrate	Number of Movies	Movie Duration [h]	Total Cell Count, Start	Total Cell Count, End	Survival Rate per Day
Glass	2	7.33	82	83	104%
Si	2	7.33	75	85	151%
bs17c	2	7.33	39	39	100%
bs17m	2	7.33	41	39	85%
bs17e	2	7.33	-	-	-
bs12c	2	7.33	54	58	126%
bs12m	2	7.33	46	41	69%

7 Modelling Cell Behaviour

This chapter describes how the time-lapse movies of the migrating cells are analysed in order to fit the migration patterns of the cells to a mathematical model. To do this, firstly an introduction to the current mathematical model of cell behaviour will be made. The manner in which the time-lapse movies are analysed and the results of this analysis will afterwards be presented and the substrates will be compared by use of the mathematical model.

7.1 The Ornstein-Uhlenbeck Process

Mathematical motility models of cell behaviour have remained relative simple over many decades. The standard model still used today is the Ornstein-Uhlenbeck (OU) process (Ornstein and Burger 1919), though better models are sought after (Selmeczi, Mosler, et al 2005 and Selmeczi, Li, et al. 2008). The OU process is an old model inspired by Brownian motion and can easily be derived from the Langevin equation (Eq. 16) describing Brownian motion.

$$\vec{F} = m \cdot \frac{d\vec{v}(t)}{dt} = -6\pi \cdot \eta \cdot r \cdot \vec{v}(t) + \sqrt{2D}\vec{\xi}(t) \qquad \textbf{Eq. 16}$$

Here

$\vec{F}$	[N]	is the force on the particle,
m	[kg]	is its mass,
$\vec{v}$	[m/s]	is its velocity,
η	[Pa·s]	is the fluid viscosity,
D	[μm^2/s]	is the diffusion coefficient of the particle,
$\vec{\xi}$	[$s^{-1/2}$]	is a normalized 'white noise', and
t	[s]	is the time.

Dividing on both sides by $6\pi \cdot \eta \cdot r$, setting $P = \frac{m}{6\pi \cdot \eta \cdot r}$, and defining a new diffusion coefficient *D'* gives the OU process

$$P\frac{d\vec{v}(t)}{dt} = -\vec{v}(t) + \sqrt{2D'}\vec{\xi}(t) \qquad \textbf{Eq. 17}$$

P [s] is called the persistence time of the motion and *D'* [m^2/s] is the diffusion coefficient of the OU process, also called the motility coefficient of the microorganism, which in this chapter will just be denoted *D*.

The first term of the right-hand side describes how the cell is slowed down in the direction opposite to that of its motility due to adhesion and retraction of focal adhesion sites. The second term on the right-hand side of the equation describes the random motion that the cell undergoes due to the random rearrangements of the cytoskeleton.

The left-hand side of the equation describes the acceleration of the cell, i.e. the change in velocity of the motion. The persistence time of the motion is a quantitative measure

of the cell motility memory, i.e. if a cell displays very persistent motion it has a high *P* and its direction of motion will be less affected by the diffusion-like effect of the motility compared to a cell with a lower *P*.

The velocity autocorrelation function is defined as $\phi(\mathrm{t}) =< v(t) \cdot v(0) >$. Following integration of Eq. 17 twice the velocity autocorrelation can also be expressed as (Selmeczi, Mosler, et al 2005)

$$\phi(t) =< v(t) \cdot v(0) >=< v^2 > e^{-|t|/P} = \frac{nD}{P} e^{-|t|/P} \qquad \textbf{Eq. 18}$$

Here *n* is the dimension, which in the case of this study is 2, and ϕ [m^2/s^2] is the autocorrelation, which describes the correlation between the velocity at time 0 and the velocity at time *t*. From this equation it is clear that the dependence on prior velocity is an exponentially function, where the persistence time *P* determines the rate of decay.

7.2 Analysing the Time-Lapse Movies

In order to find out how well the OU process describes the motility data obtained in this study, the recorded time-lapse movies were analysed with a MATLAB program developed by Cristian Grădinaru, PhD student at DTU Nanotech.

The program, which has yet to be given a name, tracks the cells by finding the brightest spots in each frame in the time-lapse movie. The cell edge was subsequently defined as the contour line of constant intensity set at a fraction of that of the brightest spot in the cell. The cell coordinates were finally defined as the centroid of this contour line.

After the cells had been tracked by the program the cell trajectories had to be manually checked to exclude undesired data points, such as trajectories intersecting in space and time, dividing cells, non-adherent cells, incorrectly tracked cells, cells adhering to other cells, etc. These instances had to be manually deleted from the trajectory data afterwards. This was a quite time-consuming process, and time did not permit a thorough analysis of each time-lapse movie in this fashion. Therefore only analyses on movies of cells on baseline substrates (Glass and Si) and on nanostructured substrates that seemed to affect the cells were made.

7.3 Interpreting the Motility Data

After manual post-processing of the trajectories they were processed by another MATLAB program by Cristian Grădinaru. From the trajectories it calculates the velocities and the accelerations of the cells.

In a few of the movies stage drift was seen. This drift was then simply subtracted from all the trajectories in order to get the actual cell migration patterns of the cells on the substrate. Furthermore, the average of all cell velocities was calculated for each and all frames to make sure the flow of the medium did not move the cells in a par-

ticular direction. The velocity in x and y direction was compared, as the flow was in the x direction, and no difference was seen within the error bars.

The accelerations perpendicular and parallel to the velocity are plotted as a function of the velocity. According to the OU process (Eq. 17) the acceleration perpendicular to the velocity should average to zero, as the acceleration in this direction should be white noise. The acceleration parallel to the velocity, however, is linearly dependent on the velocity and from Eq. 17 it can be seen that the slope should be $-\frac{1}{P}$. It should be noted that the length units on the graphs are pixels (1 pixel = 0.977 µm), while the time units are frames (1 frame = 4 min.).

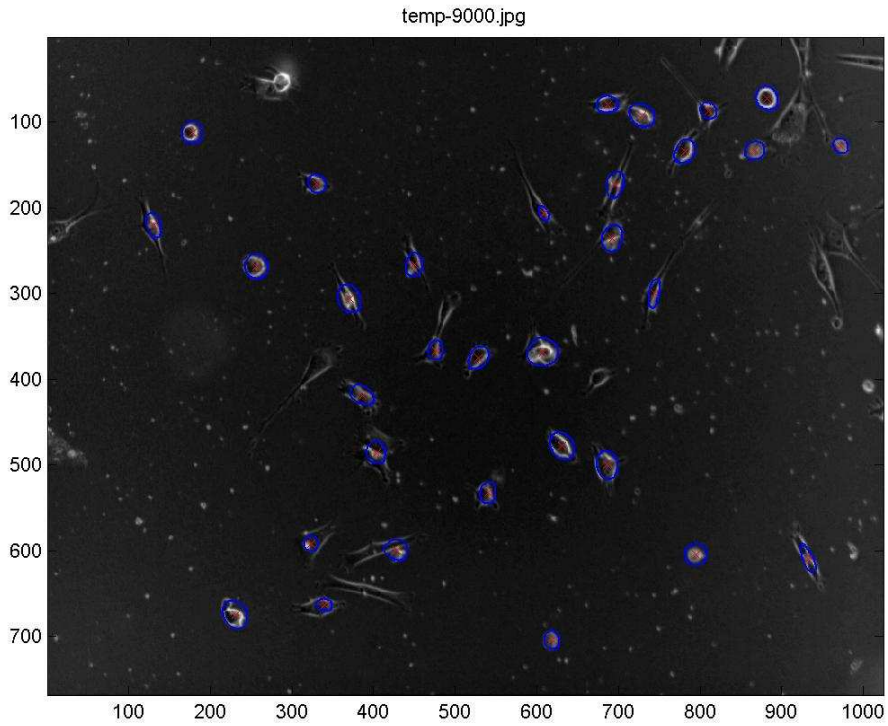

Figure 26. Pictures of the cells tracked on the 16-05 black Si substrate. The blue circles indicate the cell edges, while the small red crosses indicate the centroids.

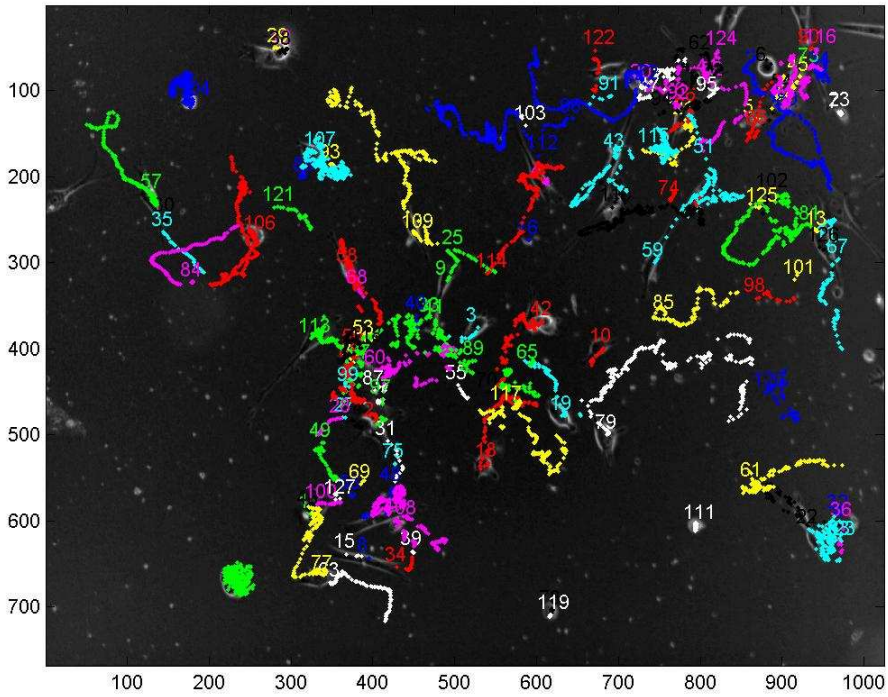

Figure 27. Figure from the MATLAB program showing the trajectories for the 16-05 black Si substrate after manually processing. The units on both axes are pixels.

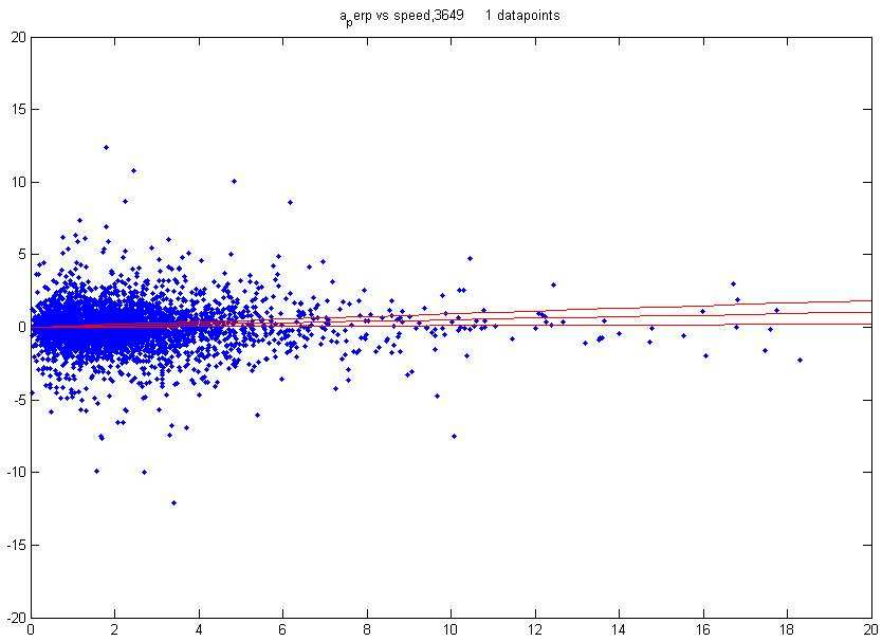

Figure 28. Figure from the MATLAB program showing the acceleration of the cells perpendicular to their velocity as a function of their velocity for the 16-05 black Si substrate. The red lines are the average with error bars. The units are pixels/frame (x axis) and pixels^2/frame (y axis).

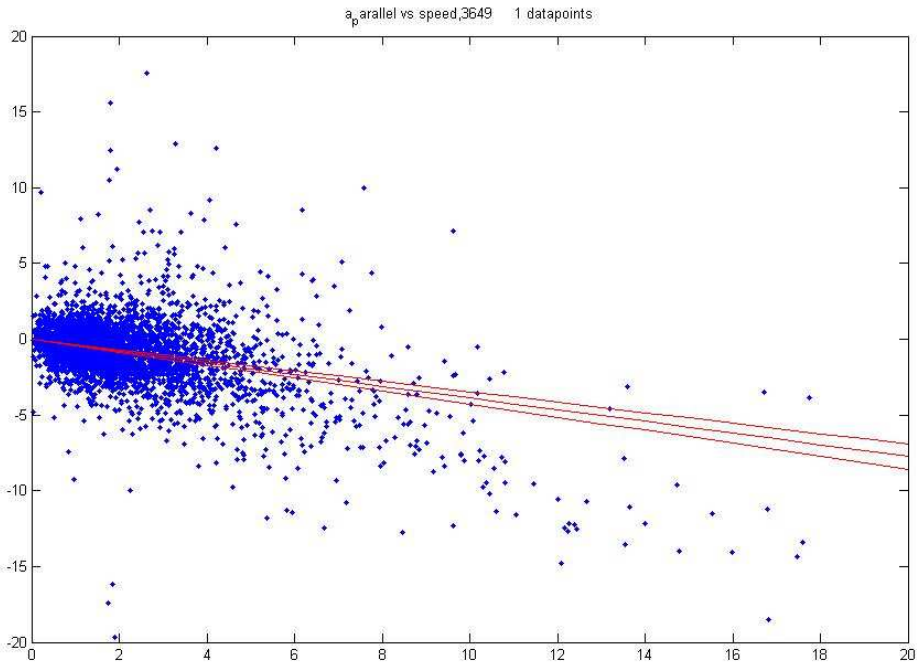

Figure 29. Figure from the MATLAB program showing the acceleration of the cells parallel to their velocity as a function of their velocity for the 16-05 black Si substrate. The red lines are the average with error bars. The units are pixels/frame (x axis) and pixels^2/frame (y axis).

As the accelerations are quite scattered as seen in Figure 28 and Figure 29, the program bins them on the velocity axis and adds error bars as seen in Figure 30 to better show the linear dependence. The figures correspond well with the OU process, although some second order effects may be seen on the graph for the parallel velocity, i.e. another term, $\alpha \cdot v^2(t)$, where α is small, should perhaps be added on the right-hand side of Eq. 17. However, it is only for this particular data set plotted in these graphs that this effect is clearly seen, because it has more than 4000 data points and hence also many data points for the cells at higher velocities where this effect is seen. For the rest of the substrates the number of data points was between 717 and 2330 resulting in larger error bars at those velocities effectively blurring these effects. Hence, for the purpose of this study the graph is assumed to be linear in order to find the persistence time P for the examined substrates.

Next, the program will calculate the standard deviations of these accelerations (Figure 31). According to the OU process the same standard deviation $\sqrt{2D}$ should apply to all velocities resulting in flat and equal graphs if plotted as a function of velocity. However, as seen in Figure 31 this is not the case. The standard deviation of the accelerations perpendicular to the velocity does show a flat behaviour, but the same thing cannot be said about the standard deviation on the accelerations parallel to the velocity. It seems that the noise term on the right-hand side of Eq. 17 is a linear function of the velocity v.

Lastly, the program calculates the velocity autocorrelation $\varphi(t)$ (Eq. 18) and displays it on both a linear plot (Figure 32) and on a semi-log plot (Figure 33) to better be able to judge whether the exponential decay predicted by the OU process actually holds. The

semi-log plot seems fairly linear for the first 5 frames, but more data would be a definite advantage for this plot.

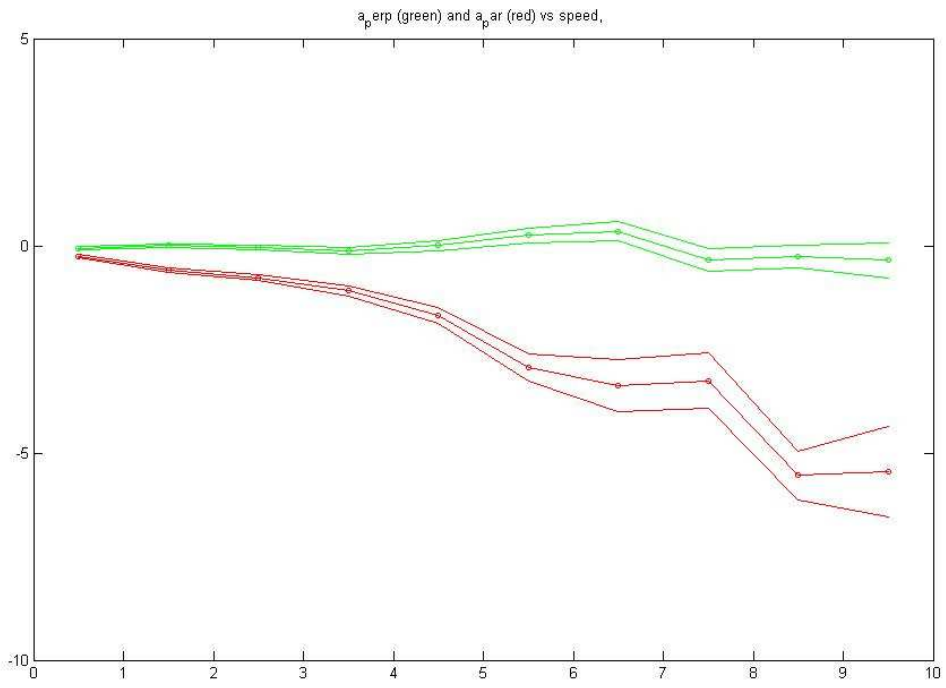

Figure 30. Figure from the MATLAB program showing the binned accelerations of the cells perpendicular (green, top) and parallel (red, bottom) to their velocity as a function of their velocity on the 16-05 substrate. The units are pixels/frame (x axis) and pixels^2/frame (y axis).

As the graphs shown here do not seem different from the graphs produced by the other substrates in this study, i.e. the linearly-dependent standard deviation as a function of velocity and the not exactly linear semi-log plot do not seem unique for this substrate, and as finding a new model will require larger amounts of data than obtained, the OU process will still be used to analyse the substrates. This finding will therefore not be further addressed, but only noted as a finding that should be studied further.

Graphs from all the analyzed substrates can be seen in Appendix C.

Since the data from all the analysed time-lapse movies, which all used the same fibroblast cell type, therefore seems to follow the same motility model in agreement with earlier studies (Selmeczi, Mosler, et al 2005), the surveyed substrates will be characterized by the parameters persistence time *P*, diffusion coefficient *D*, and the expectation value $<v^2>$ representing the velocities of the cells. By Eq. 18 these are correlated by $< v^2 >= \frac{2D}{P}$.

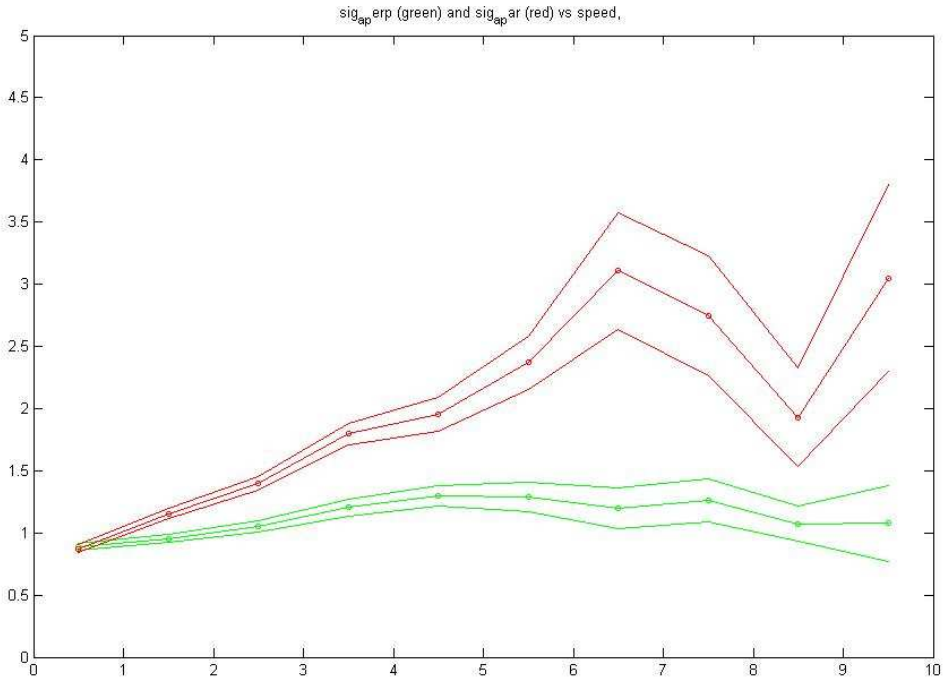

Figure 31. Figure from the MATLAB program showing standard deviation of the accelerations of the cells perpendicular (green, bottom) and parallel (red, top) to their velocity as a function of their velocity on the 16-05 substrate. The units are pixels/frame (x axis) and pixels^2/frame (y axis).

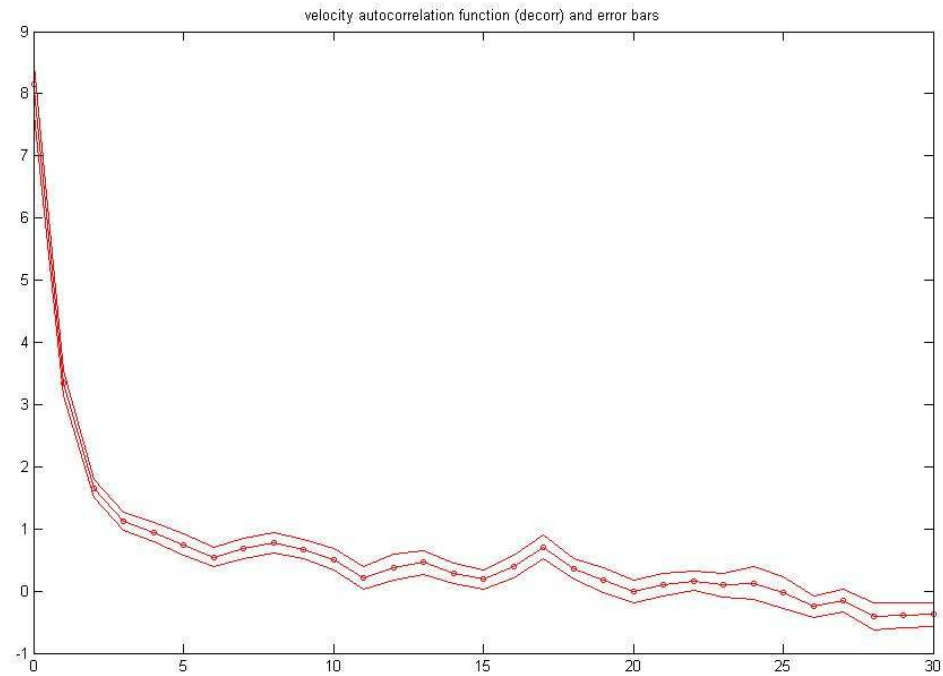

Figure 32. Figure from the MATLAB program showing a linear plot of the autocorrelation function as a function of time on the 16-05 substrate. The units are frames (x axis) and pixels^2/frame^2 (y axis).

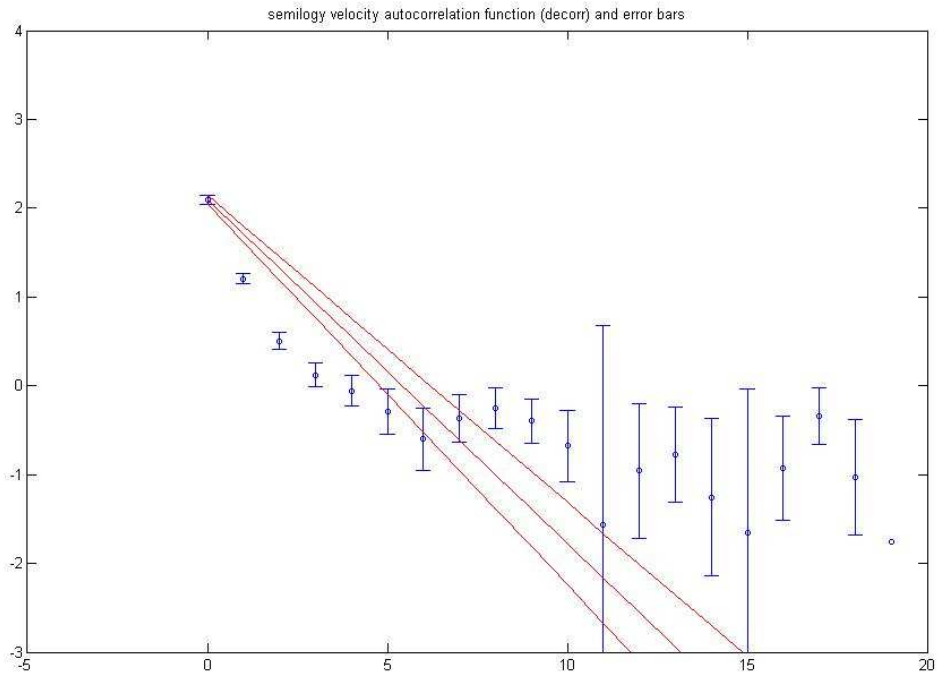

Figure 33. Figure from the MATLAB program showing a semi-log plot of the autocorrelation function as a function of time on the 16-05 substrate. The units are frames (x axis) and ln(pixels^2/frame^2) (y axis).

Table 5. Persistence Time, Diffusion Coefficient, and $<v^2>$ for Different Substrates.				
Substrate (Date)	**Data Points**	***P* [min.]**	***D* [μm^2/min.]**	**$<v^2>$ [μm^2/min.^{2}]**
Si (07092009)	966	5.5±0.7	0.52±0.15	0.38±0.06
Si (21092009)	1272	5.5±0.6	0.32±0.06	0.23±0.02
Glass (07092009)	717	5.9±0.6	0.50±0.12	0.34±0.04
16-05 (21092009)	4026	10±1.1	1.5±0.2	0.58±0.03
15-19 (21092009)	1415	9.6±1.1	1.9±0.5	0.80±0.10
bs17c (21092009)	2330	2.8±0.1	0.09±0.01	0.13±0.01
bs17m (21092009)	1632	5.5±0.5	0.31±0.05	0.23±0.02

All the measured persistence times, diffusion constants and $<v^2>$ are seen in Table 5 and in Figure 34. When comparing the persistence times with the time interval of 4 min. between obtaining images for the time-lapse movie, it can be seen that a shorter interval than 4 min. would have been preferable. However, two things limit the ability to make this interval shorter. For one thing, with a 1-min. interval each time-lapse movie will generate approximately 1 GB of data per day. When doing several time-lapse movies on each of several substrates for many days, this can amount to quite a large amount of data. Furthermore, the speed of the microscope stage also hinders the minimum time interval between obtaining images. The microscope stage took almost 2 min. to obtain images from 15 different places in the chamber, which was a normal amount of images when doing experiments with several substrates at once. If obtaining images with a shorter time interval than 2 min. is needed, fewer substrates or fewer places on each substrate will have to be monitored.

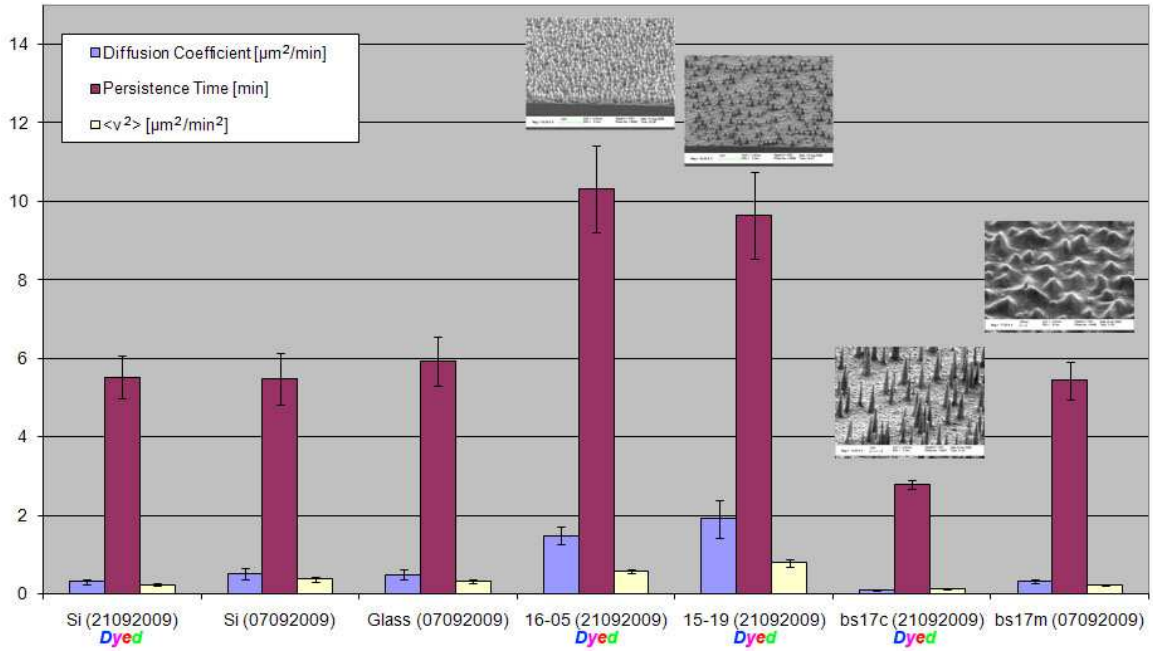

Figure 34. Diffusion coefficient *D*, persistence time *P*, and expectation value of the velocity squared $<v^2>$ for the analysed substrates. A clear difference in all parameters is seen between the substrates with small spikes (16-05, 15-19) and the substrate with large spikes (bs17c). In parentheses are noted the experiment numbers.

The two different measurements on Si are from two different experiments simply to get an idea of reproducibility to check that other factors than the different substrates do not change the cell behaviour in the used setup. The *P* for the two experiments is exactly the same, but the *D* and $<v^2>$ differ a bit, though only the $<v^2>$ differs outside the error bar. If comparing these two measurements to the measurements on the nanostructured substrates, though, it is seen that they are very similar to each other and that things like the dye in the 21092009 experiment and the slightly lower flow rate in the end of the 07092009 experiment have very little influence, if any at all, compared to the influence of the nanostructured substrates. The small difference seen could very well be explained by the few data points obtained from the Si substrate in the 07092009 experiment, as fewer than 1000 data points were on the low side.

Unfortunately not that many data points were obtained and analysed on a glass substrate. More time-lapse movies would have to be analysed to get precise figures for the glass substrate, but time did not allow this. From the data available it does seem, though, that the fibroblast cells migrate alike on Si and glass.

On the single pyramid-like black Si substrate analysed (bs17m) the numbers do not seem to differ much from the flat Si. However, when looking at the black Si with spikes of different sizes things change.

In the prior chapter it was already seen that cells were not able to live on the 15-17 substrate, which had large and dense spikes, and on the bs17c substrate, which had large, but sparse spikes, the migration of the fibroblast cells seemed very confined. This is confirmed by the $<v^2>$, which is about half that of the flat Si. At the same time the *P* measured on the bs17c substrate is also half that of flat Si, while the *D* is less than a third that of flat Si. In other words, the fibroblast cells tend to forget where they

are going, while at the same time doing very little random motion, resulting in very little movement at all.

Taking a look at the black Si with small spikes the opposite trend is seen. Both on the 15-19 substrate (small, sparse spikes) and on the 16-05 substrate (small, dense spikes) the $<v^2>$ is roughly double that of flat Si. At the same time the *P* is also double that of flat Si, while the *D* is at least 3-4 times larger. In other words, the fibroblast cells keep their course a longer time, while also doing more random motion on the black Si substrates with the small spikes (15-19 and 16-05) than on a flat Si substrate, resulting in a higher velocity overall, which was not obvious from just looking at the movies.

Figure 35 shows an overview of the dependence between spike size and pitch and cell velocity and persistence time. The cell persistence time is clearly very dependent on the spike size, while the velocity-dependence is far less pronounced. Of course, this overview is only a representation of the results obtained in this study, e.g. the persistence time will not continue to increase as the spikes get smaller and smaller, since this decrease in spike size would eventually mean the substrate would become a flat Si substrate, which, as measured, has a lower persistence time than the small spikes. Some optimum spike size, and probably also pitch, to get the highest persistence time is probably attainable.

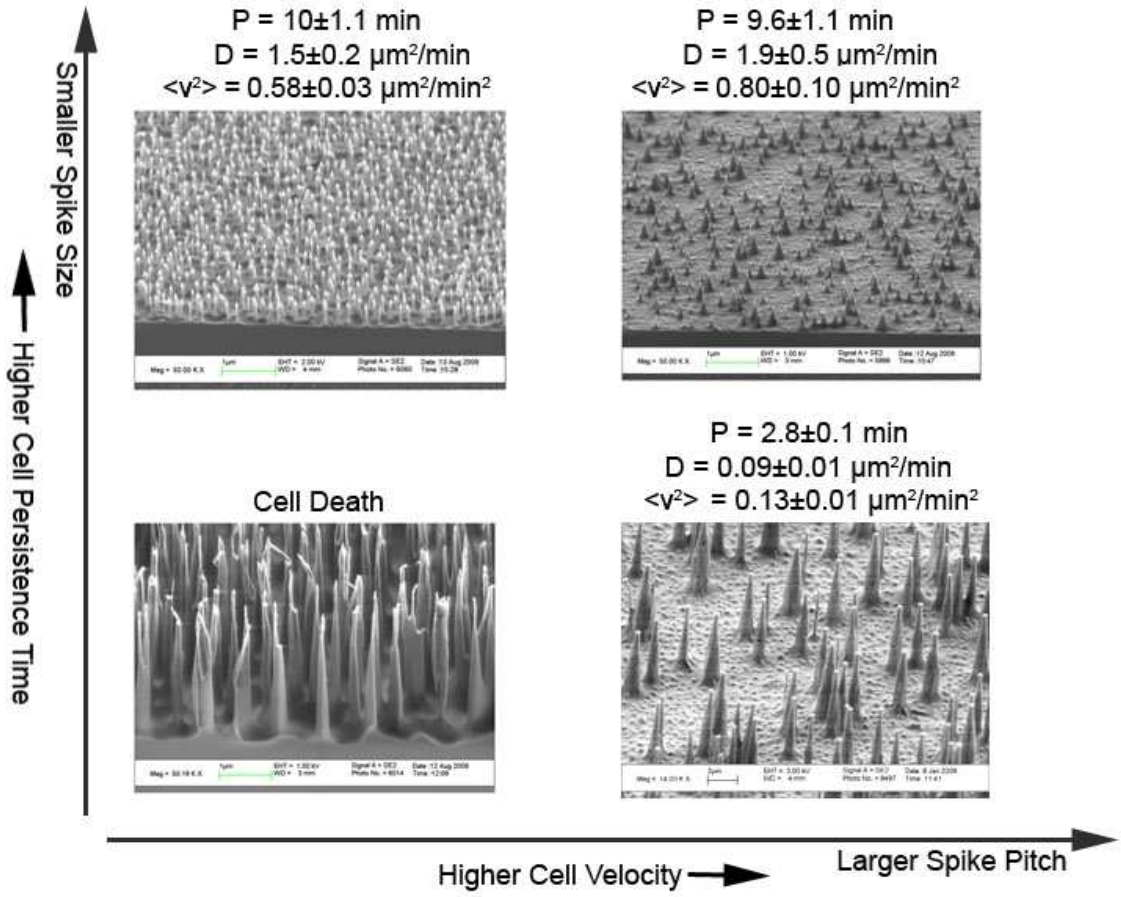

Figure 35. Chart showing the dependence between cell persistence time and velocity and spike size and pitch.

8 Making Nanostructured Substrates using Electron Beam Lithography

In addition to the black Si substrates electron beam lithography (EBL) was used to make finely tuned nanostructured substrates. Due to time-constraints and the time-consuming process of e-beam writing and characterization these were not thoroughly characterized, which is why the data obtained on these substrates are presented in this stand-alone chapter.

In this chapter an introduction to the creation and characterization of EBL substrates will first be made, and then the results obtained on these substrates will be presented in the same fashion as with the black Si substrates with a comparison to a baseline substrate.

8.1 Introduction to Electron Beam Lithography

The e-beam writer used to make finely tuned nanostructured surfaces in these experiments is a FEI Helios 600 NanoLab™ DualBeam belonging to Center for Electron Nanoscopy at DTU. It functions both as an electron beam (e-beam) writer and supports the focused ion beam (FIB) technique. For making the finely-tuned nanostructured surfaces only the e-beam writer capability was be used.

EBL works by scanning electrons across a surface covered in an e-beam resist. When exposed to the scanning electrons the e-beam resist will have cross-links (bonds) broken or created depending on whether the resist is positive or negative. The areas on the resist which have its crosslinks broken (in the case of a positive resist) can later be selectively removed by so-called development in a chemical solution and vice-versa if the resist is negative**.**

EBL enables the making of structures with a resolution in the nanometre range though several things limit its resolution. Among these things are aberration and stability of the electron source, which are related to the e-beam writer and its electron beam, though the resist used plays the largest role, as the incoming electrons will be scattered and give rise to proximity effects. This leads to an exposure of adjacent regions, which should not have been exposed. If two exposed regions are too close, the region between them may get exposed too, and this will limit the pitch resolution as illustrated in Figure 36.

The resist used in this study is poly(methyl methacrylate) (PMMA), which allows for a fairly high resolution at about 10 nm. Furthermore, it allows cell growth, which of course is a crucial feature for these experiments. For development a 3:1 mixture of isopropyl alcohol (IPA) and methyl isobutyl ketone (MIBK) was used for 50 s, followed by 20 s in IPA.

The largest problem with making EBL surfaces for these cell experiments was the slow nature of the e-beam writer. The serial technique makes it a time-consuming process, which means a structure of just 1 mm^2, corresponding to the field of view in the microscope used for the observation of cells in this study, would usually take 15-30 min. of writing time. In the same time one can produce several hundreds if not thousands of mm^2 black Si, which can be used for obtaining several time-lapse movies at once, making it far less dependent on e.g. where the cells settle on the sub-

strate.

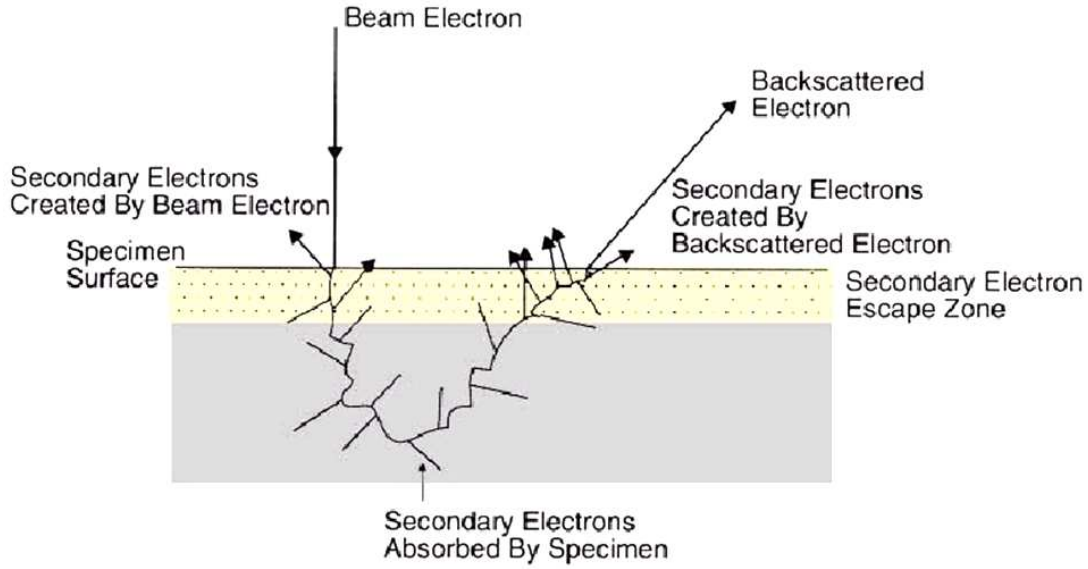

Figure 36. Sketch showing the incident beam's way through the specimen (Bøggild 2008).

8.2 Making the Nanostructured Surfaces

As the e-beam writer was new and not thoroughly characterized, different structures were made and characterized with an atomic force microscope (Veeco CP-II). Atomic force microscopes (AFM) use a sharp tip at the free end of a cantilever to characterize the surface structure. As the tip gets close to the surface it will be exposed to van der Waals forces, which will result in a deflection of the cantilever. In the AFM used this deflection would be measured via a position-sensitive photodiode measuring the displacement of a laser beam reflected on the back of the cantilever as illustrated in Figure 37.

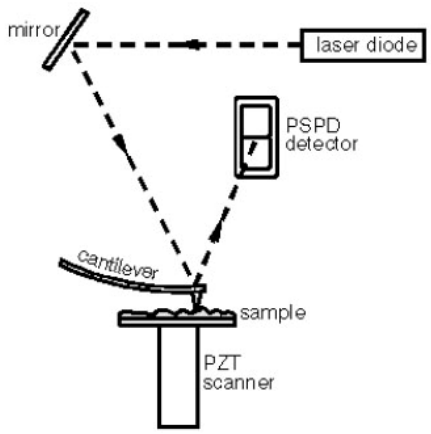

Figure 37. Laser detecting system of the AFM (Howland, R, Lisa Benatar, L. 2000).

Several different modes can be used in order to get the contour of the surface using AFM. In this study the tapping mode or intermittent-contact (IC-AFM) was used. This mode offers the same force sensitivity as contact mode without introducing its dragging forces as it scans the surface, which could potentially damage the surface. At the same time the lateral forces on the tip is reduced, which improves the resolution. In tapping mode the cantilever is set to vibrate just below the eigenfrequency of its free oscillation. As the cantilever is then brought closer to the surface the attractive van der Waals forces shown on Figure 38 will first make the resonance frequency of the cantilever lower, which result in the amplitude getting higher, since the resonance

frequency is now closer to the frequency it is set to vibrate at. The cantilever is then brought even closer to the surface in order to get it to vibrate at the same amplitude as in its free oscillation. This will happen when there are no attractive or repulsive forces, which corresponds to where two axes cross on Figure 38 . A feedback loop is then keeping the amplitude constant, hence keeping the forces on the tip constant and thereby making the tip follow the surface contour. Using the photo-sensitive diodes a 3-dimensional representation of the surface is made with nm resolution as the tip is scanned across the surface.

The resolution of the AFM images is primarily limited by the radius of the end of the tip. The tip used in this study (BudgetSensors ElectriMulti75E-G) had a tip radius of <25 nm, which should provide a resolution high enough for the EBL surfaces made.

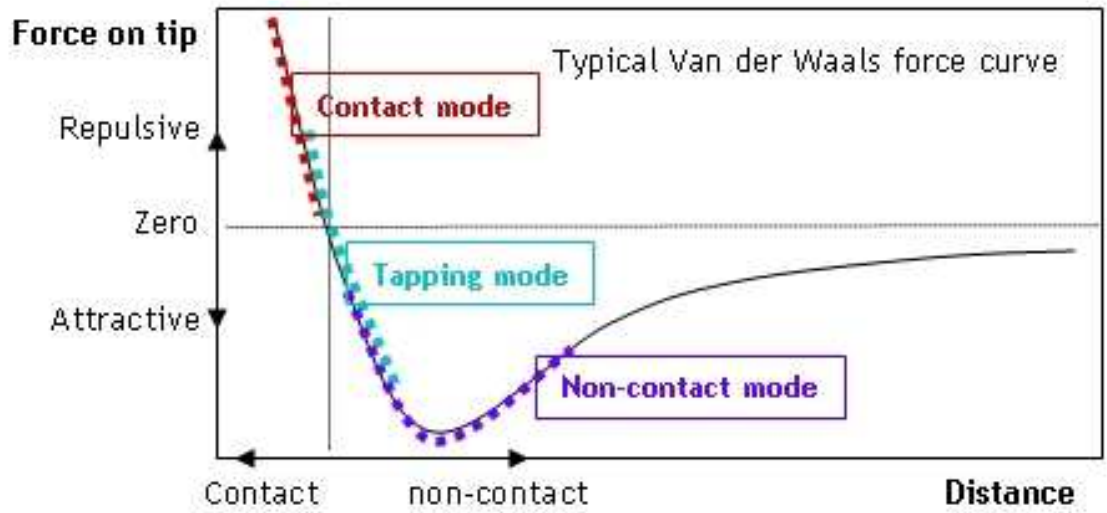

Figure 38. Interatomic forces experienced by the tip of the AFM (AFM, WikiBooks 2009).

8.3 Surface Characterization

A variety of structures was written with the e-beam writer in 200 nm thick PMMA spun on a 2” Si wafer. Some settings did not create any structures in the PMMA at all, some created very sparse structures, and yet some created structures visible by the naked eye.

The settings which seemed to give good results from the first test run are seen in Table 6. All of the described surfaces in this section used these settings. The number of passes differed, and will therefore be stated for each surface made.

Table 6. E-Beam Writer Settings.

Accelerating Voltage	Beam Current	Working Distance	Dwell Time
30 keV	0.17 nA	6 mm	15 µs

Due to the time-consuming process of producing and characterizing each EBL surface made, the surfaces which in the end resulted in time-lapse movies with cells on them were unfortunately not characterized in the AFM prior to the experiments, and the surfaces could not be characterized afterwards due to residue in the form of cells and proteins from the medium adhering to the surface after an experiment lasting several

days. However, by comparing the settings used to produce these surfaces with the settings used to produce the surfaces which were characterized it is possible to get a good idea of how the surface structures of these actually were.

When analyzing the surfaces it was seen that it was not easily possible to make narrow lines with a small pitch in the PMMA surface with the used e-beam writer. Figure 39 shows a surface that was written with a mask consisting of lines with their centres 200 nm apart. The e-beam writer did not seem to expose the dots close enough to actually produce lines of this size, resulting in a surface with lines of dots instead.

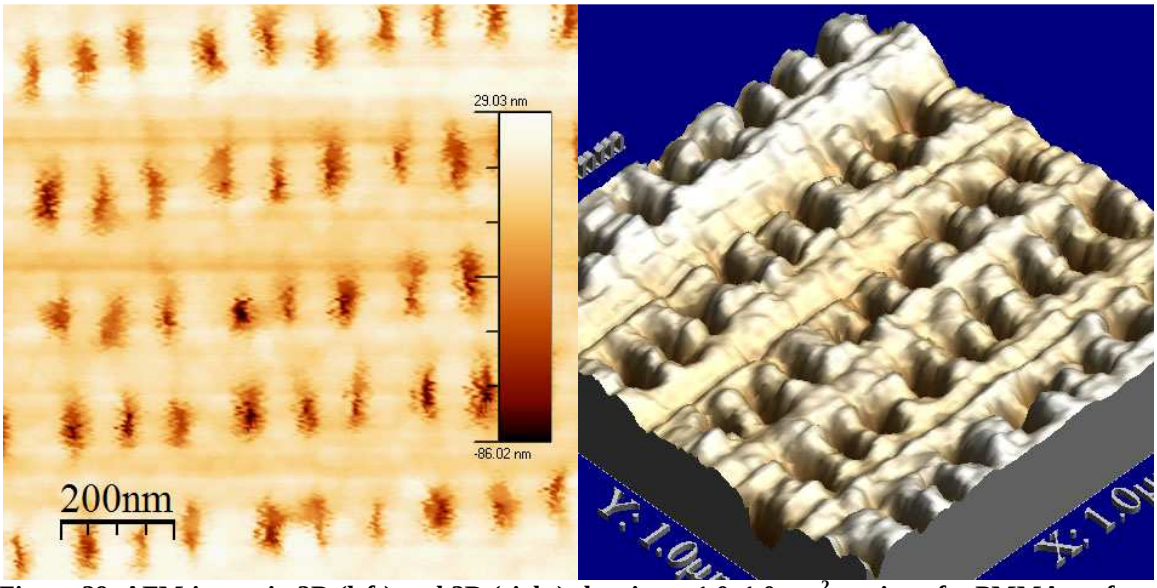

Figure 39. AFM image in 2D (left) and 3D (right) showing a 1.0x1.0 µm^2 section of a PMMA surface, which was produced with a mask consisting of horizontal lines with a pitch of 200 nm.

The mask was an image (BMP) file written so that 1 pixel corresponds to 100 nm on the surface, and from the dotted lines it is seen that each pixel in the mask image corresponds to an elongated dot with a depth of about 100 nm and a size of approximately 30-60 nm (width and height) when writing 2 passes as done on this sample. The elongation seems to stem from the direction of writing as the lines in the mask were orthogonal to the writing direction.

Looking at another sample most of the trends seem to be confirmed. Figure 40 shows a surface made with a mask consisting of dots, again with 1 pixel corresponding to 100 nm. The centres of the dots should be 200 nm apart and this time 5 passes were used for writing. The dots are about 60 nm in diameter but only 80 nm deep. The larger dots are explained by the extra passes, whereas the smaller depth could be explained by the smaller proximity effect on these more sparse dots. No elongation due to writing direction is seen this time, which is maybe avoided due to the higher number of passes causing wider and more circular dots.

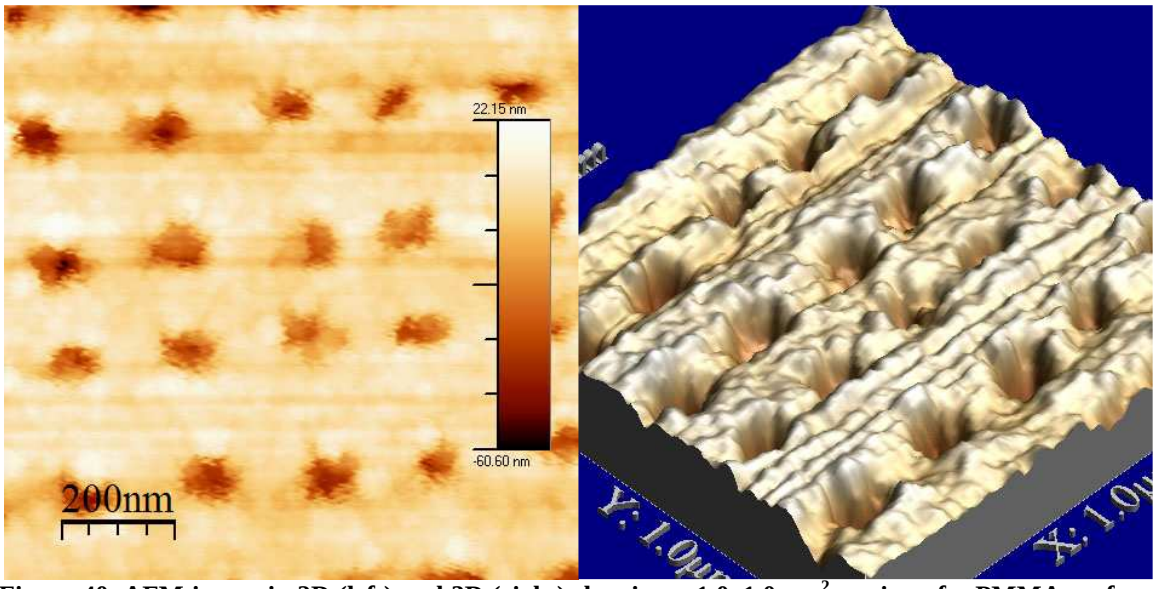

Figure 40. AFM image in 2D (left) and 3D (right) showing a 1.0x1.0 µm^2 section of a PMMA surface, which was produced with a mask consisting of dots with a spacing of 200 nm.

A more thorough examination of the e-beam writer is needed, but these observations should be enough to get an idea of the surface structures of the substrates, which did result in time-lapse movies with cells.

8.4 Electron Beam Structures for Cells

3 EBL structures with fibroblast cells were successfully monitored. Each structure had a size of 500x500 µm^2 and hence only a single time-lapse movie was possible on each of these surfaces. Figure 41 shows the two different masks used to produce these surfaces.

The first structure (EBL1) used the mask shown in Figure 41A, where the white part is exposed and the black part is not. It was written with 1 pas, and 1 pixel corresponds to 100 nm. Each big white dot is 9 pixels in diameter with an edge-edge-pitch of 10 pixels. From the characterized surfaces it is known that these big dots will not be fully exposed, so the surface at the dots will be like the surface shown in Figure 39, but with a pitch of approximately 50 nm in each direction and possibly a bit smaller dots due to the use of only 1 pas. Dots with a diameter of 30-40 nm, a depth of 80-100 nm, and a pitch of 50 nm are therefore assumed to have been written at the big white dots.

The second structure (EBL2) was written with 2 passes using the mask shown in Figure 41B. It is the exact same mask used to produce the surface characterized in Figure 40. The only difference on this structure is then the 2 passes used instead of 5. Hence, the surface will look the same except for the fact that the dots should be a bit smaller. Comparing with Figure 39 it is seen, however, that the dots do not seem to get much smaller when only 2 passes are used. Therefore dots with a diameter of 30-40 nm, a depth of 80 nm, and a pitch of 200 nm are assumed to be on this surface.

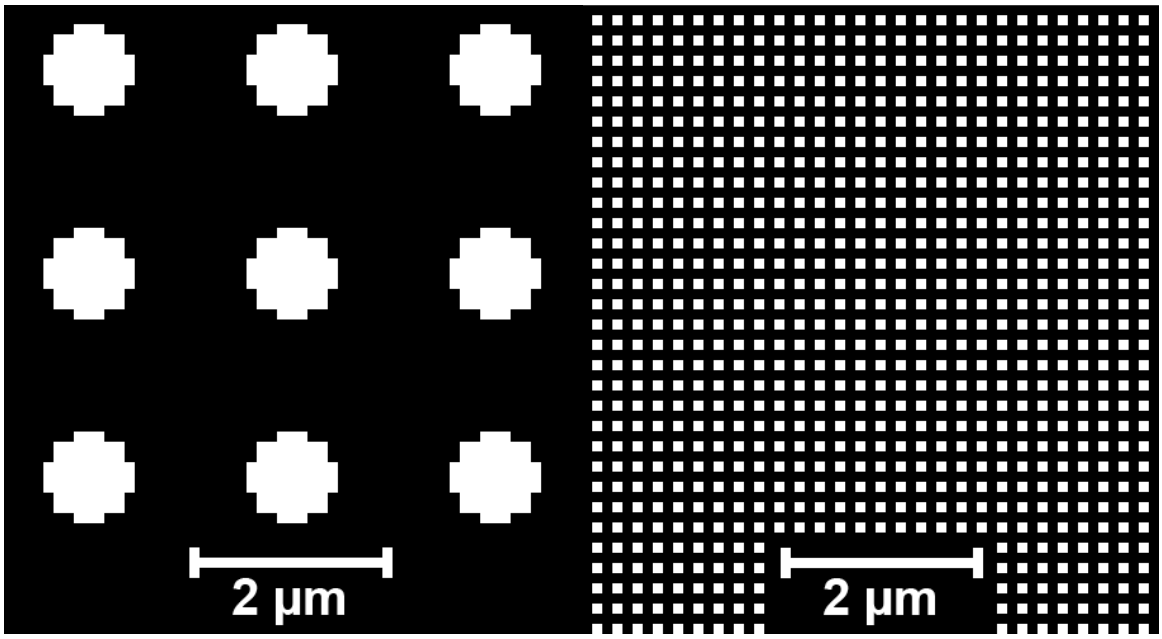

Figure 41A (left) & Figure 41B (right). The 2 different masks used for the 3 EBL structures successfully monitored with cells.

The last structure (EBL3) was written with the same mask as EBL1 (Figure 41A) but with 2 passes instead of 1. The dots written at the big white dots in the mask are therefore assumed to be a bit larger, hence dots with a diameter 40-50 nm, a depth of 80-100 nm and a pitch of 50 nm are assumed to be on this surface.

8.5 Observations on Cell Behaviour on Electron Beam Structures

Like in the previous chapter describing the time-lapse movies in a qualitative manner, the cell survival rate, motility and morphology will be described here. It is again important to bear in mind that the actual density of cells seen on a substrate does not necessarily reflect cell-substrate interaction. Furthermore, all the results obtained on the e-beam structures are from the same experiment, which started 1 day after the cell seeding. From looking at both the survival rate and the time-lapse movies, though, the lag period for the cells did seem to be over.

Flat PMMA

Flat PMMA was used as a baseline to see the interactions of the fibroblast cells with this material. A picture of the cells on this substrate can be seen in Figure 42. Almost every cell adhered to the substrate making elongated and polygonal shapes, often with tails of about 100 µm. The motility seemed good, and the proliferation very high. After a few days most of the substrate was completely covered in cells. This is reflected in the survival rate, which at 183% was the highest encountered. It should be noted that actually 3 time-lapse movies with cells on flat PMMA was obtained. The last movie had a measured survival rate of 272%, which was a lot higher than 181% and 184% measured on the two other time-lapse movies on flat PMMA. This, however, seemed to be largely because of cells migrating into the field of view during the experiment, which is why this measurement has been discarded.

Table 7. Cell Counts and Survival Rates (Experiment 10102009).					
Substrate	Number of Movies	Movie Duration [h]	Total Cell Count, Start	Total Cell Count, End	Survival Rate per Day
PMMA	2	51.13	30	109	183%
EBL1	1	16.00	72	100	164%
EBL2	1	51.13	21	54	156%
EBL3	1	51.13	8	23	164%

The Electron Beam Structures

The time-lapse movies of fibroblast cells on the e-beam structures looked very alike the time-lapse movies obtained on the flat PMMA. Pictures of cells on these substrates can be seen in Figure 42 and Figure 43. Cell adhesion was high with almost exclusively elongated and polygonal shapes and only very few round shapes. The cells also seemed to migrate just as much as on the flat PMMA substrate. The proliferation was again very high, although the survival rates, which were all about 160%, are a bit lower than on flat PMMA. The shorter movie duration seen on EBL1 in Table 7 was caused by the cells being too dense to be counted properly after 16 h.

To sum it up shortly, no obvious qualitative difference could be seen when looking at the time-lapse movies. A possible explanation for this could be the coating that the cell culture medium and the cells themselves make on the substrate. If the thickness of this coating is in the same size range as the dots written in the substrates, the cells are not likely to be affected of the dots. As the dots are significantly smaller than the smallest black Si substrates studies, this cannot be ruled out as a possibility.

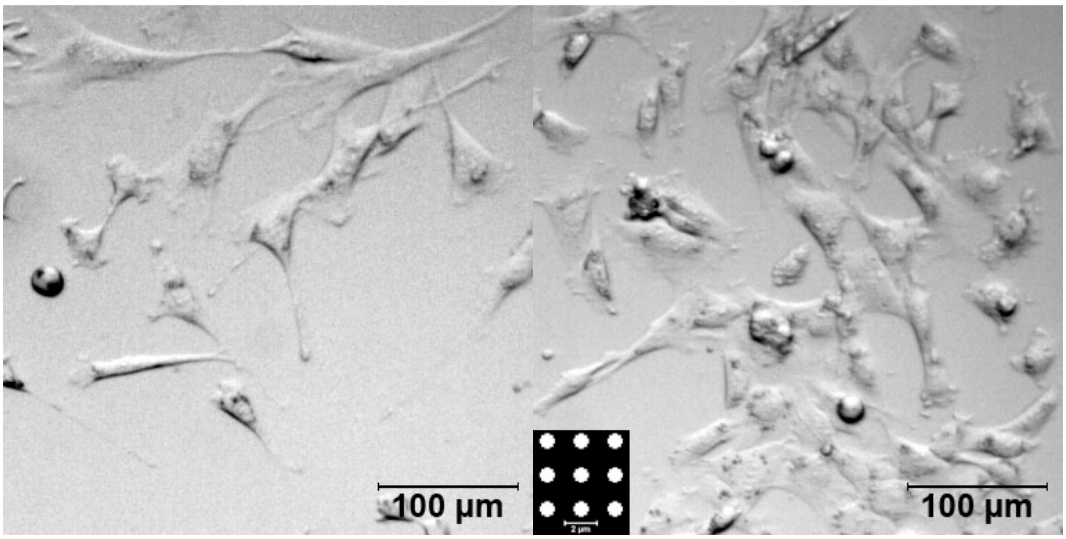

Figure 42. The flat PMMA (left) and EBL1 (right) substrate with cell as seen in the microscope. The e-beam mask used for EBL1 can be seen in the lower left corner.

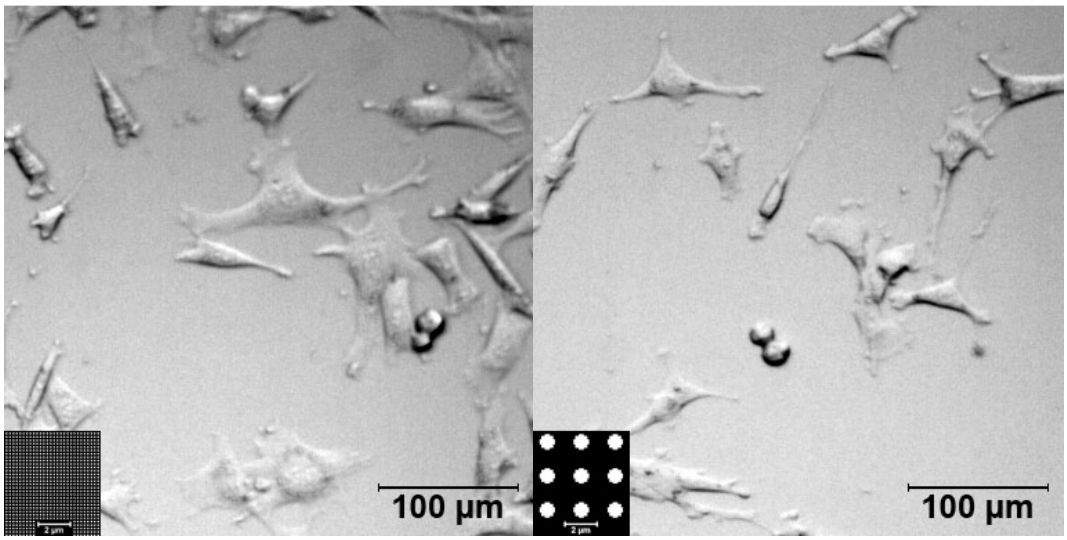

Figure 43. The EBL2 (left) and EBL3 (right) substrate with cell as seen in the microscope. The e-beam mask used for the 2 structures can be seen in the lower left corners of each image.

8.6 Modelling Cell Behaviour

As with the black Si substrates the time-lapse movies of cells on the flat PMMA and on the EBL2 substrate were analysed with the cell tracking MATLAB program made by Cristian Grădinaru. The EBL2 substrate was chosen as the cell density on this substrate was most appropriate for cell tracking, i.e. a decent amount of cells to give enough data points, but at the same time not so many that several cells would be incorrectly tracked as a single cell. The other EBL substrates were not analyzed in this way due to time-constraints. The results from the analysis can be seen in Table 8.

Table 8. Persistence Time, Diffusion Coefficient, and $<v^2>$ for Different Substrates.

Substrate	Data Points	*P* [min.]	*D* [µm^2/min.]	$<v^2>$ [µm^2/min.^{2}]
PMMA	2078	5.4±0.4	0.80±0.13	0.59±0.05
EBL2	2133	5.0±0.3	0.59±0.10	0.48±0.05

There seems to be no clear difference between persistence time, diffusion coefficient, or the expectation value of the velocity squared between flat PMMA and the EBL2 substrate. In other words, the fibroblast cells seem to migrate at the same velocity and with both the same persistence and random motion on the e-beam structure as on the flat PMMA.

However, more experimental data is needed and more diverse structures should be made to get a better picture of the cell interaction with nanosized structures made in PMMA. It should be made clear, though, that making nanostructured surfaces using EBL is a time-consuming and expensive process and is probably not the most well-suited for testing cell behaviour because of these reasons.

9 Conclusion

In this study a temperature stage fitting in a microscope and keeping the temperature steady at 37 °C was made. Several aspects that could cause temperature fluctuations and imprecision of temperature measurements were looked into. Testing showed that the stage was able to keep the temperature within ±0.2 °C for several days.

A cell culture chamber suitable for culturing cells inside the temperature stage was also created. The chamber allowed for a continuous flow rate of cell culture medium without it having a detrimental effect on the cells inside. Furthermore, the chamber allowed for experiments with several substrates at once, and these were easily placed inside the chamber via removal of the detachable lid.

Using the temperature stage and the cell culture chamber a survey on the motility of NIH3T3 fibroblast cells was successfully made on several different nanostructured substrates. The topography size ranges in this study was not directly comparable to that of prior studies. Like in the prior studies, though, a very clear dependence between cell behaviour and topography was seen on some of the substrates.

While the survival rate of fibroblast cells on black Si substrates with pyramid-like structures (bs12c, b12m, bs17m, and bs17e) seemed lower than that of flat Si, no clear difference in persistence time, diffusion coefficient, or velocity of the cells could be seen for the one substrate mathematically analysed.

On the black Si substrates with spikes a very clear dependence on the size of these spikes was seen. On dense large spikes (15-17), which had a height and a diameter of 1.5 µm and 200 nm, respectively, and a pitch of less than 1 µm, the fibroblast cells were not able to adhere.

On more sparse large spikes (bs17c), with a height and diameter of 6.0 µm and 1.2 µm, respectively, and a pitch of about 3 µm, the fibroblast cells were able to adhere, but the motility was clearly affected, as the migration was very confined. This was also confirmed by mathematical analysis of the cell trajectories, which showed that the persistence time, diffusion coefficient and velocity of the fibroblast cells on this substrate was significantly lower than on a flat Si substrate.

On black Si with small spikes the opposite trend was seen. Both of these surveyed substrates had spikes with a height of approximately 300 nm and a diameter of approximately 100 nm, whereas the pitch was 200 nm (16-05) and 300 nm (15-19), respectively. Though the survival rate on both substrates seemed a bit lower than on the flat Si substrate, a clear change in motility was seen when the cell trajectories were analysed mathematically. Persistence time, diffusion coefficient, and velocity increased dramatically on both substrates compared to flat Si. Persistence time and diffusion coefficient were very alike for both of these black Si substrates, while the fibroblast cells on the substrate with more sparse spikes seemed to have a higher velocity. Both of these nanostructures hold potential for making biomaterials more suitable for cells.

The behaviour of fibroblast cells on dots in PMMA made by an e-beam writer was also surveyed. The dots were all about 30-50 nm in diameter with a depth of 80-100 nm, while pitches of 50 nm and 200 nm were tested. None of these nanostructured substrates did seem to have a significant impact on the cell motility or survival rate compared to a flat PMMA substrate. An explanation for this could be the coating caused by the medium and the cells, which could potentially cover the small dots making them invisible to the cells.

Furthermore, it should be noted that the Ornstein-Uhlenbeck process, which is the standard mathematical model used today for cell migration and also used in this study, does not seem to hold according to the experimental data obtained in this study. More experimental data then was obtained in the experiments carried out in this study is needed, though, to be able to find a better model.

9.1 Future Work

This study has investigated the migration of cells, but not how the migration takes place on the cellular and sub-cellular level. What causes the difference in motility across the different nanostructured substrates might be of interest for further study. It seems that spikes with features in the sub-500-nm-range enhance motility of fibroblast cells, perhaps due to easier formation and retraction of focal adhesion sites on such spikes. Spikes in the µm-range, however, seem to decrease the migration of fibroblast cells significantly. It would be interesting to study how the actual adhesion on the 15-19, 16-05, and bs17c substrate takes place and establish whether the cells are pierced by the large spikes on the bs17c substrate or simply migrate on top of them.

Black Si with spike sizes in between those used in this study might also be interesting to test. Since small spikes (<500 nm) seem to enhance motility and tall spikes (>1 µm) seem to decrease motility, it remains an open question how black Si with spike sizes in between will affect cell motility.

When performing experiments with these fibroblast cells it would also be advantageous to record frames more frequently than every 4 min. as in this study, as it was seen from the data analysis that data with a higher time resolution would be preferable. Especially in the case of the substrate on which cells migrate slowly (bs17c), where the persistence time was less than 3 min., frames obtained with 1 min. intervals would allow for a much better fitting of the data. Such time resolution could possibly also provide sufficient data to make a better model for cell motility.

For the observations of proliferation and survival rate longer continuous time-lapse movies providing at least one week of surveillance would be preferable. This would allow for better study of the lag period and the period of exponential growth until the cells become confluent, which could be interesting to study, since it is very possible that the nanostructures affect the cell behaviour also in this regard. This, however, would require either a very large hard drive or some manual interactions if it is to be combined with time-lapse movies with a higher time resolution.

10 References

Ozturk, S. S.,Wei-Shou H. (2006). “Cell culture technology for pharmaceutical and cell-based therapies.” Taylor & Francis Group.

Grădinaru, C., Lopacinska, J. M., Mølhave, K., Flyvbjerg, H. (Aug 2009). “Deliverable Report T9.1, D9.1, FP7.” Nanotech - Department of Micro- and Nanotechnology, Technical University of Denmark.

Stangegaard, M. (Dec 2005) “A biocompatible micro cell culture chamber (μCCC) for culturing and on-line monitoring of Eukaryotic cells,” PhD Thesis, Microarray Technology, Nanotech - Department of Micro- and Nanotechnology, Technical University of Denmark.

Masters, J. R.W. (Aug 2000). “Animal Cell Culture: A Practical Approach”, Third Edition. Oxford University Print.

Bøggild, P. (Jun 2008). Nanolithography course, lecture notes, “Day 9 (EBL 4)”, Kongens Lyngby, Nanotech - Department of Micro- and Nanotechnology, Technical University of Denmark.

Selmeczi, D., Mosler, S., Hagedorn, P. H., Larsen, N. B., Flyvbjerg, H. (2005). “Cell Motility as Persistent Random Motion: Theories from Experiments.” Biophysical Journal **89**(2): 912-931

Selmeczi, D., Li, L., Pedersen, L. I. I., et al. (2008). ” Cell motility as random motion: A review.” European Physical Journal - Special Topics **157**: 1.

Brammer, K. S., S. H. Oh, et al. (2008). "Enhanced cellular mobility guided by TiO2 nanotube surfaces." Nano Letters **8**(3): 786-793.

Kim, D. H., K. Han, et al. (2009). "Mechanosensitivity of fibroblast cell shape and movement to anisotropic substratum topography gradients." Biomaterials **30**(29): 5433-5444.

Park, J., S. Bauer, et al. (2007). "Nanosize and vitality: TiO2 nanotube diameter directs cell fate." Nano Letters **7**(6): 1686-1691.

Aoki, N., Yokoyama, A., et al. (2006). “Strikingly Extended Morphology of Cells Grown on Carbon Nanotubes.” Chemistry Letters **35**(5): 508.

Ornstein, L. S. and H. C. Burger (1919). “On the theory of the brownian motion.” Proceedings Koninklijke Akademie van Wetenschappen te Amsterdam **21**: 922-931.

Howland, R, Lisa Benatar, L. (2000). “A Practical Guide to Scanning Probe Microscopy.” ThermoMicroscopes.

AFM, Nanotechnology, WikiBooks (Oct 2009).

Wikipedia (Oct 2009), Conduction (heat),
http://en.wikipedia.org/wiki/Fourier%27s_Law

Wikipedia (Oct 2009), Heat transfer - Newton's law of cooling,
http://en.wikipedia.org/wiki/Heat_transfer#Newton.27s_law_of_cooling

Wikipedia (Oct 2009), Heat transfer coefficient,
http://en.wikipedia.org/wiki/Heat_transfer_coefficient

Wikipedia (Oct 2009), Heat transfer coefficient - Heat transfer coefficient of pipe wall,
http://en.wikipedia.org/wiki/Heat_transfer_coefficient#Heat_transfer_coefficient_of_pipe_wall

Wikipedia (Oct 2009), Heat transfer coefficient - Combining heat transfer coefficients,
http://en.wikipedia.org/wiki/Heat_transfer_coefficient#Combining_heat_transfer_coefficients

The Engineering ToolBox (Oct 2009), Thermal Conductivity of some common Materials, http://www.engineeringtoolbox.com/thermal-conductivity-d_429.html

Appendix A - Library of Black Si Surfaces

Wafer overview

A series of SEM pictures have been taken for each wafer. In this document the best pictures is shown. The pictures have been taken from approximately the same areas on each wafer. These areas are the Center, the Middle and the Edge of the wafer, where it is important to note that the Middle is between the Center and the Edge of the wafer.

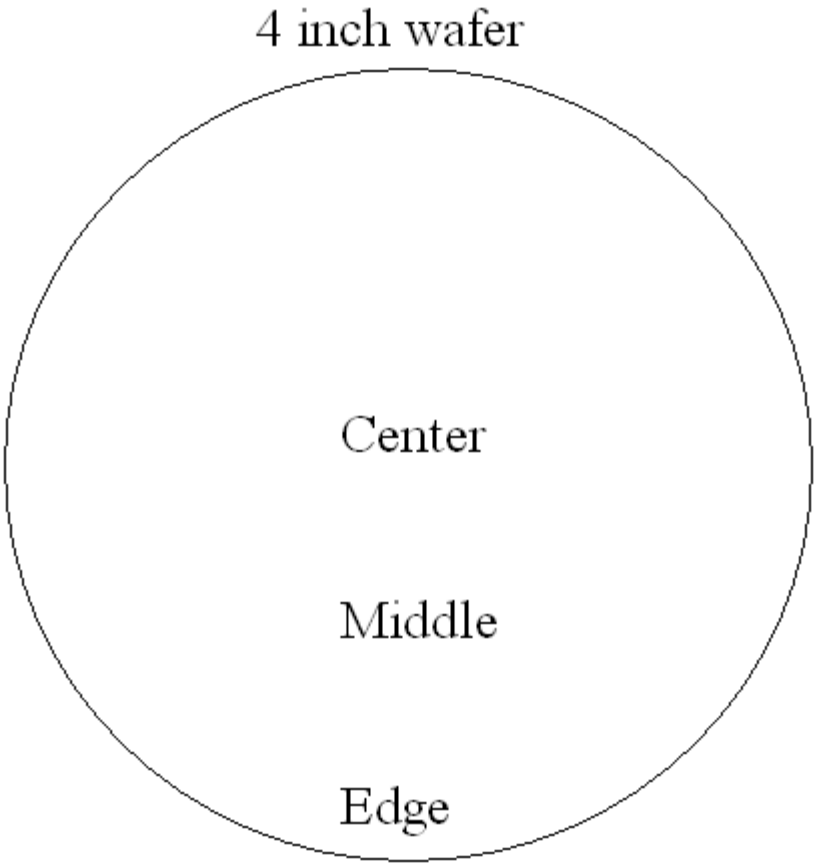

The pictures are shown in tables, where each page consists of one table with SEM pictures from one wafer. To the left of the table are shown the pictures from the Center of the wafer, in the middle are the pictures from the Middle and to the right are shown the pictures from the Edge of the wafer. At the top of the table are shown overview pictures, where the viewing angle is 0 degrees, the angle between the wafer and the camera was 0 degrees. Below are pictures with viewing angles of 45 degrees with zooms of 14k, 35k and 77k. Some pictures are missing because it was deemed unnecessary to spend time taking the pictures either because the structures on the sample were too large or too small in comparison to the zoom. As can be seen there are a lot of dirt and residue on some samples which originates from the etching processes. Wafer 14 was rinsed to try to remove some of the residue which can be seen on the 14skyl table. By comparing the pictures in table 14 with those on table 14skyl it can be seen that most of the dirt has been removed. However this was only done on wafer 14 because of time constraints. In the future it would be wise to rinse

all the samples before putting them into the SEM. This would make it easier to see the etched surfaces in the SEM on some samples.

Centre 09 Middle 09 Edge

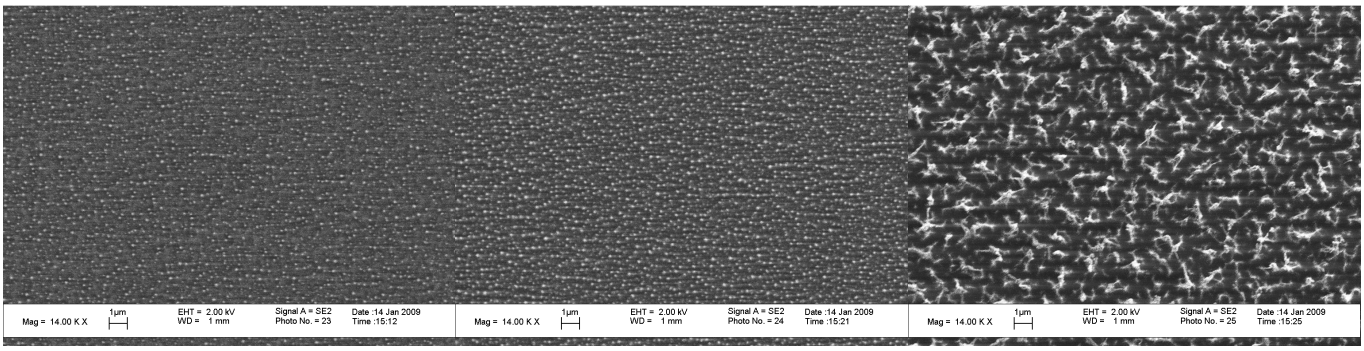

14k x zoom, no tilt (0 degrees)

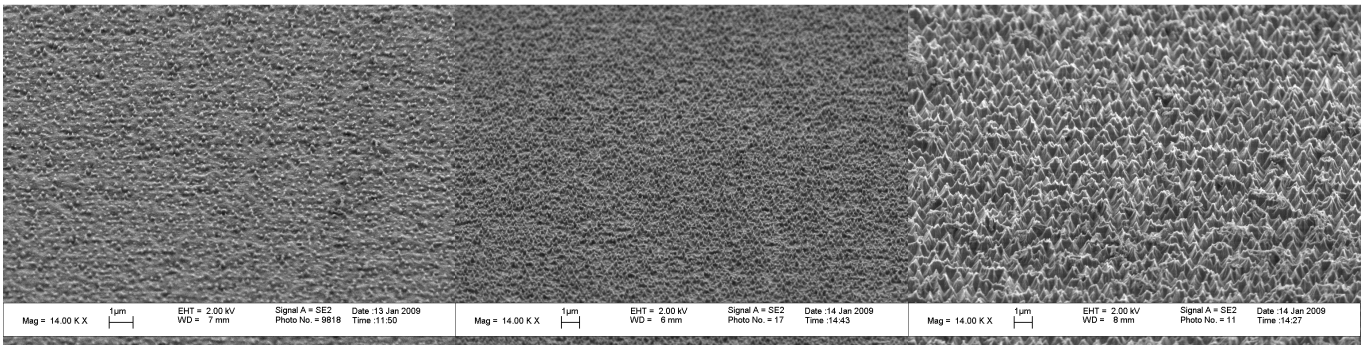

14k x zoom, 45 degrees tilt

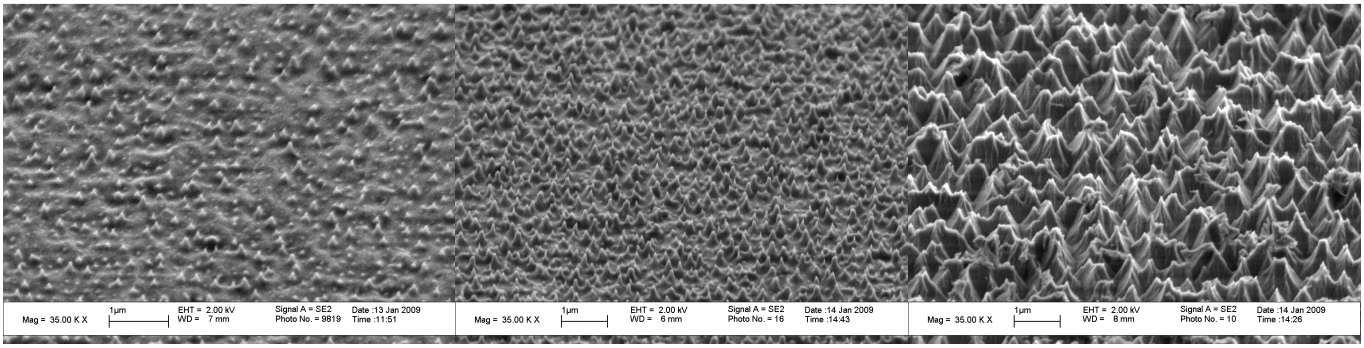

35k x zoom, 45 degrees tilt

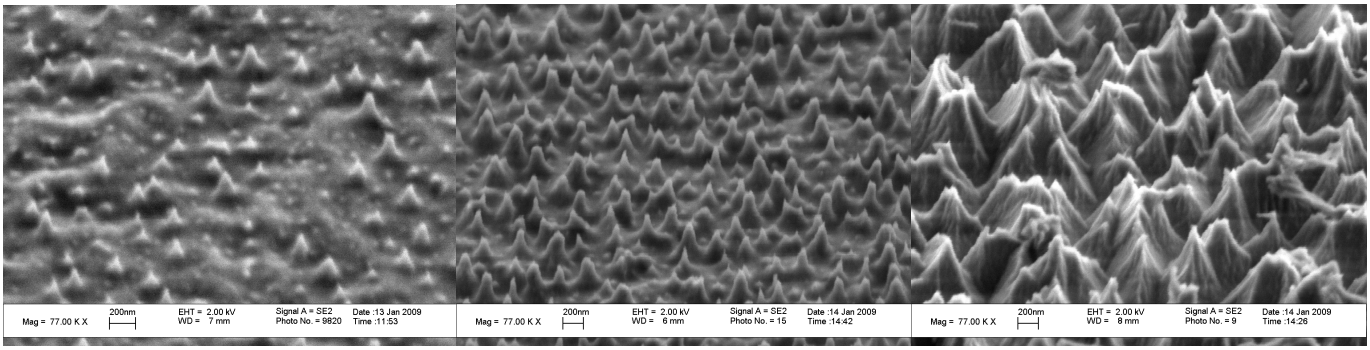

77k x zoom, 45 degrees tilt

Coil Power [W]	Process time [min]	Pressure [mTorr]	SF6 flow [sccm]	O2 flow [sccm]	Platen power [W]	Temp [ºC]
0	08:00	85	80	80	200	-10

Centre	10	Middle	10	Edge

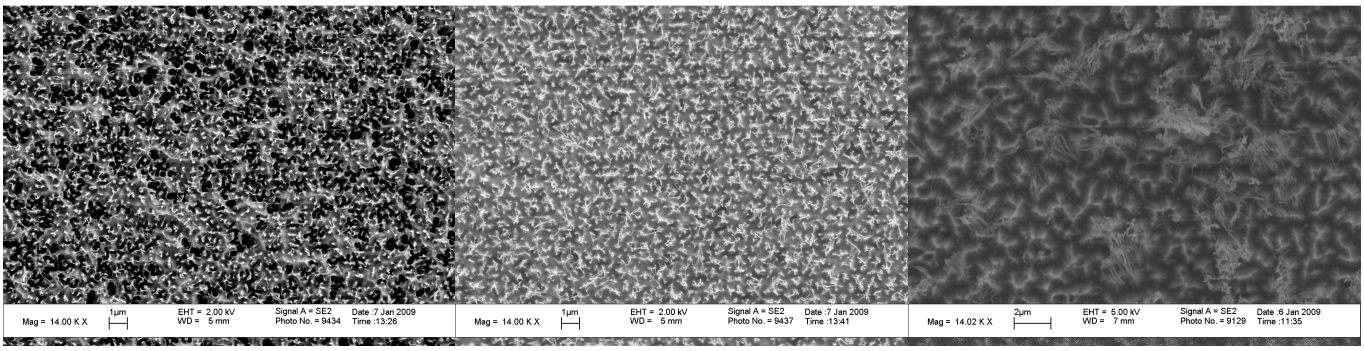

14k x zoom, no tilt (0 degrees)

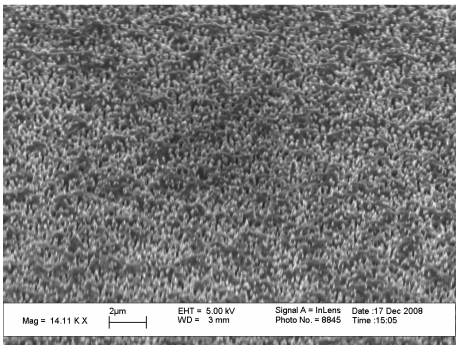

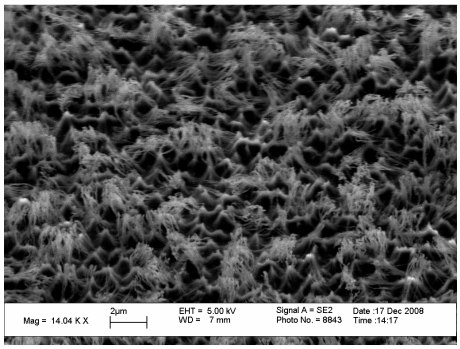

14k x zoom, 45 degrees tilt

35k x zoom, 45 degrees tilt

77k x zoom, 45 degrees tilt

Coil Power [W]	Process time [min]	Pressure [mTorr]	SF6 flow [sccm]	O2 flow [sccm]	Platen power [W]	Temp [ºC]
0	08:00	85	80	80	300	-10

Centre	11	Middle	11	Edge

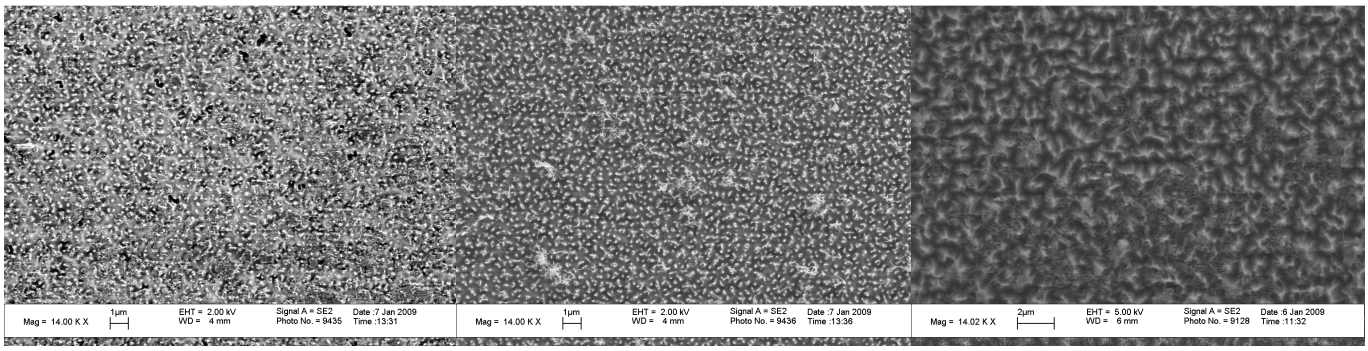

14k x zoom, no tilt (0 degrees)

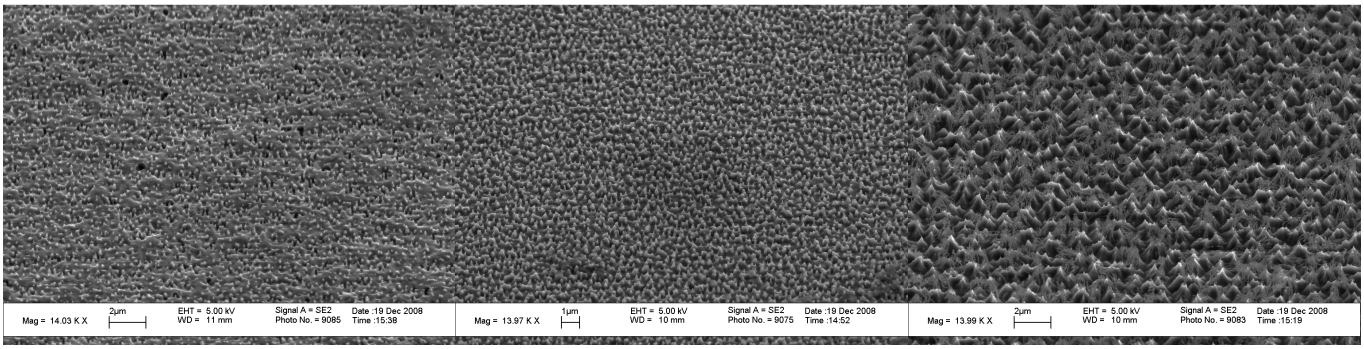

14k x zoom, 45 degrees tilt

35k x zoom, 45 degrees tilt

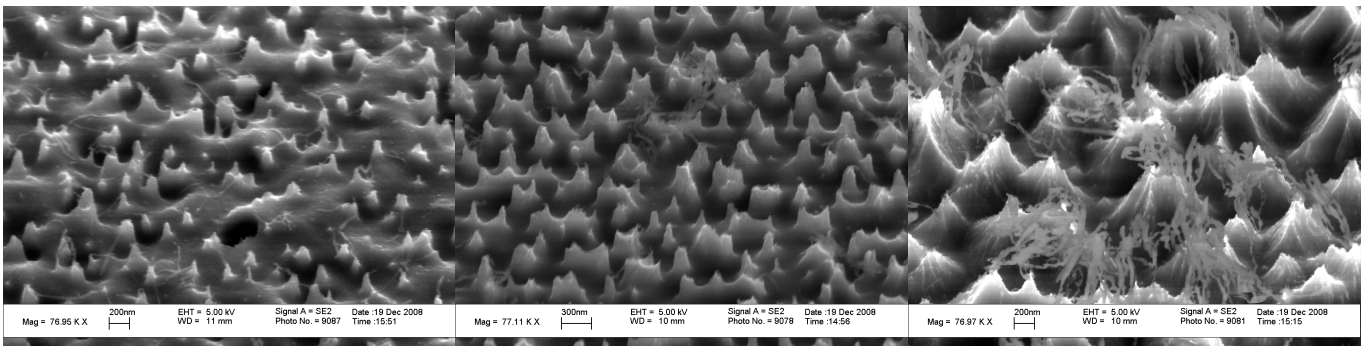

77k x zoom, 45 degrees tilt

Coil Power [W]	Process time [min]	Pressure [mTorr]	SF6 flow [sccm]	O2 flow [sccm]	Platen power [W]	Temp [ºC]
0	08:00	85	80	80	250	-10

Centre	12	Middle	12	Edge

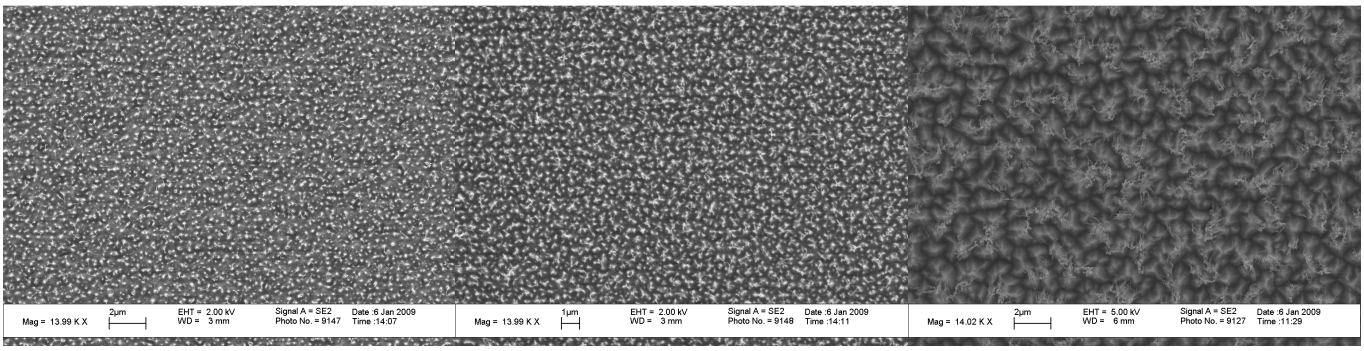

14k x zoom, no tilt (0 degrees)

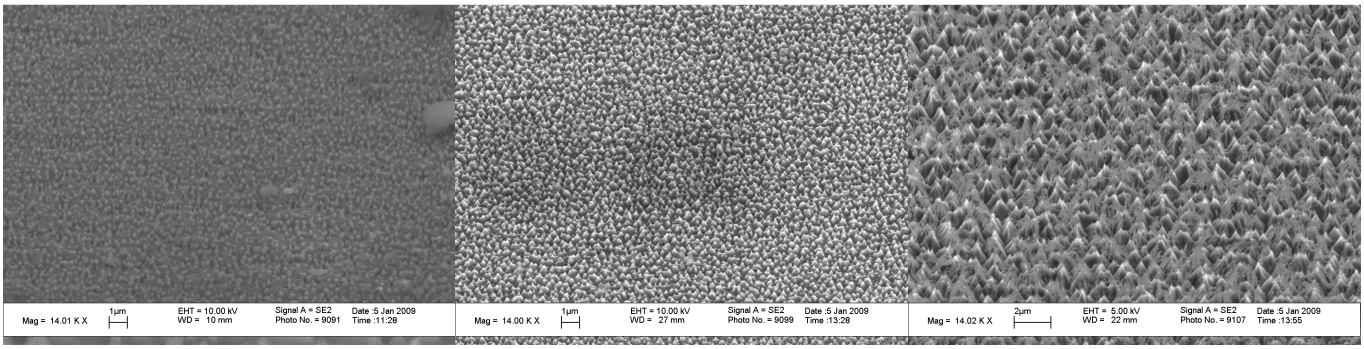

14k x zoom, 45 degrees tilt

35k x zoom, 45 degrees tilt

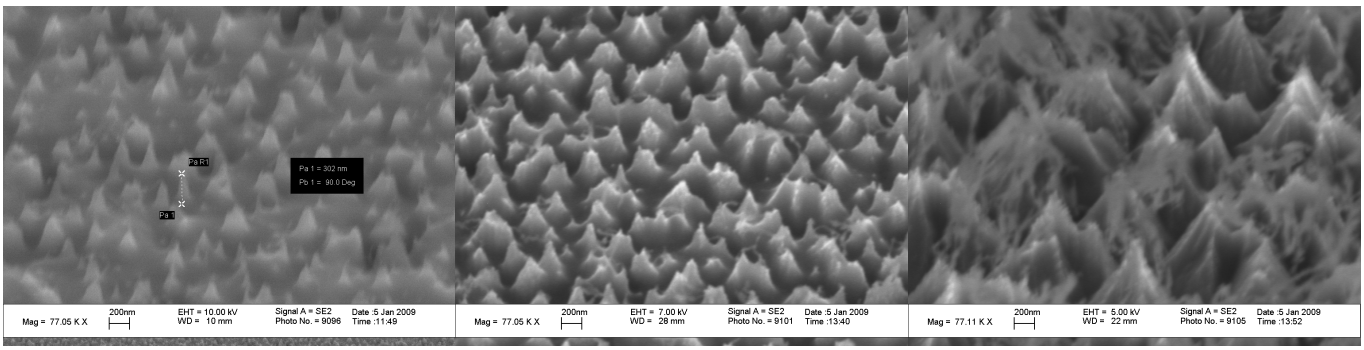

77k x zoom, 45 degrees tilt

Coil Power [W]	Process time [min]	Pressure [mTorr]	SF6 flow [sccm]	O2 flow [sccm]	Platen power [W]	Temp [ºC]
0	12:00	85	80	80	200	-10

Centre	13	Middle	13	Edge

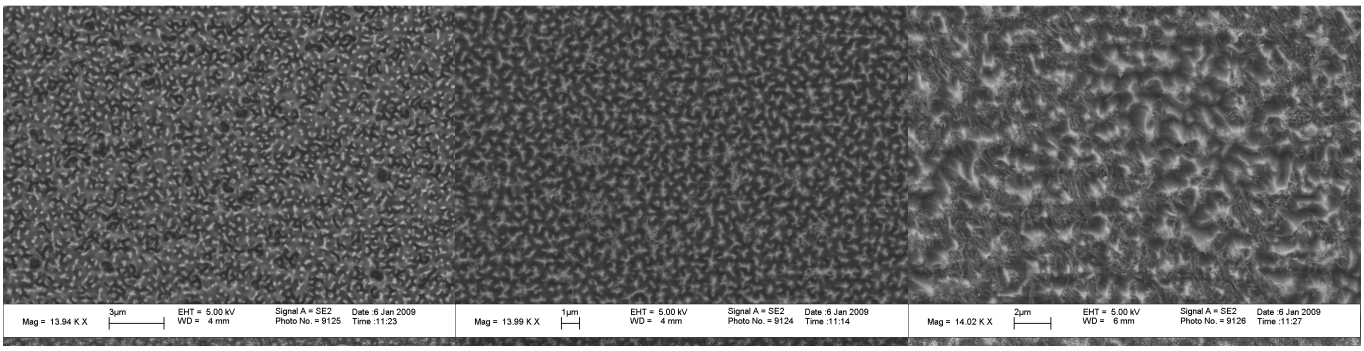

14k x zoom, no tilt (0 degrees)

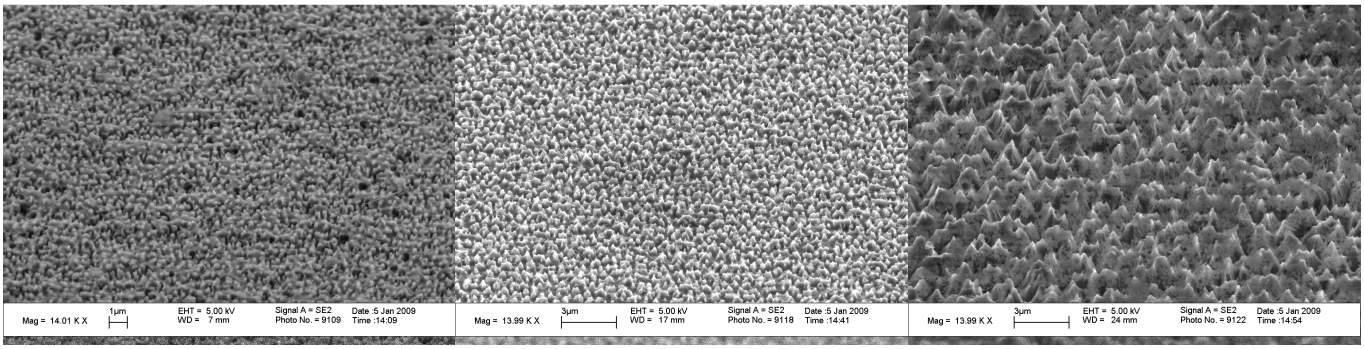

14k x zoom, 45 degrees tilt

35k x zoom, 45 degrees tilt

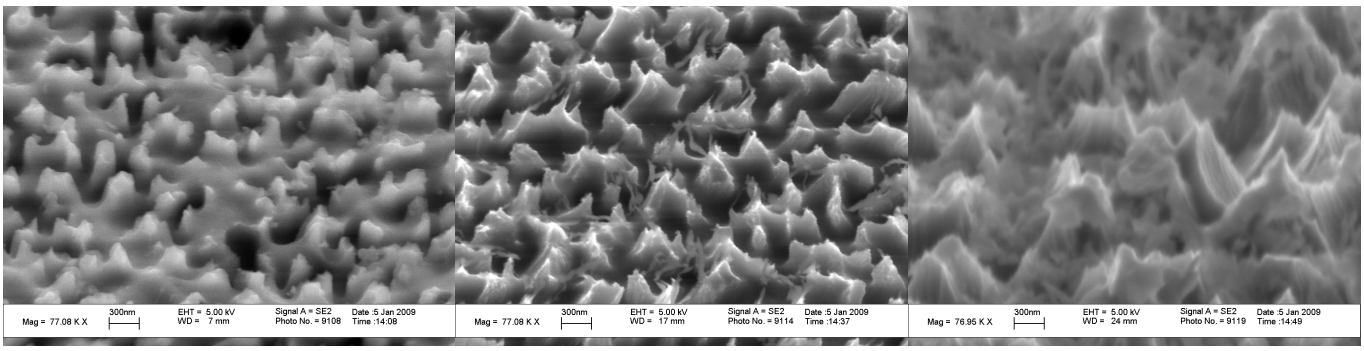

77k x zoom, 45 degrees tilt

Coil Power [W]	Process time [min]	Pressure [mTorr]	SF6 flow [sccm]	O2 flow [sccm]	Platen power [W]	Temp [ºC]
0	12:00	85	80	80	250	-10

Centre	14	Middle	14	Edge

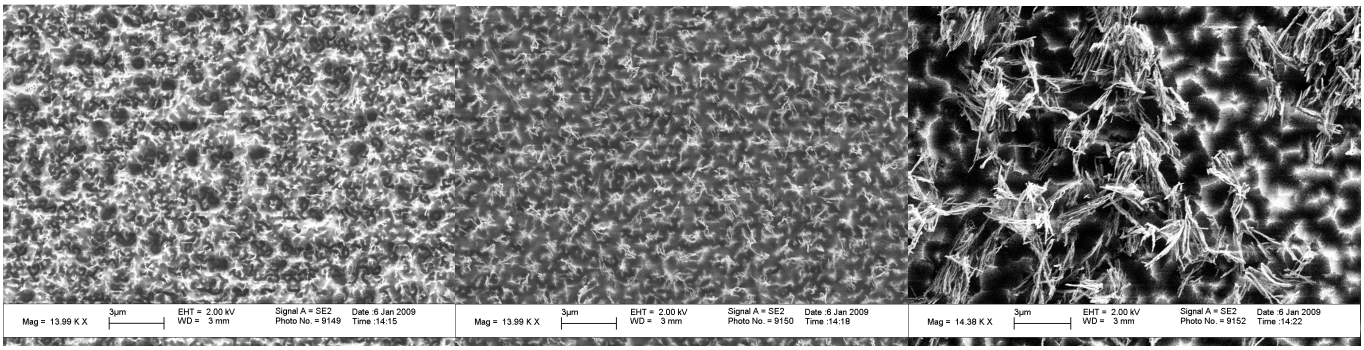

14k x zoom, no tilt (0 degrees)

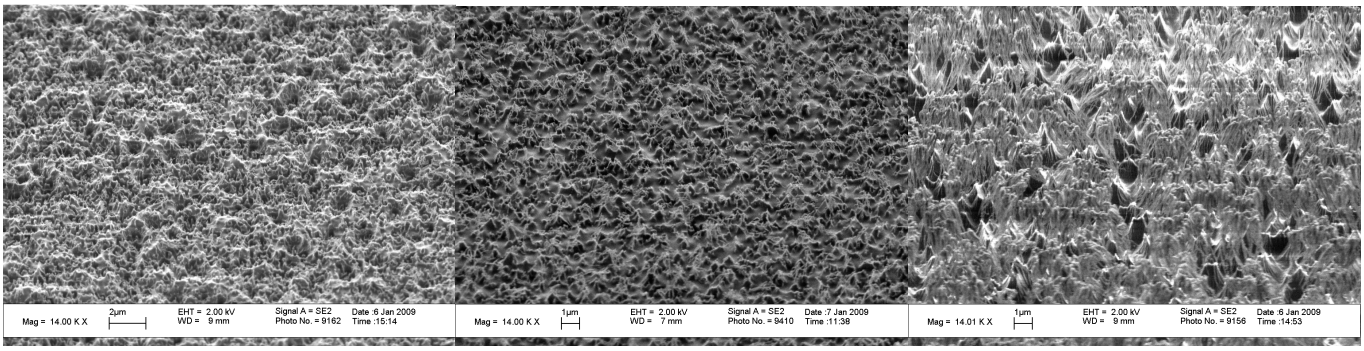

14k x zoom, 45 degrees tilt

35k x zoom, 45 degrees tilt

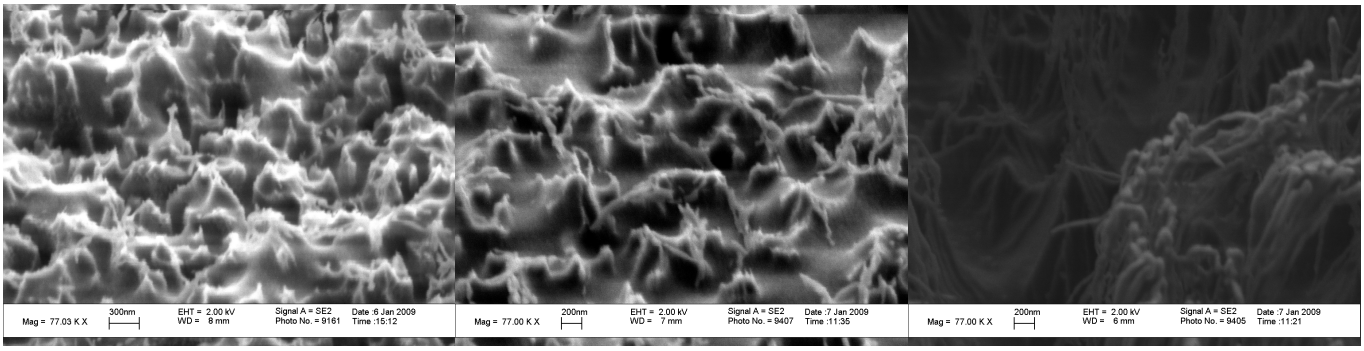

77k x zoom, 45 degrees tilt

Coil Power [W]	Process time [min]	Pressure [mTorr]	SF6 flow [sccm]	O2 flow [sccm]	Platen power [W]	Temp [ºC]
0	12:00	85	80	80	300	-10

Centre 14 rinsed Middle 14 rinsed Edge

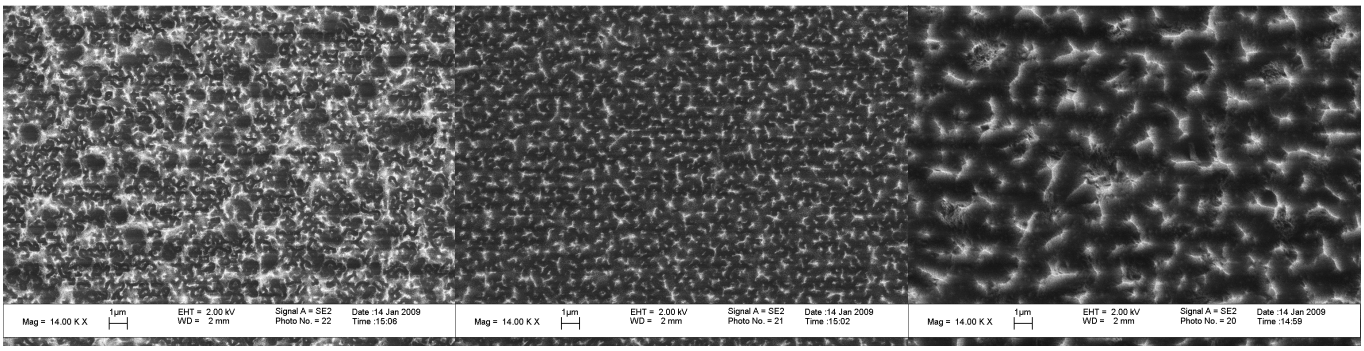

14k x zoom, no tilt (0 degrees)

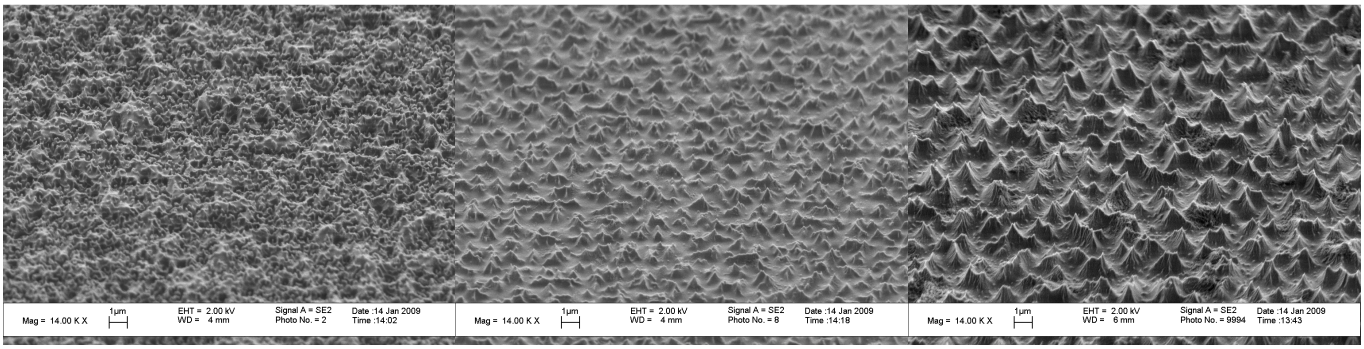

14k x zoom, 45 degrees tilt

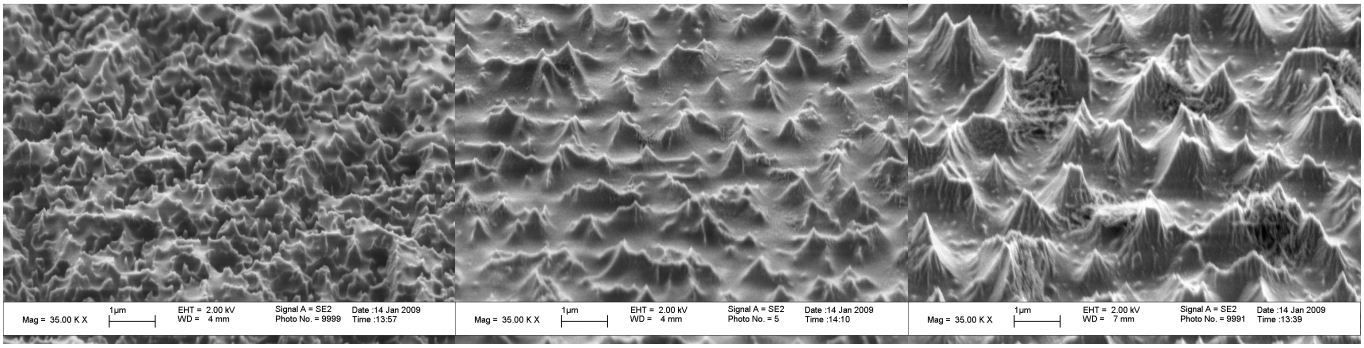

35k x zoom, 45 degrees tilt

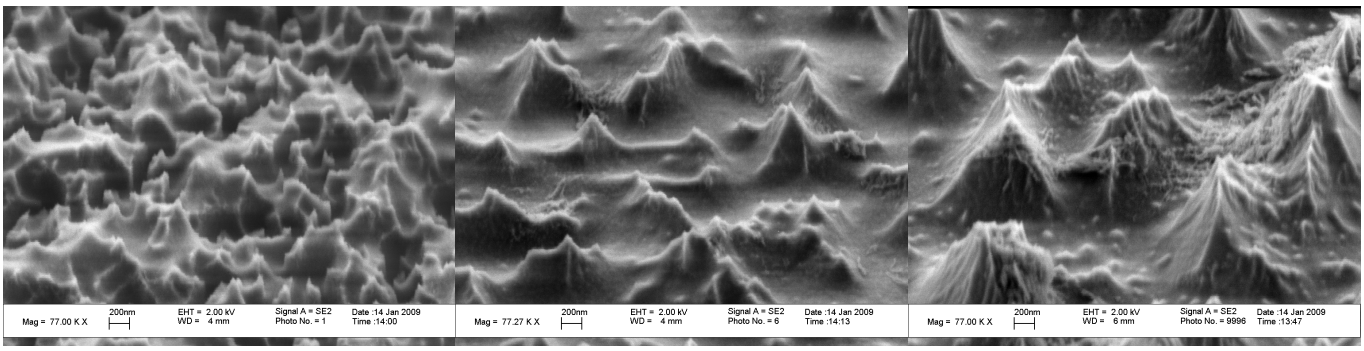

77k x zoom, 45 degrees tilt

Coil Power [W]	Process time [min]	Pressure [mTorr]	SF6 flow [sccm]	O2 flow [sccm]	Platen power [W]	Temp [ºC]
0	12:00	85	80	80	300	-10

Centre	15	Middle	15	Edge

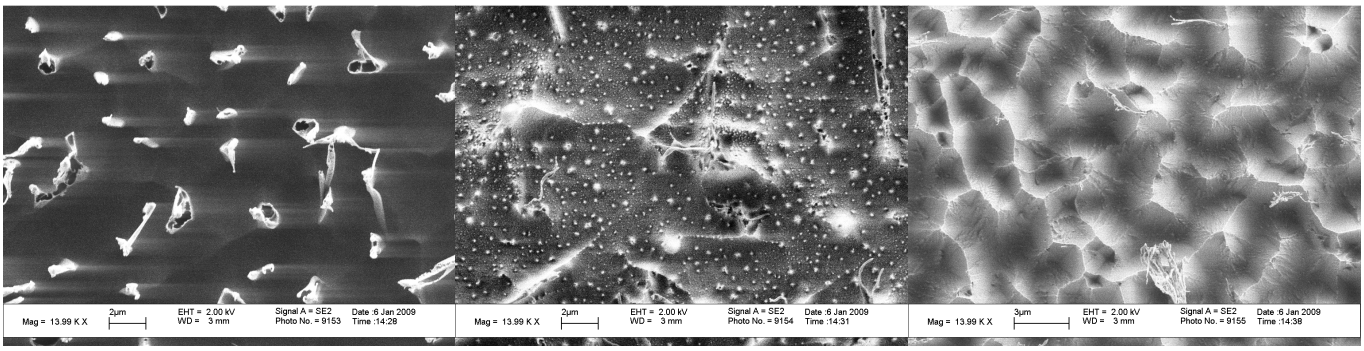

14k x zoom, no tilt (0 degrees)

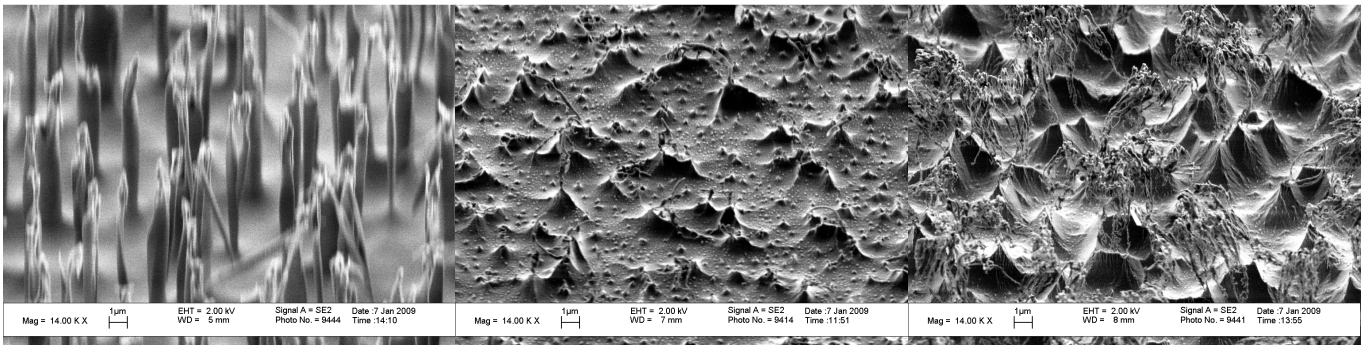

14k x zoom, 45 degrees tilt

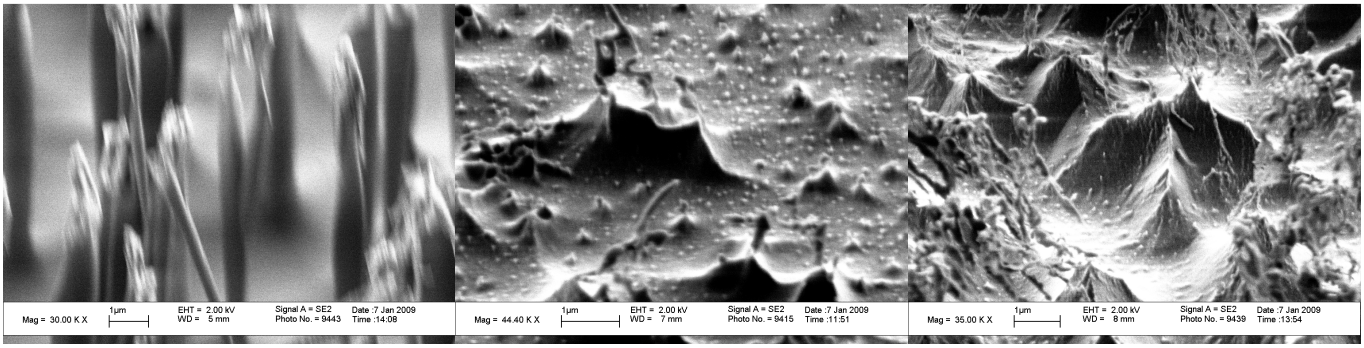

30k, 44.40k, 35k x zoom, 45 degrees tilt

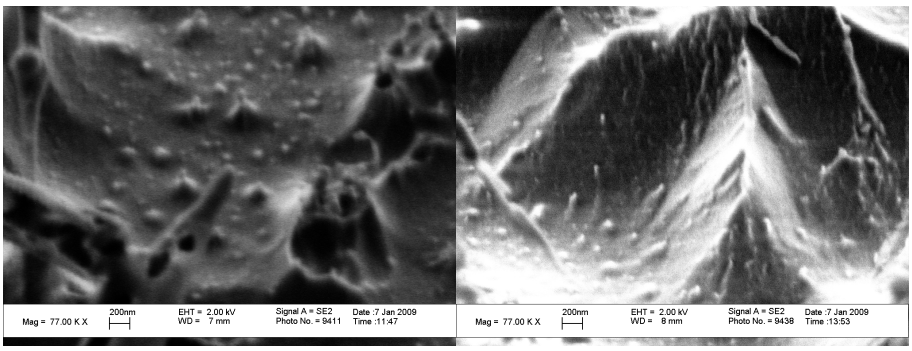

77k x zoom, 45 degrees tilt

Coil Power [W]	Process time [min]	Pressure [mTorr]	SF6 flow [sccm]	O2 flow [sccm]	Platen power [W]	Temp [ºC]
300	12:00	85	80	80	300	-10

Centre	16	Middle	16	Edge

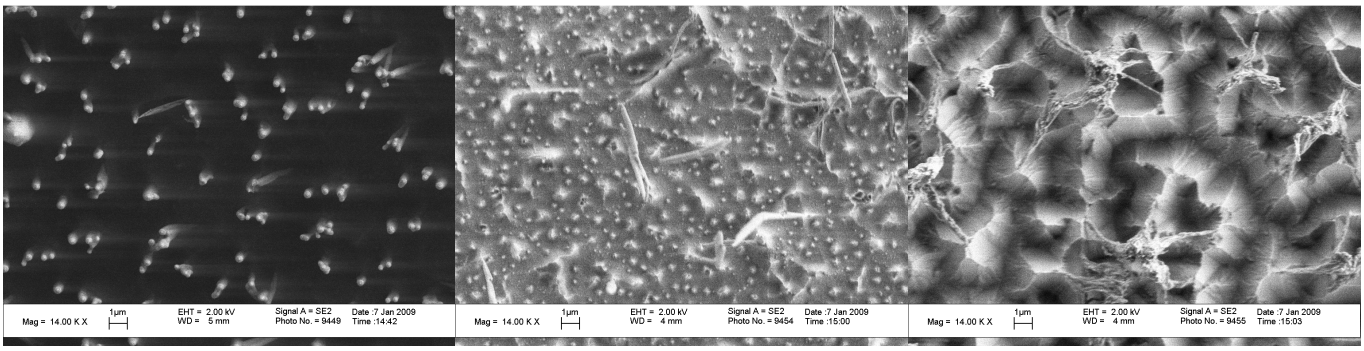

14k x zoom, no tilt (0 degrees)

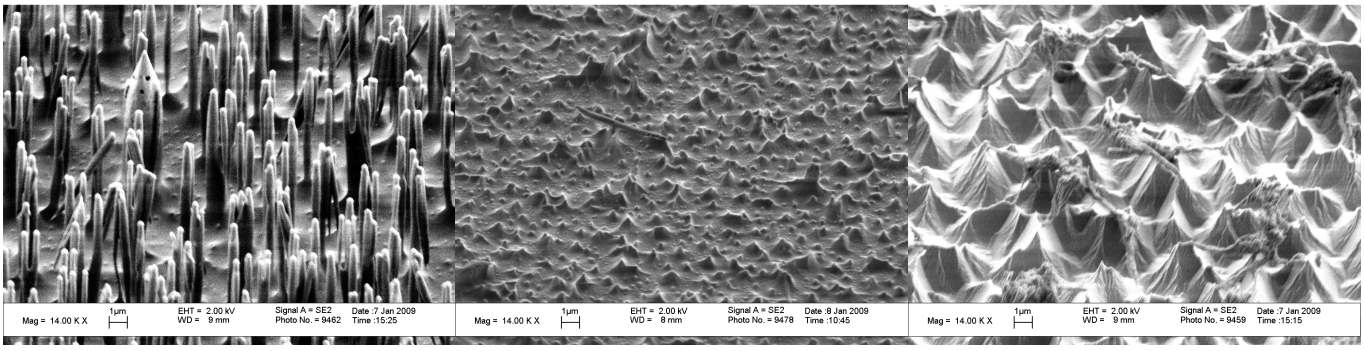

14k x zoom, 45 degrees tilt

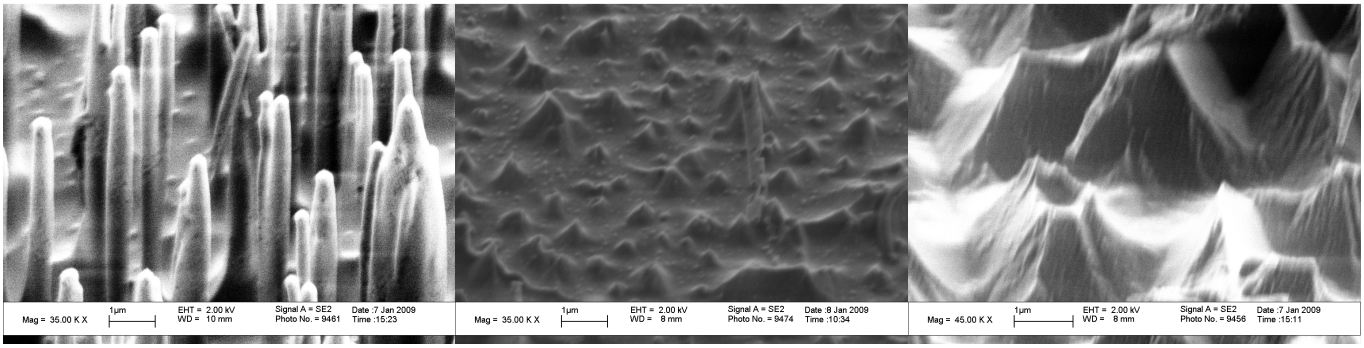

35k, 35k, 45k x zoom, 45 degrees tilt

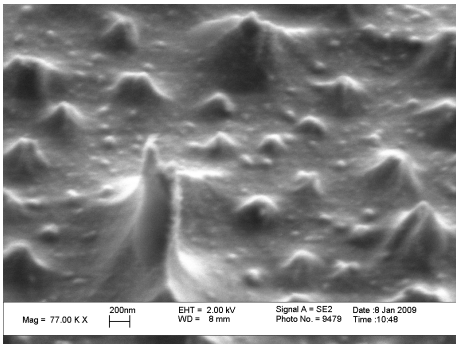

77k x zoom, 45 degrees tilt

Coil Power [W]	Process time [min]	Pressure [mTorr]	SF6 flow [sccm]	O2 flow [sccm]	Platen power [W]	Temp [ºC]
300	12:00	85	80	80	250	-10

Centre	17	Middle	17	Edge

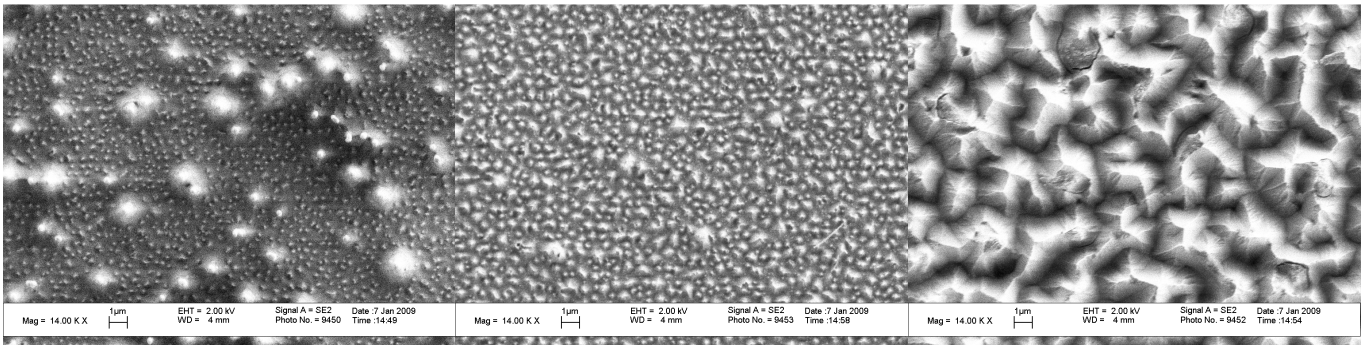

14k x zoom, no tilt (0 degrees)

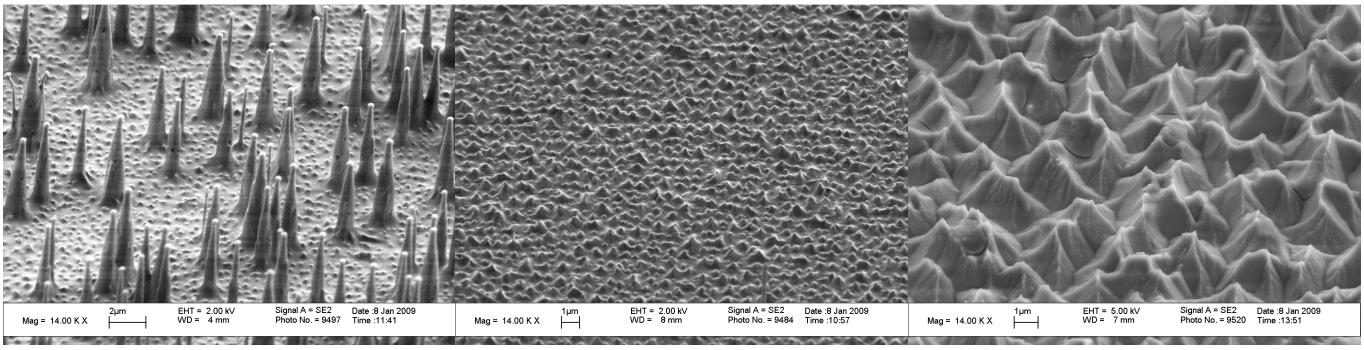

14k x zoom, 45 degrees tilt

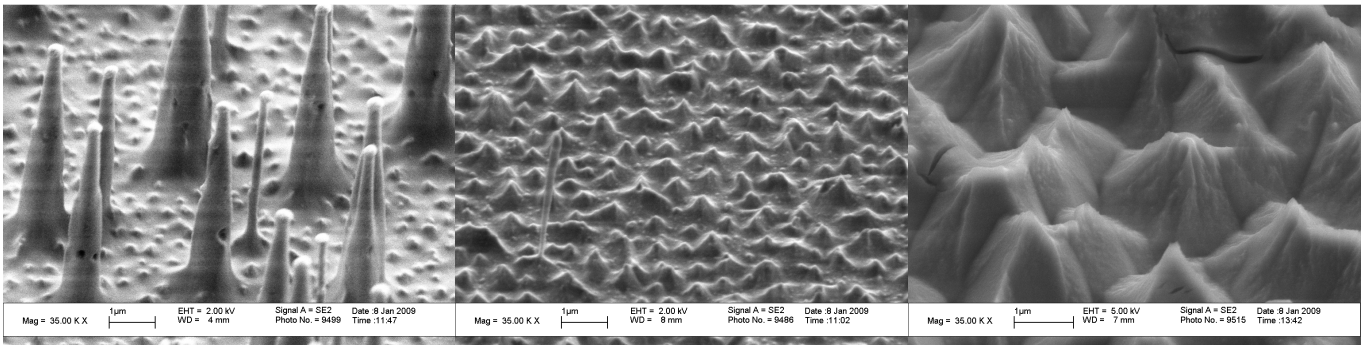

35k x zoom, 45 degrees tilt

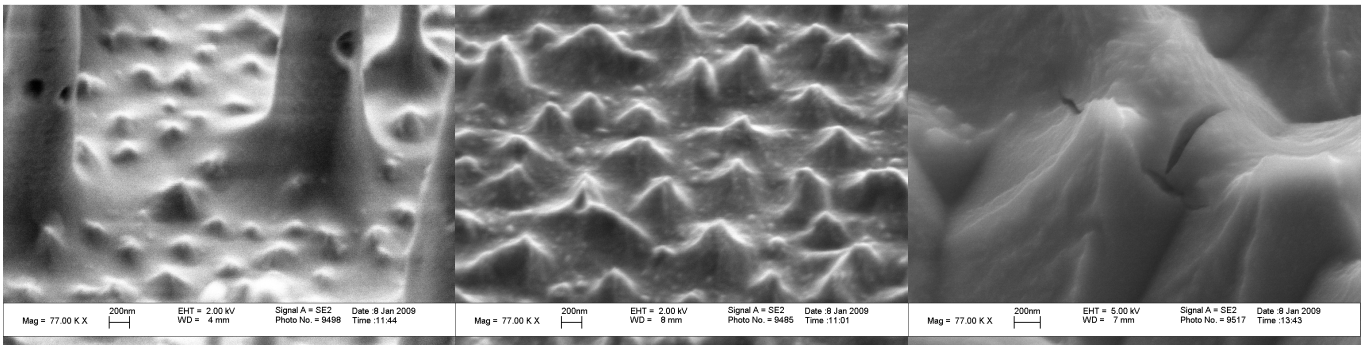

77k x zoom, 45 degrees tilt

Coil Power [W]	Process time [min]	Pressure [mTorr]	SF6 flow [sccm]	O2 flow [sccm]	Platen power [W]	Temp [ºC]
300	12:00	85	80	80	200	-10

Centre	18	Middle	18	Edge

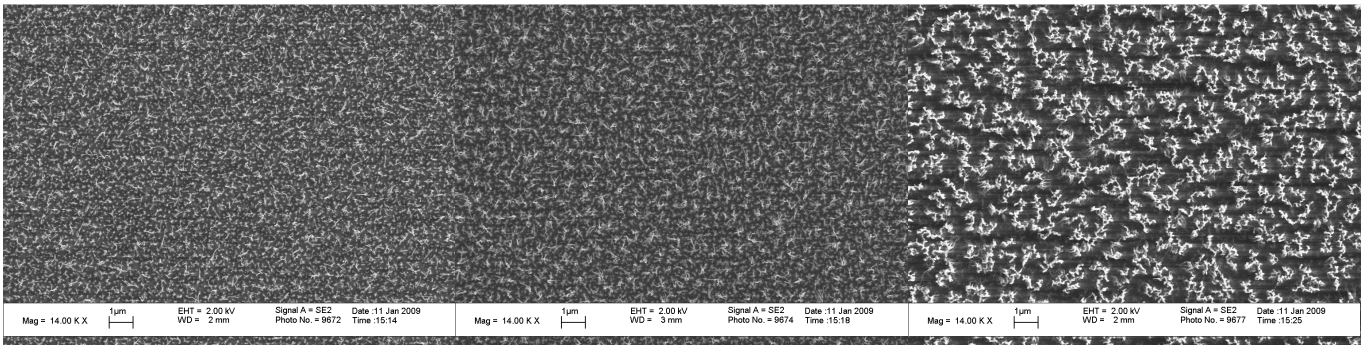

14k x zoom, no tilt (0 degrees)

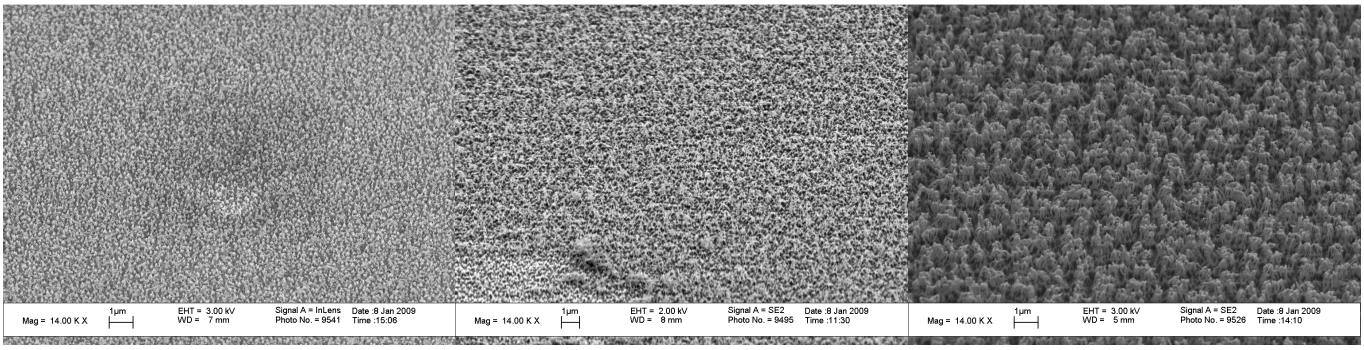

14k x zoom, 45 degrees tilt

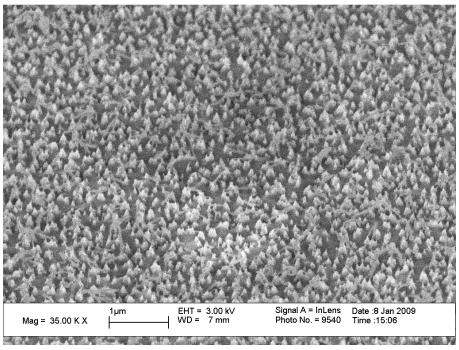

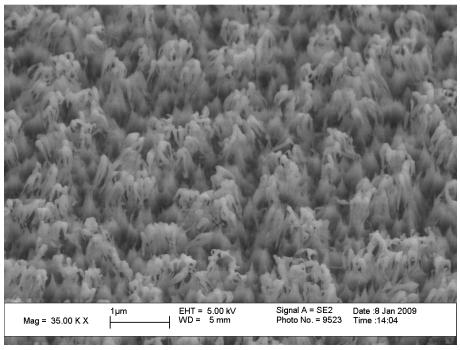

35k x zoom, 45 degrees tilt

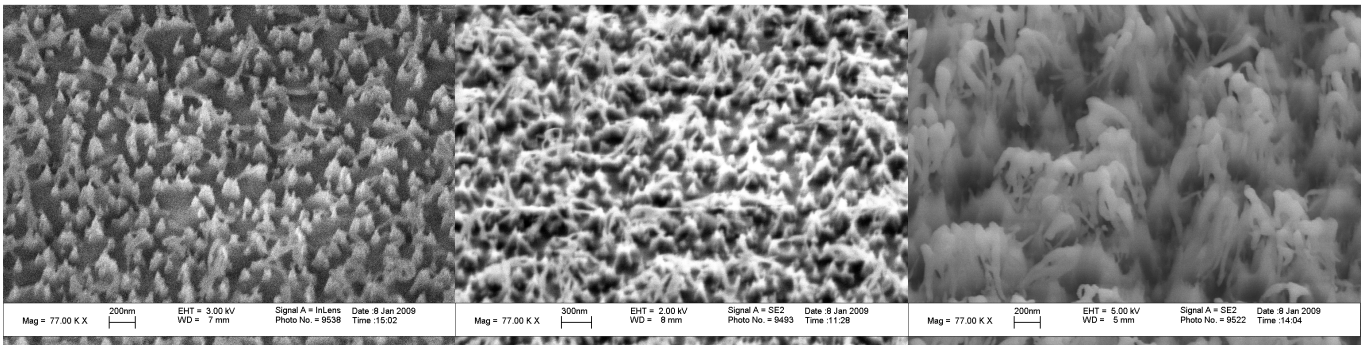

77k x zoom, 45 degrees tilt

Coil Power [W]	Process time [min]	Pressure [mTorr]	SF6 flow [sccm]	O2 flow [sccm]	Platen power [W]	Temp [ºC]
0	08:00	38	80	80	200	-10

Centre	19	Middle	19	Edge

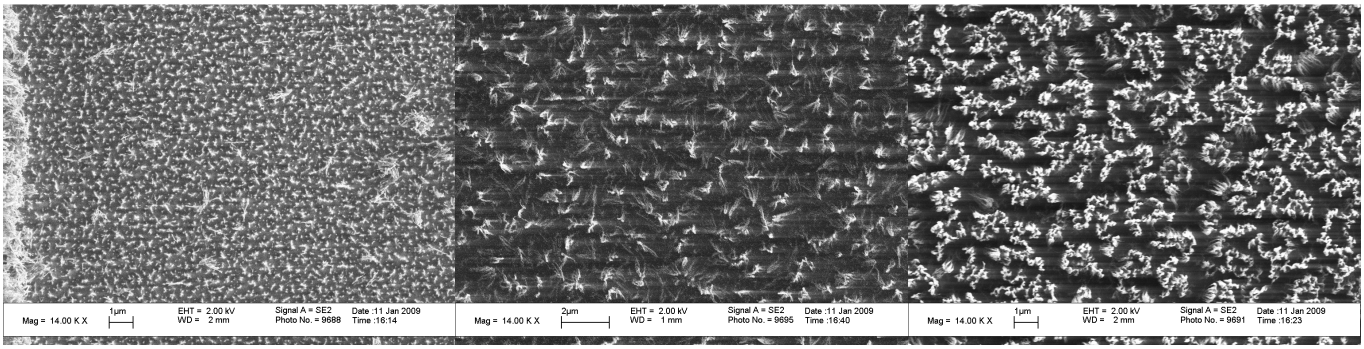

14k x zoom, no tilt (0 degrees)

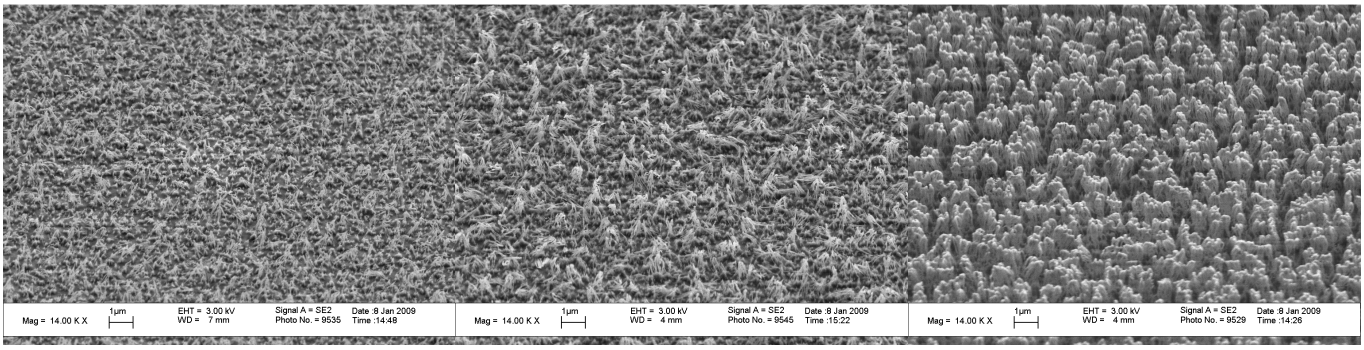

14k x zoom, 45 degrees tilt

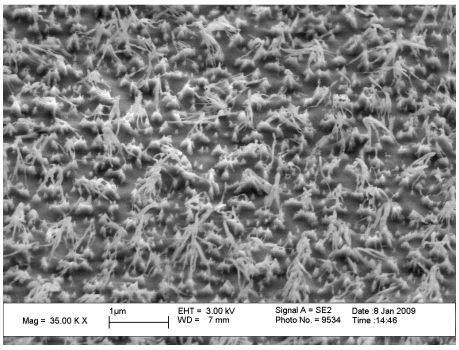

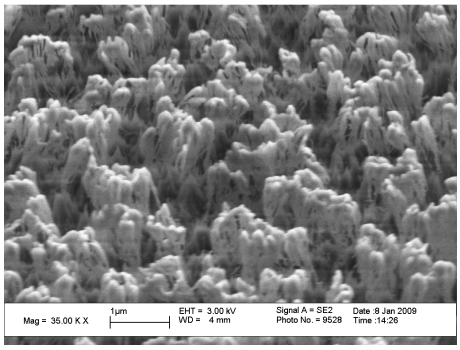

35k x zoom, 45 degrees tilt

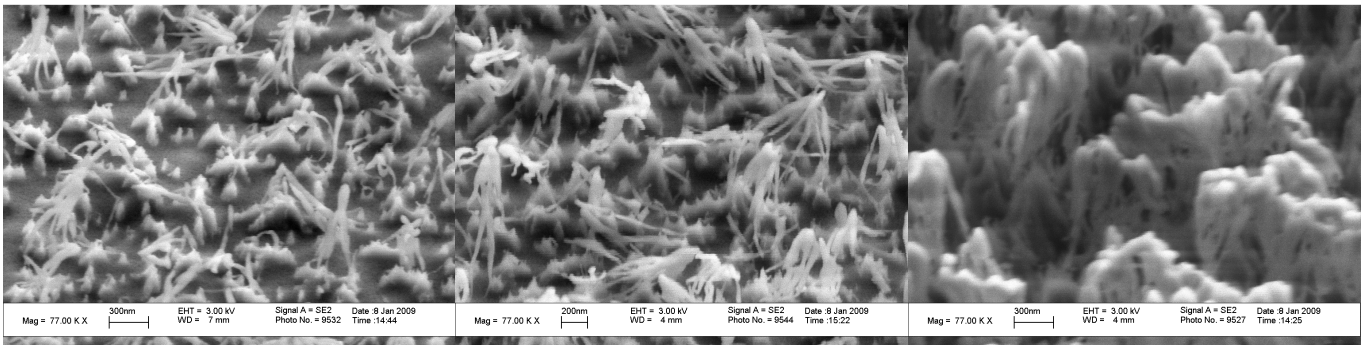

77k x zoom, 45 degrees tilt

Coil Power [W]	Process time [min]	Pressure [mTorr]	SF6 flow [sccm]	O2 flow [sccm]	Platen power [W]	Temp [ºC]
0	08:00	38	80	80	300	-10

First glance views of the wafers

Wafers bs09, bs10 and bs11

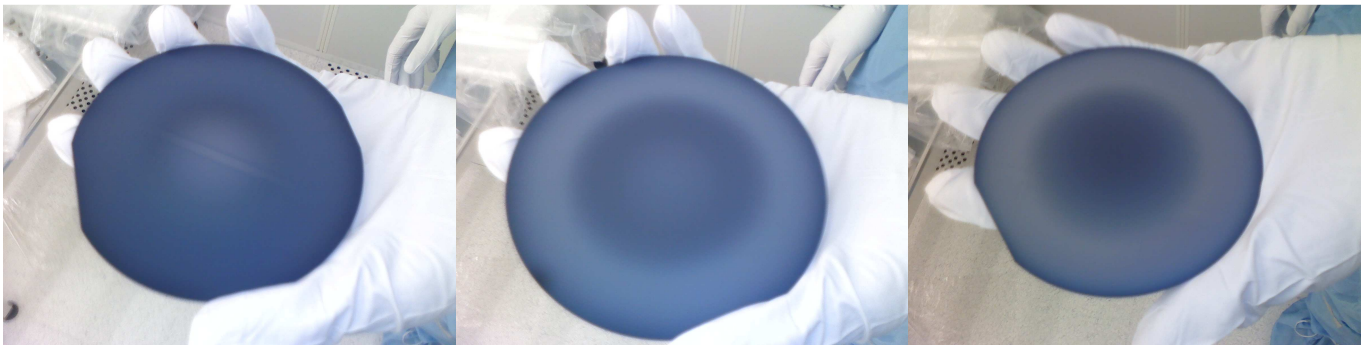

Wafers bs12, bs13 and bs14

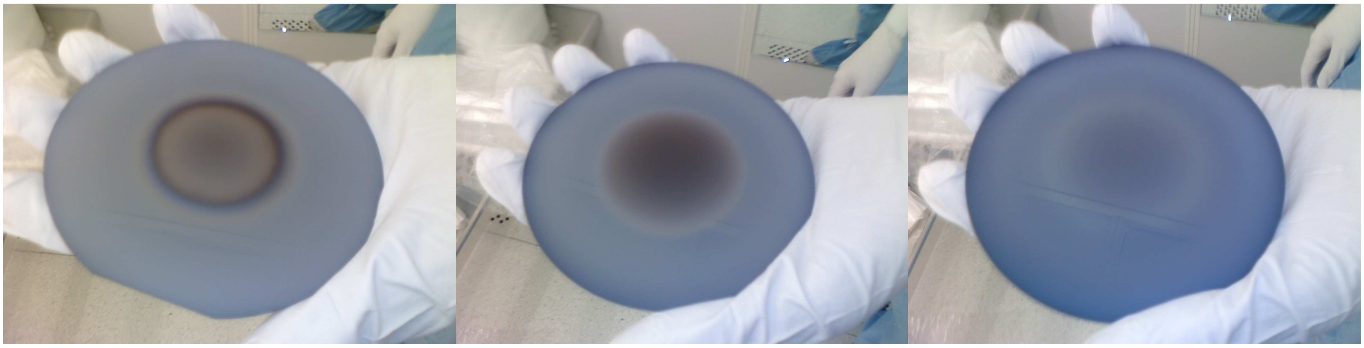

Wafers bs15, bs16 and bs17

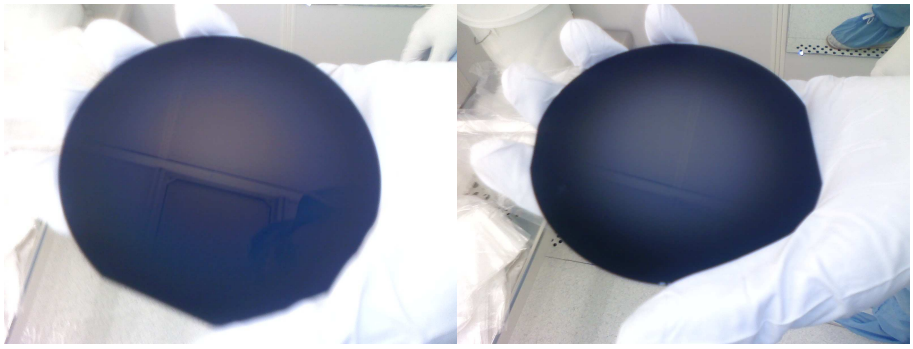

Wafers bs18 and bs19

Due to the nature of the light emitted from the blitz on the camera used, the wafers look more bluish on the pictures compared to how they look when they are illuminated by normal light.

Appendix B - Black Si Substrates from Rasmus Davidsen

15-17 Black Si

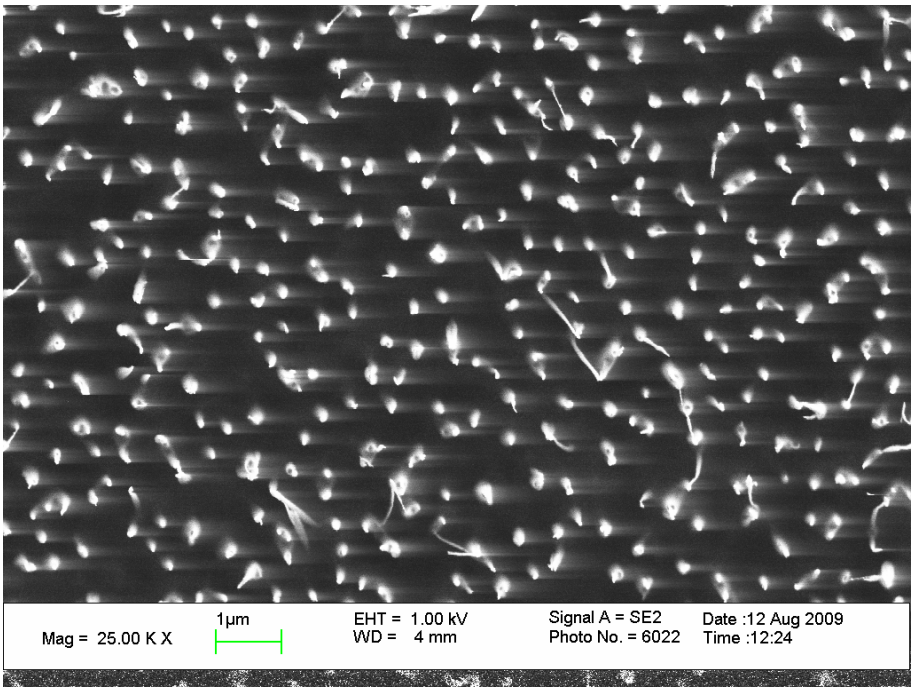

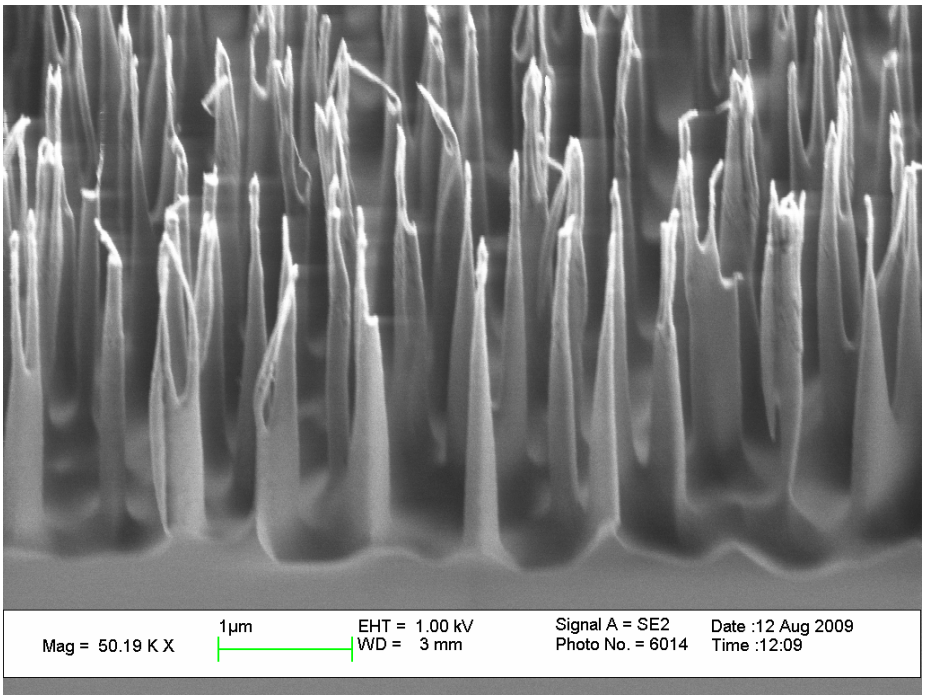

15-19 Black Si

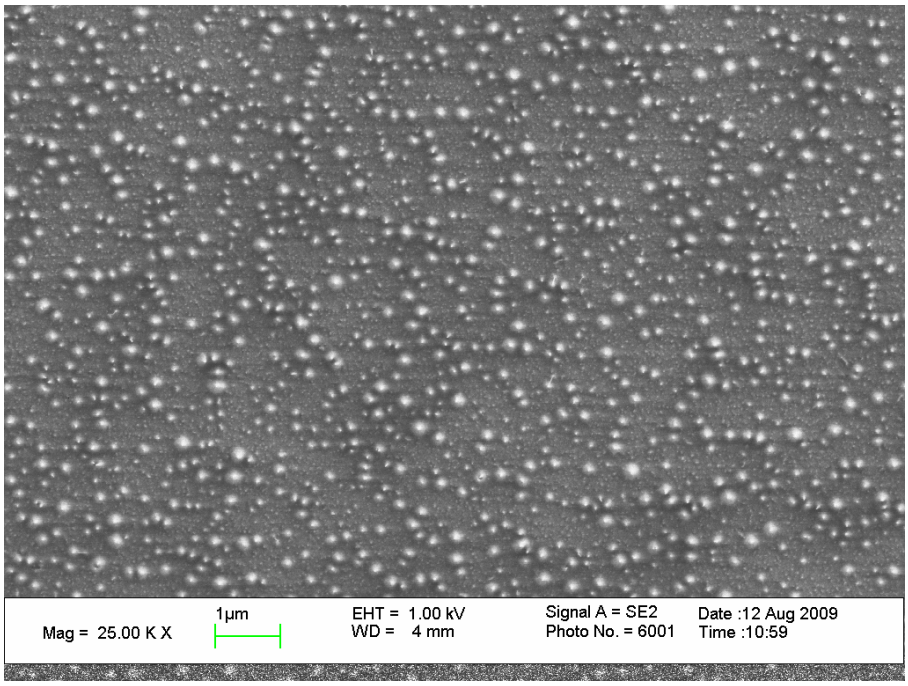

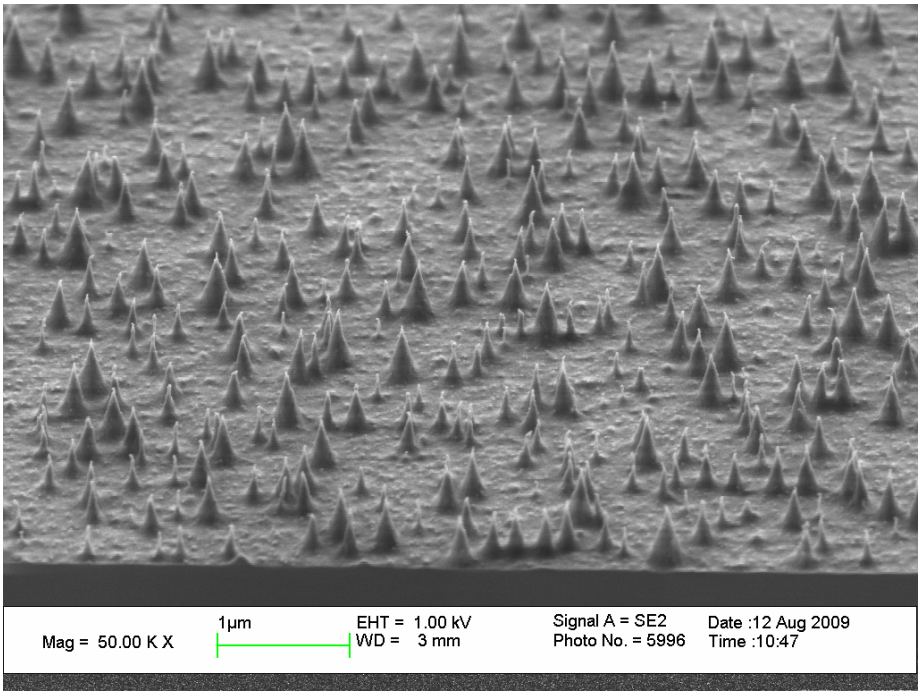

16-05 Black Si

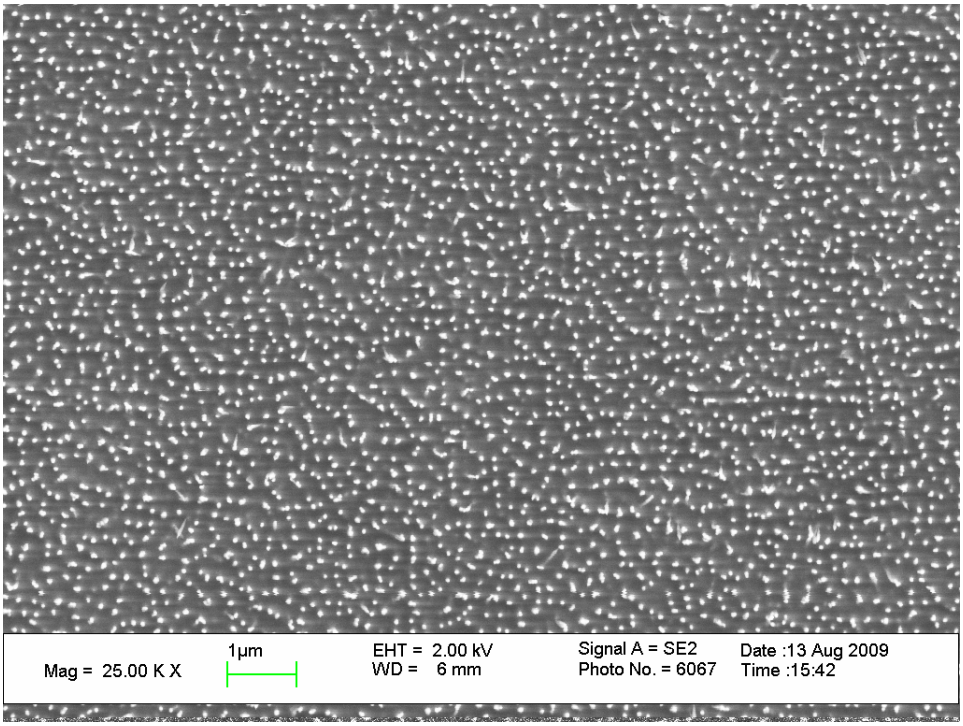

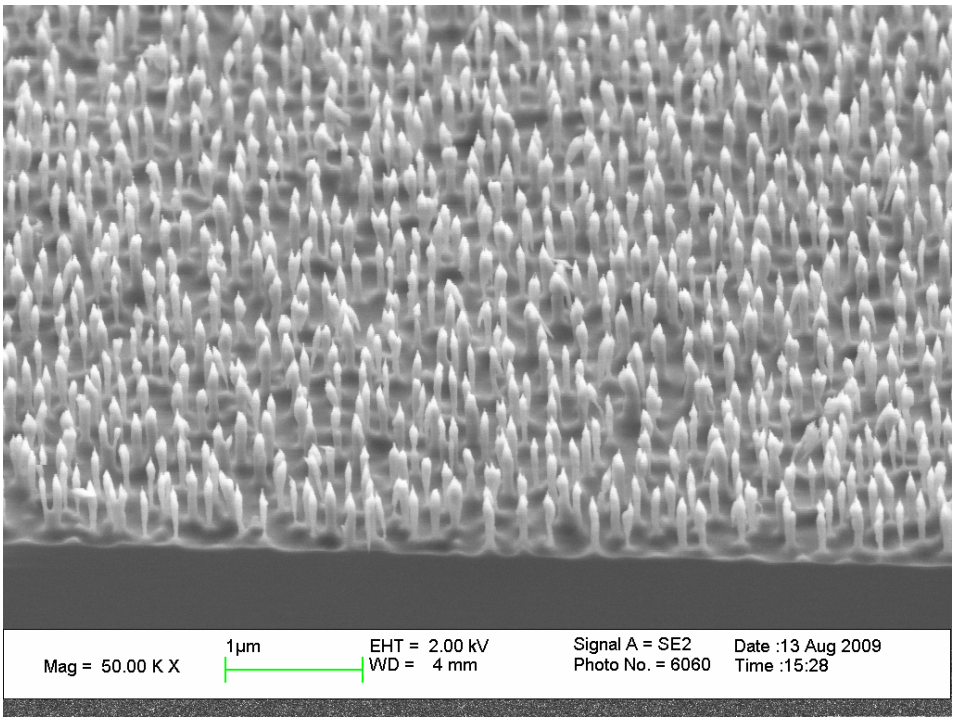

Appendix C - Graphs Modelling Cell Behaviour

Si (21092009), 1272 data points

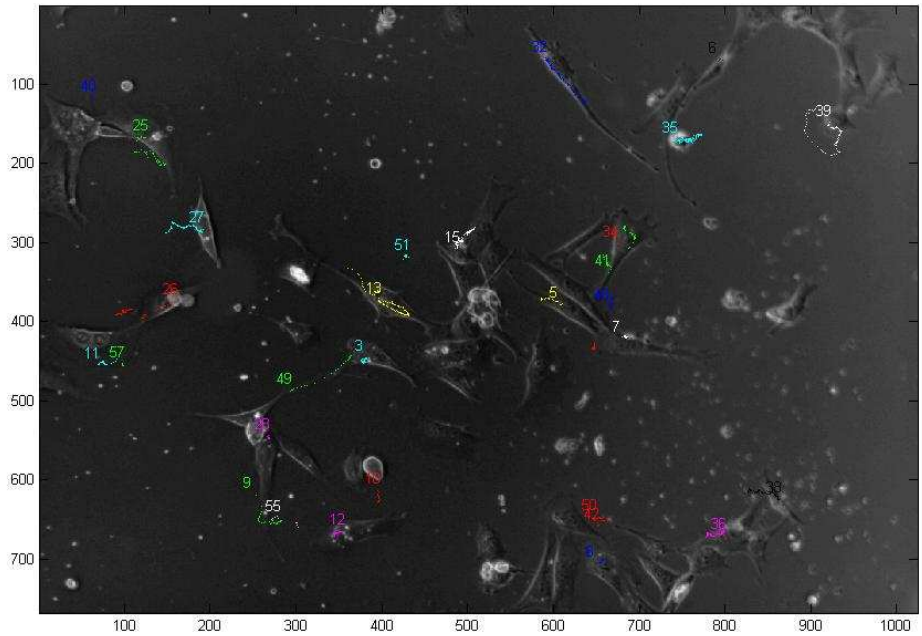

Cell trajectories. Units on both axes are pixels. 1 pixel = 0.977 µm.

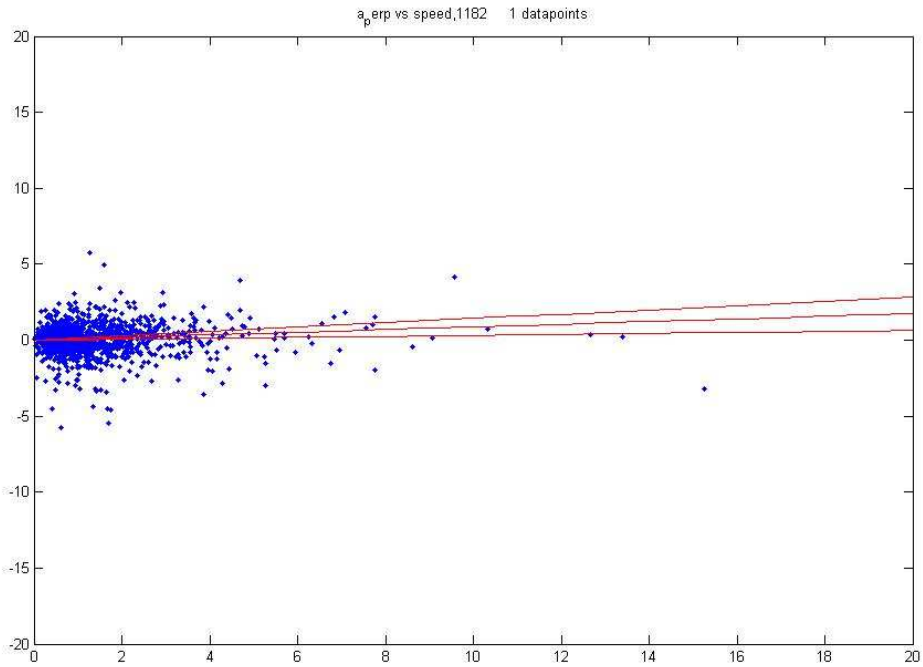

Cell acceleration perpendicular to cell velocity as a function of cell velocity. Units are µm/frame (x axis) and µm^2/frame (y axis). 1 pixel = 0.977 µm and 1 frame = 4 min.

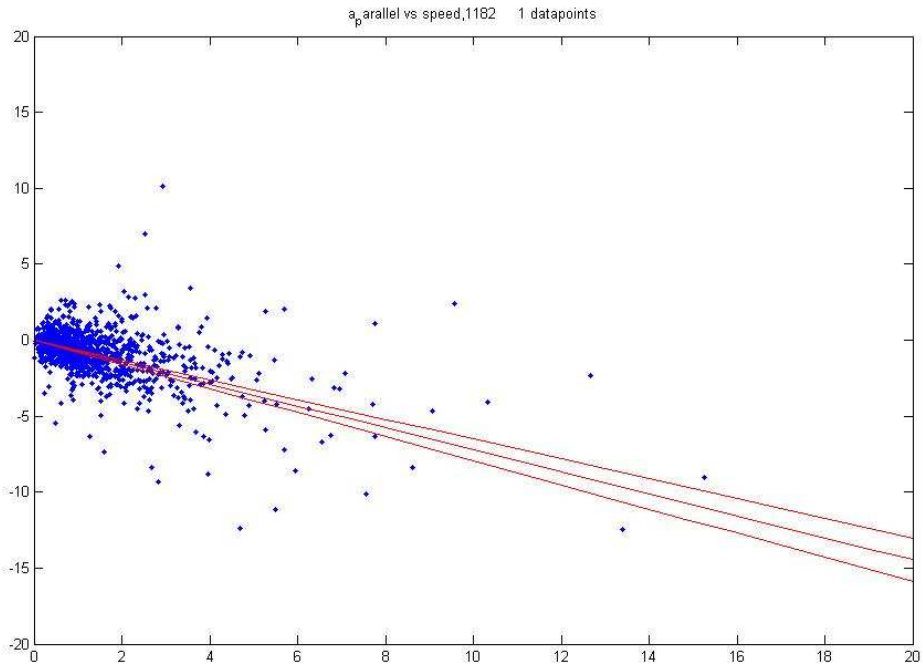

Cell acceleration parallel to cell velocity as a function of cell velocity. Units are µm/frame (x axis) and µm^2/frame (y axis). 1 pixel = 0.977 µm and 1 frame = 4 min.

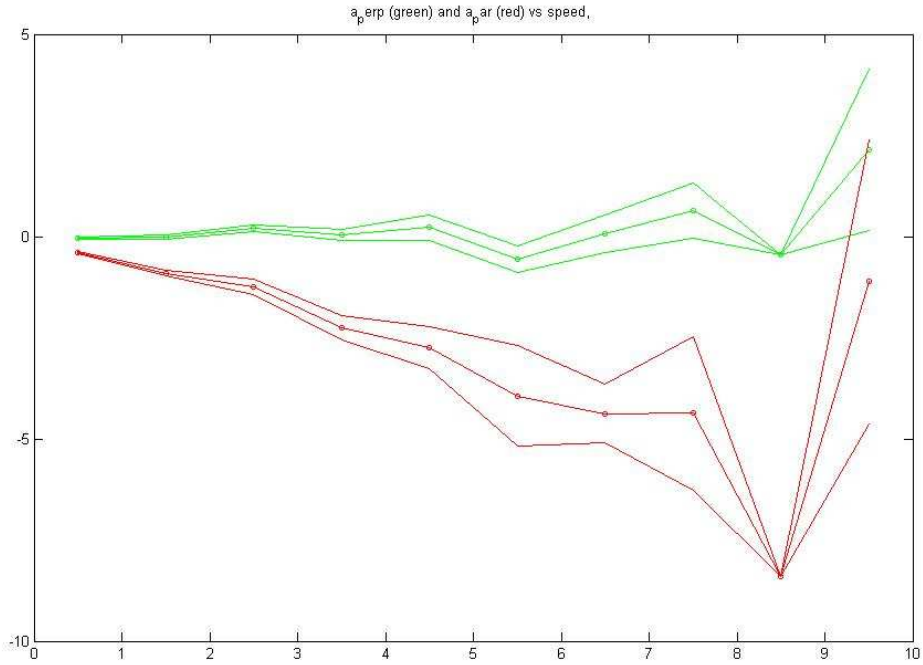

Cell acceleration perpendicular (green, top) and parallel (red, bottom) to cell velocity as a function of cell velocity. Units are µm/frame (x axis) and µm^2/frame (y axis). 1 pixel = 0.977 µm and 1 frame = 4 min.

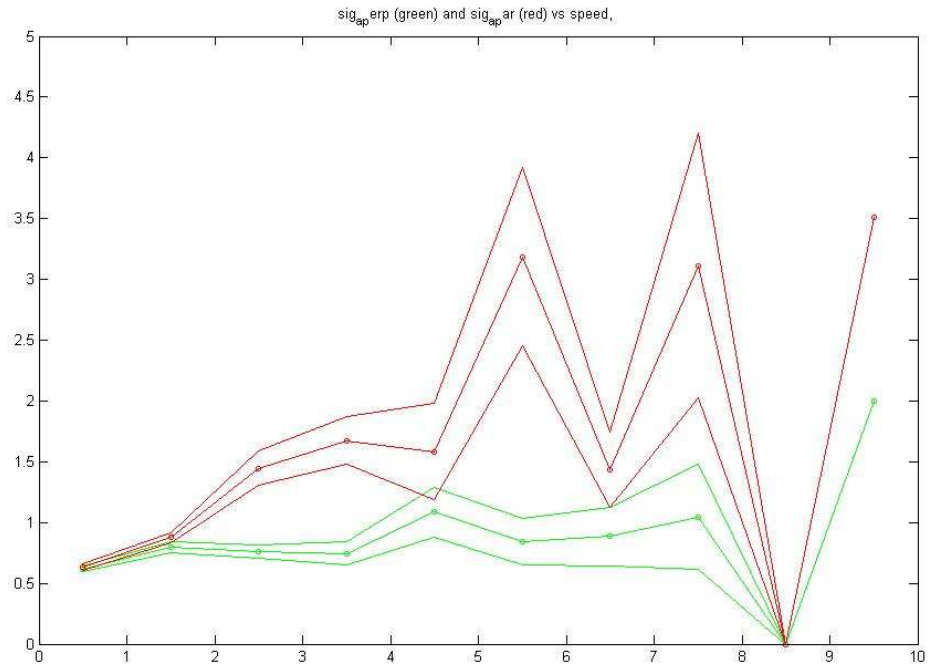

Standard deviation of cell acceleration perpendicular (green, bottom) and parallel (red, top) to cell velocity as a function of cell velocity. Units are µm/frame (x axis) and µm^2/frame (y axis). 1 pixel = 0.977 µm and 1 frame = 4 min.

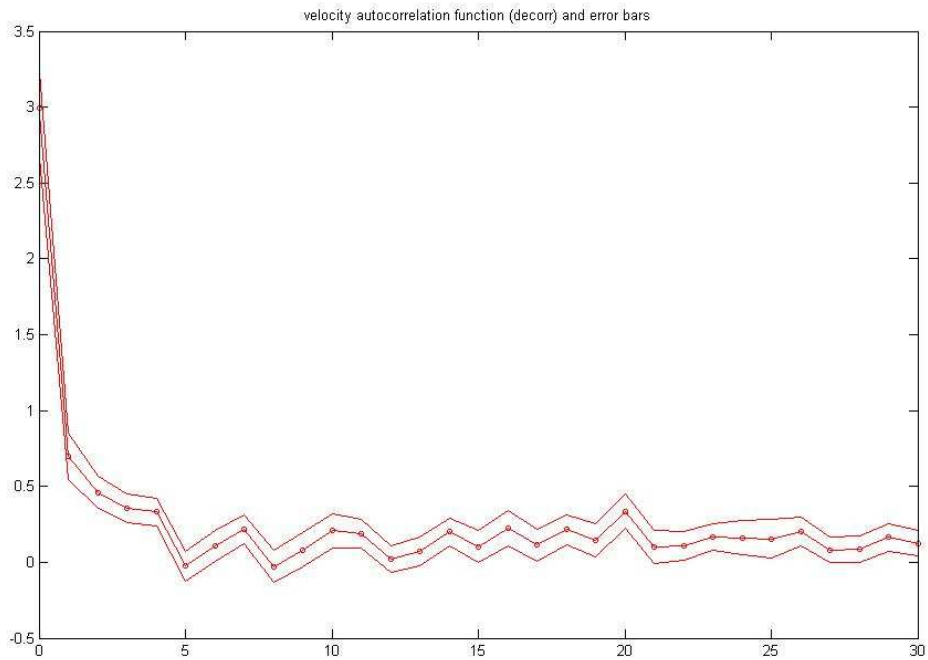

Autocorrelation of the cell velocities as a function of time. Units are frames (x axis) and µm^2/frame^2 (y axis). 1 pixel = 0.977 µm and 1 frame = 4 min.

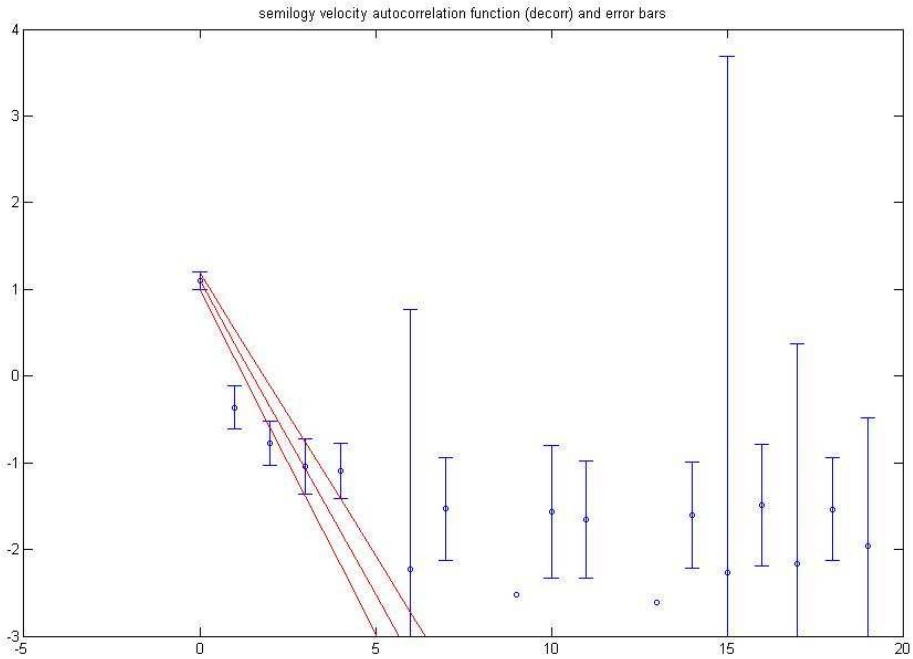

Semi-log plot of the atocorrelation of the cell velocities as a function of time. Units are frames (x axis) and ln(µm^2/frame^2) (y axis). 1 pixel = 0.977 µm and 1 frame = 4 min.

Si (07092009), 966 data points

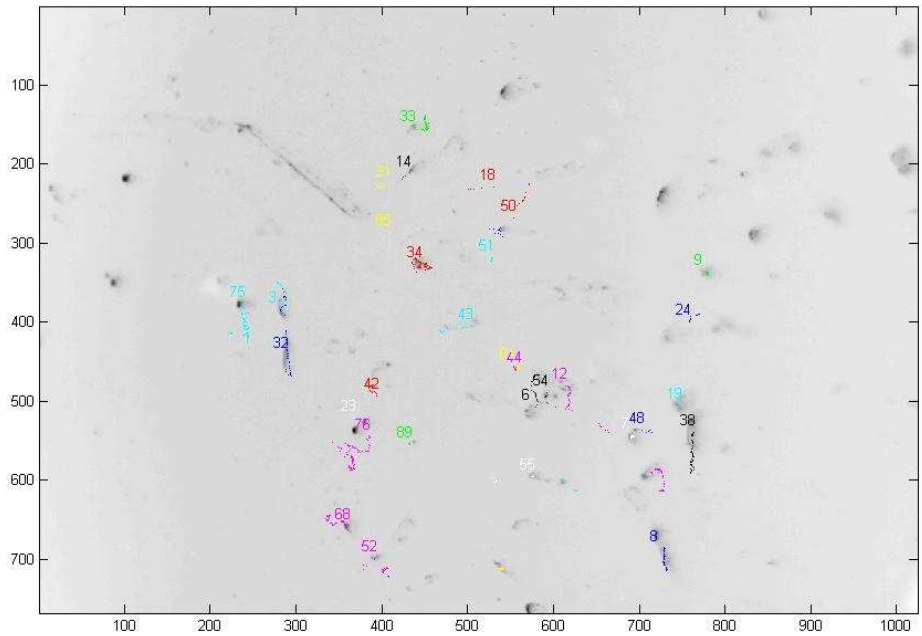

Cell trajectories. Units on both axes are pixels. 1 pixel = 0.977 µm.

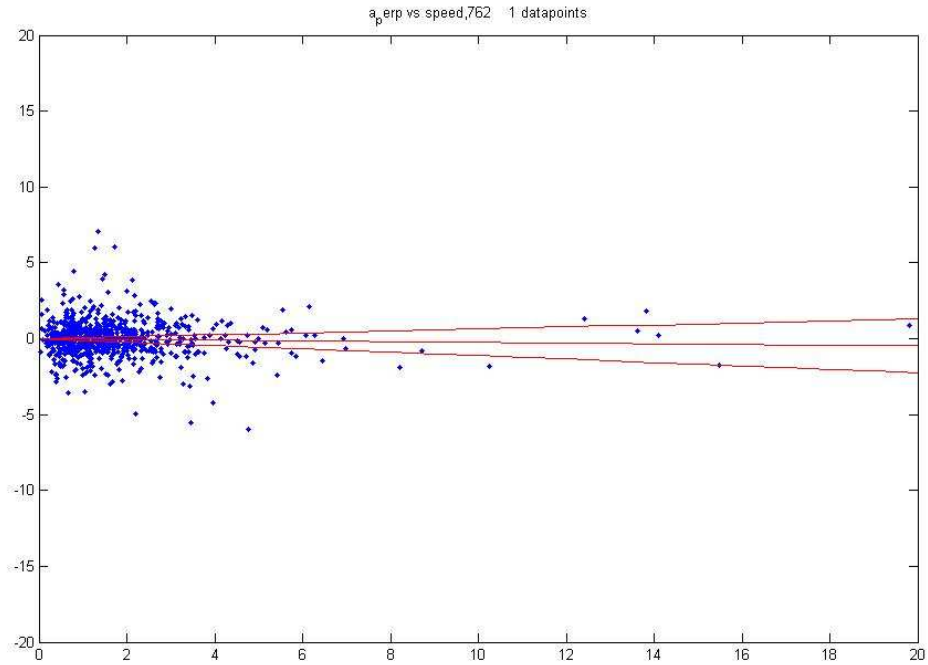

Cell acceleration perpendicular to cell velocity as a function of cell velocity. Units are µm/frame (x axis) and µm^2/frame (y axis). 1 pixel = 0.977 µm and 1 frame = 4 min.

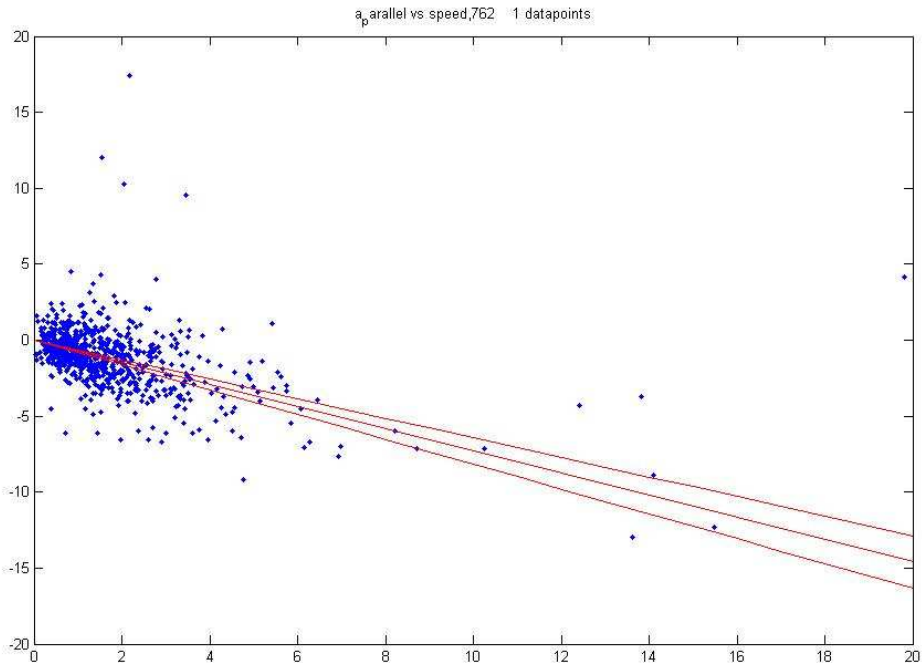

Cell acceleration parallel to cell velocity as a function of cell velocity. Units are µm/frame (x axis) and µm^2/frame (y axis). 1 pixel = 0.977 µm and 1 frame = 4 min.

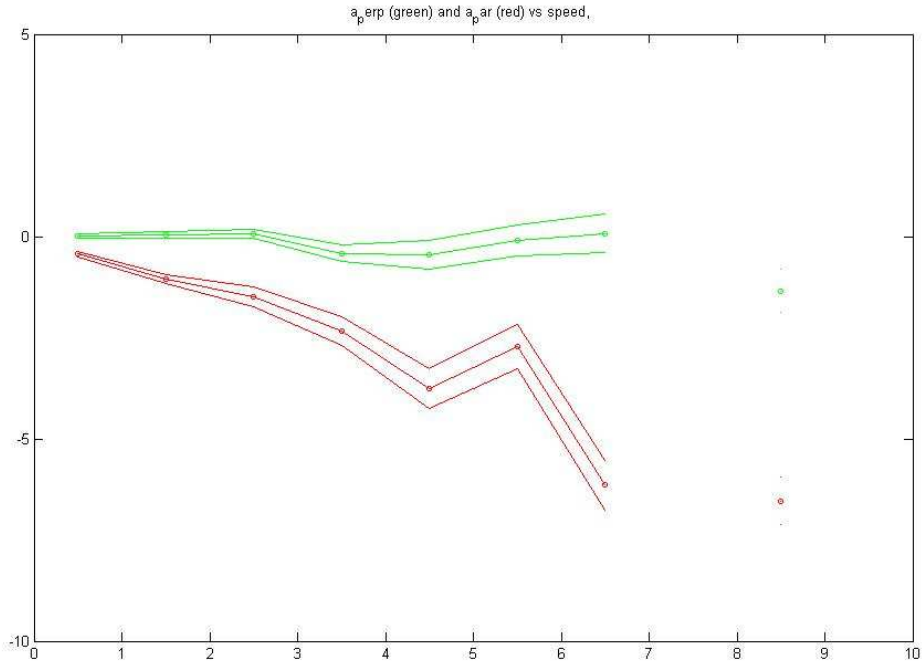

Cell acceleration perpendicular (green, top) and parallel (red, bottom) to cell velocity as a function of cell velocity. Units are µm/frame (x axis) and µm^2/frame (y axis). 1 pixel = 0.977 µm and 1 frame = 4 min.

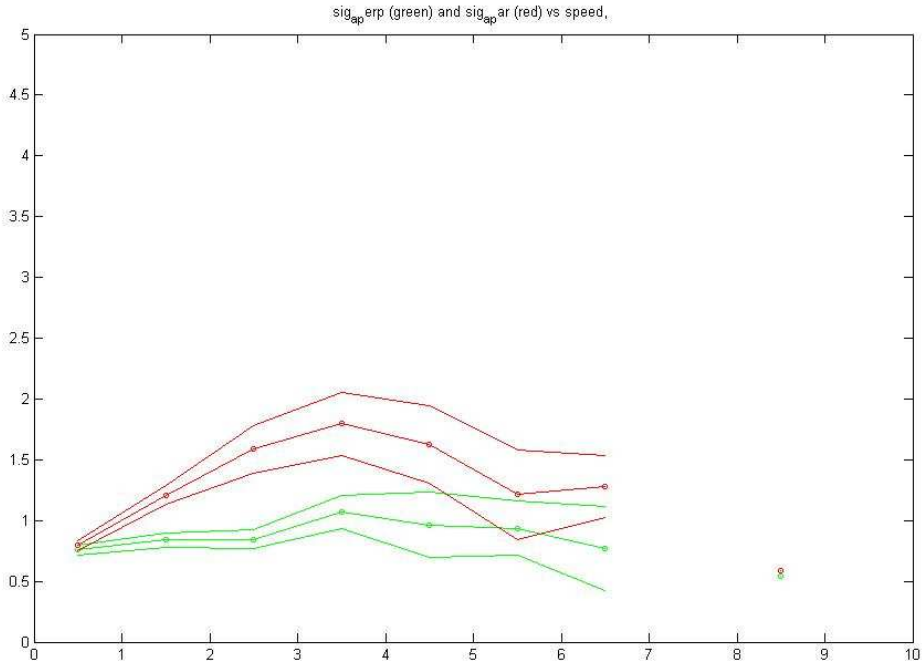

Standard deviation of cell acceleration perpendicular (green, bottom) and parallel (red, top) to cell velocity as a function of cell velocity. Units are µm/frame (x axis) and µm^2/frame (y axis). 1 pixel = 0.977 µm and 1 frame = 4 min.

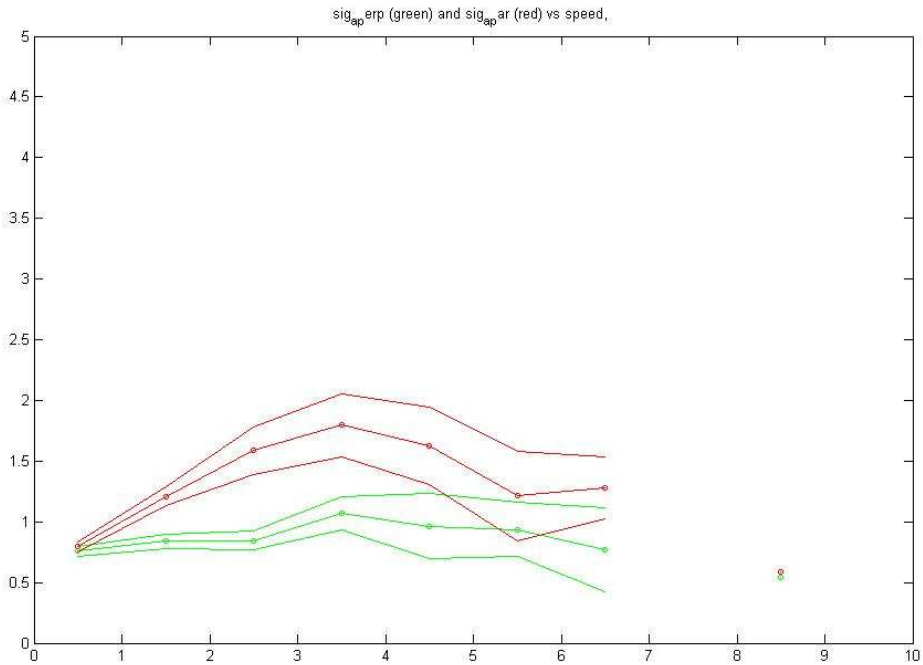

Autocorrelation of the cell velocities as a function of time. Units are frames (x axis) and µm^2/frame^2 (y axis). 1 pixel = 0.977 µm and 1 frame = 4 min.

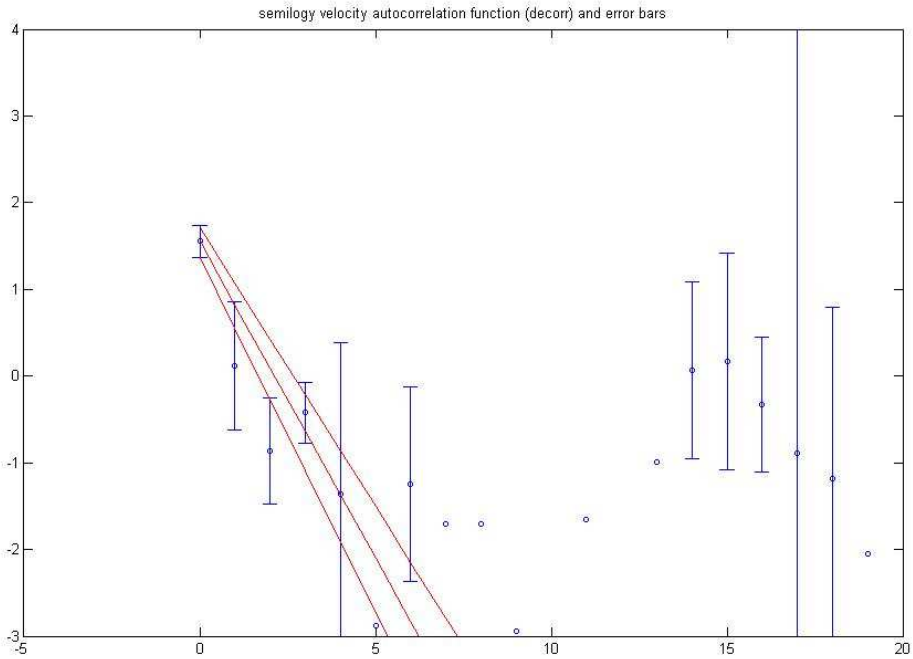

Semi-log plot of the atocorrelation of the cell velocities as a function of time. Units are frames (x axis) and ln(µm^2/frame^2) (y axis). 1 pixel = 0.977 µm and 1 frame = 4 min.

Glass (07092009), 717 data points

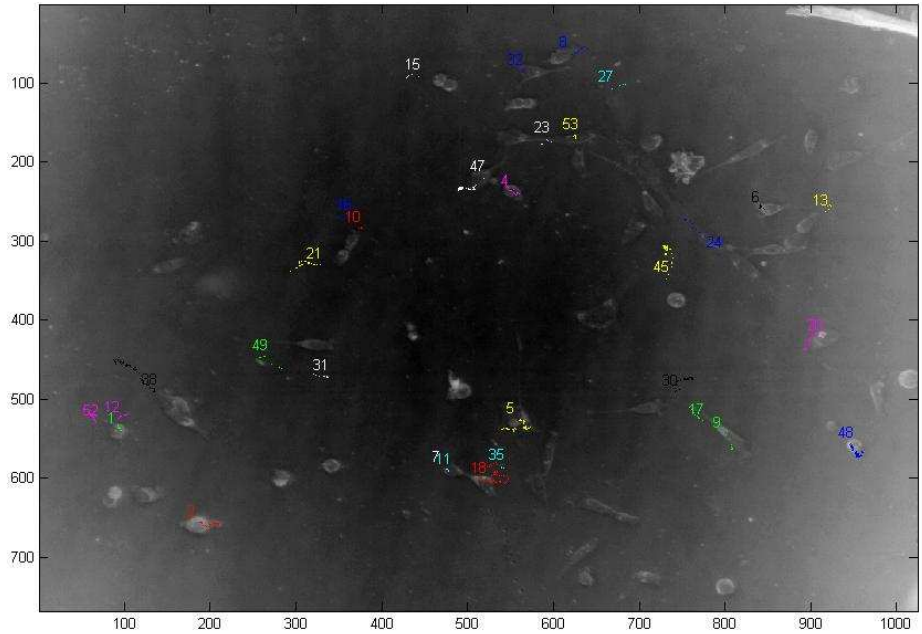

Cell trajectories. Units on both axes are pixels. 1 pixel = 0.977 µm.

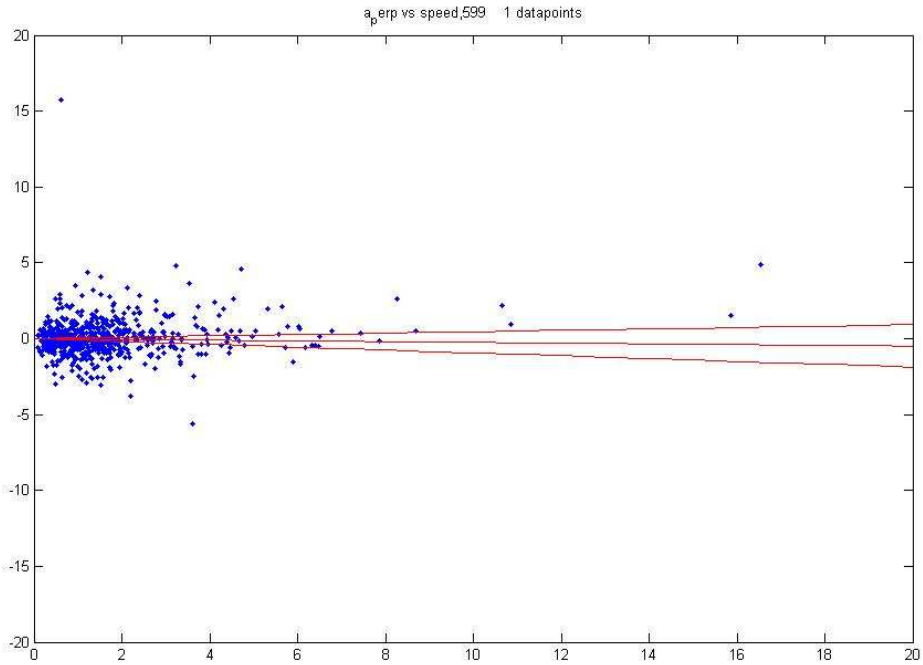

Cell acceleration perpendicular to cell velocity as a function of cell velocity. Units are µm/frame (x axis) and µm^2/frame (y axis). 1 pixel = 0.977 µm and 1 frame = 4 min.

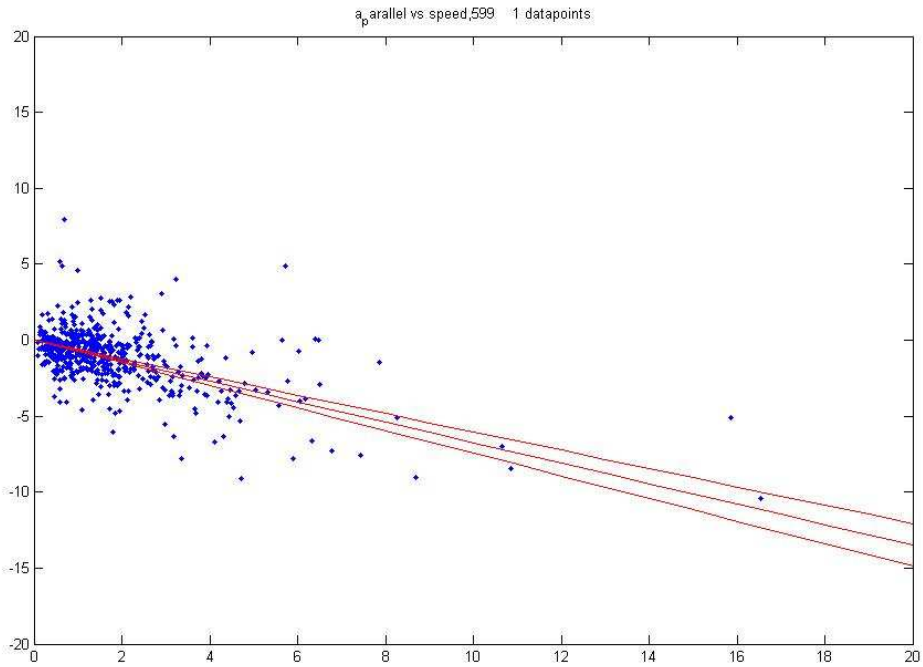

Cell acceleration parallel to cell velocity as a function of cell velocity. Units are µm/frame (x axis) and µm^2/frame (y axis). 1 pixel = 0.977 µm and 1 frame = 4 min.

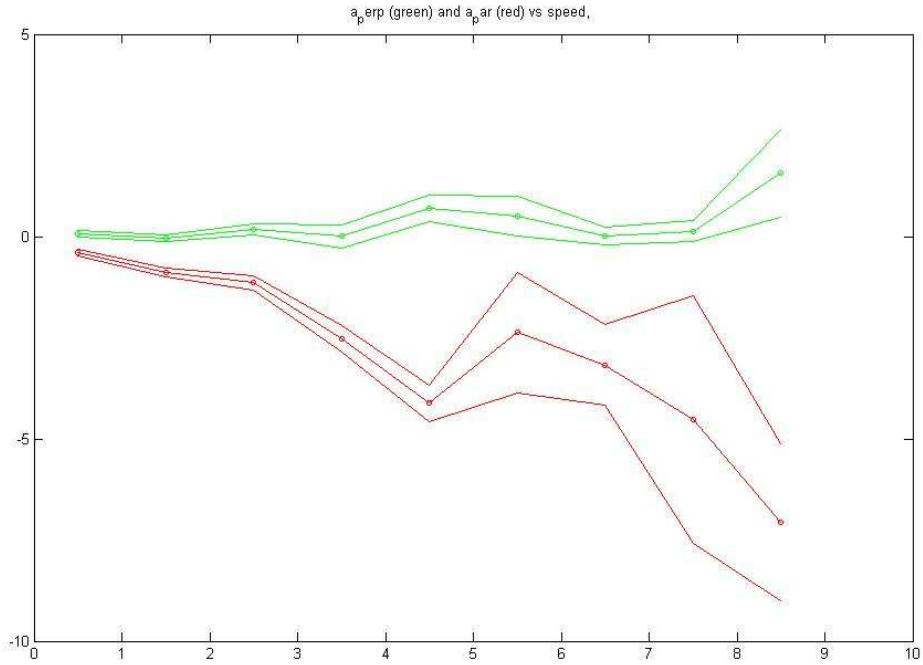

Cell acceleration perpendicular (green, top) and parallel (red, bottom) to cell velocity as a function of cell velocity. Units are µm/frame (x axis) and µm^2/frame (y axis). 1 pixel = 0.977 µm and 1 frame = 4 min.

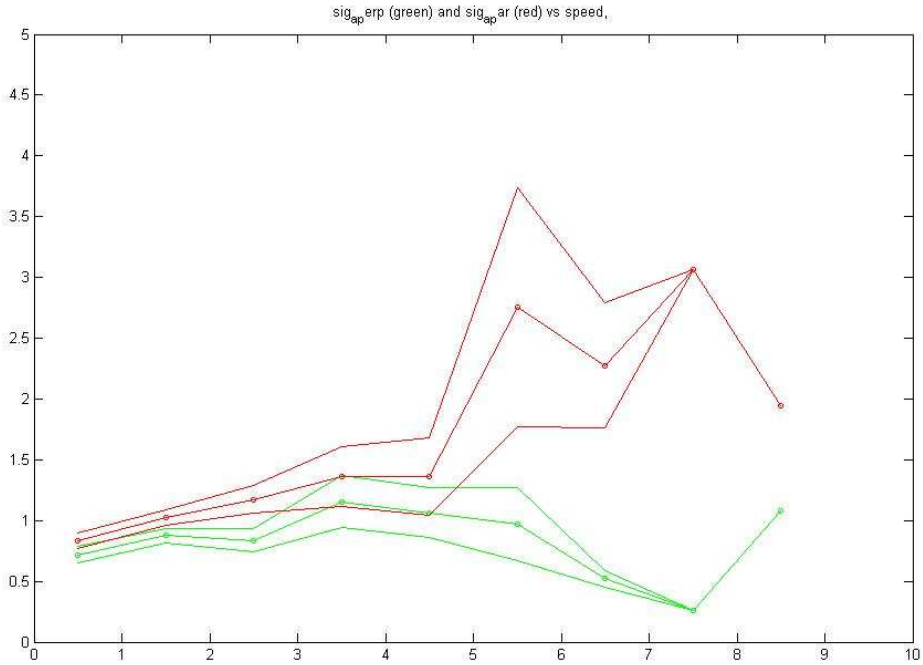

Standard deviation of cell acceleration perpendicular (green, bottom) and parallel (red, top) to cell velocity as a function of cell velocity. Units are µm/frame (x axis) and µm^2/frame (y axis). 1 pixel = 0.977 µm and 1 frame = 4 min.

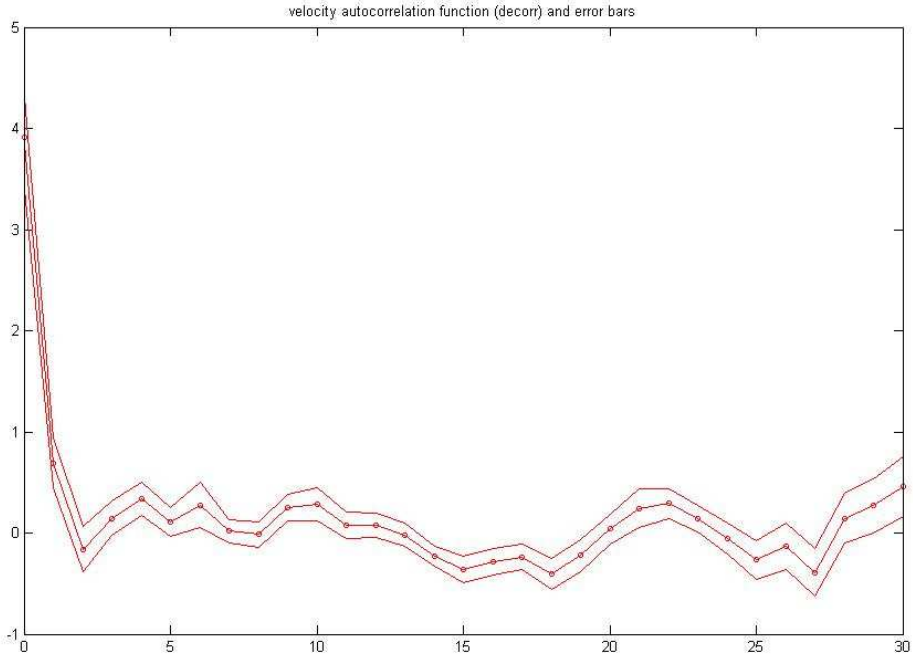

Autocorrelation of the cell velocities as a function of time. Units are frames (x axis) and µm^2/frame^2 (y axis). 1 pixel = 0.977 µm and 1 frame = 4 min.

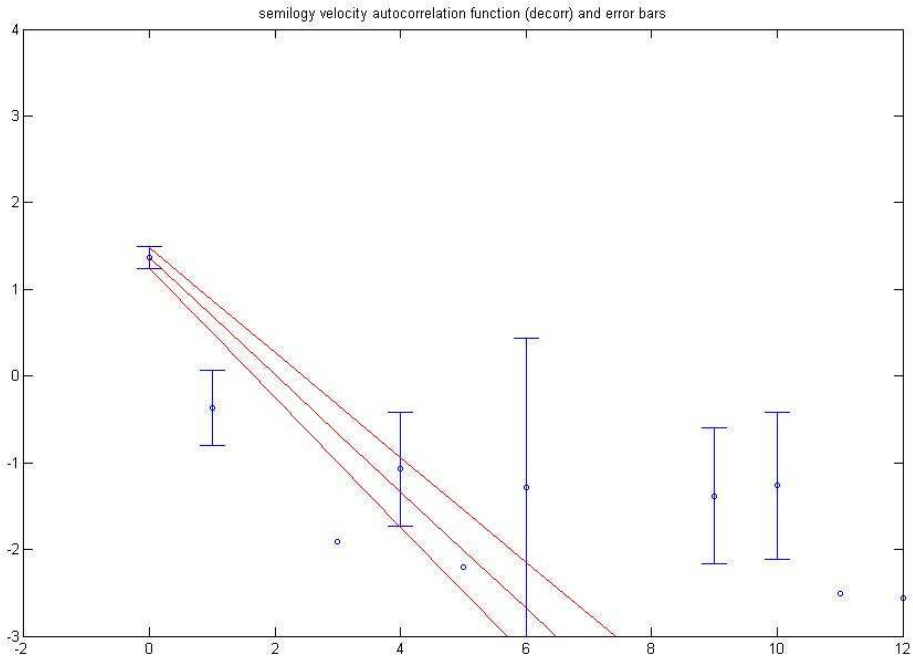

Semi-log plot of the atocorrelation of the cell velocities as a function of time. Units are frames (x axis) and ln(µm^2/frame^2) (y axis). 1 pixel = 0.977 µm and 1 frame = 4 min.

15-19 Black Si (21092009), 1415 data points

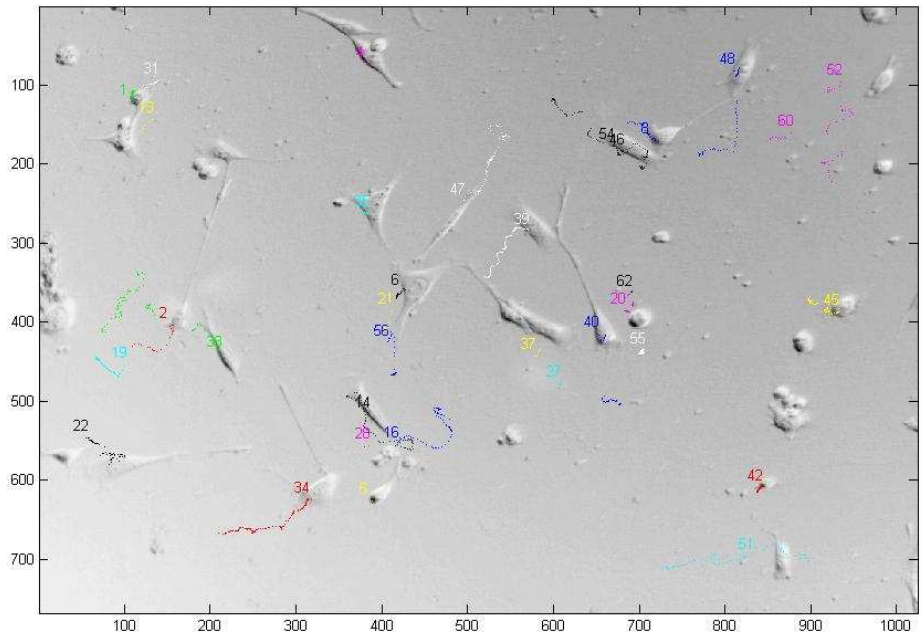

Cell trajectories. Units on both axes are pixels. 1 pixel = 0.977 µm.

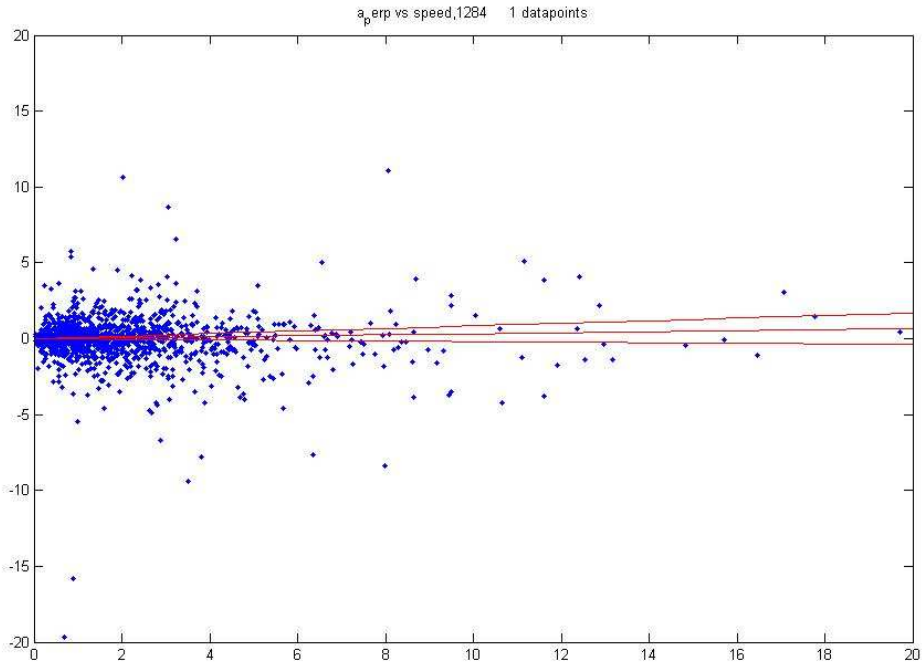

Cell acceleration perpendicular to cell velocity as a function of cell velocity. Units are µm/frame (x axis) and µm^2/frame (y axis). 1 pixel = 0.977 µm and 1 frame = 4 min.

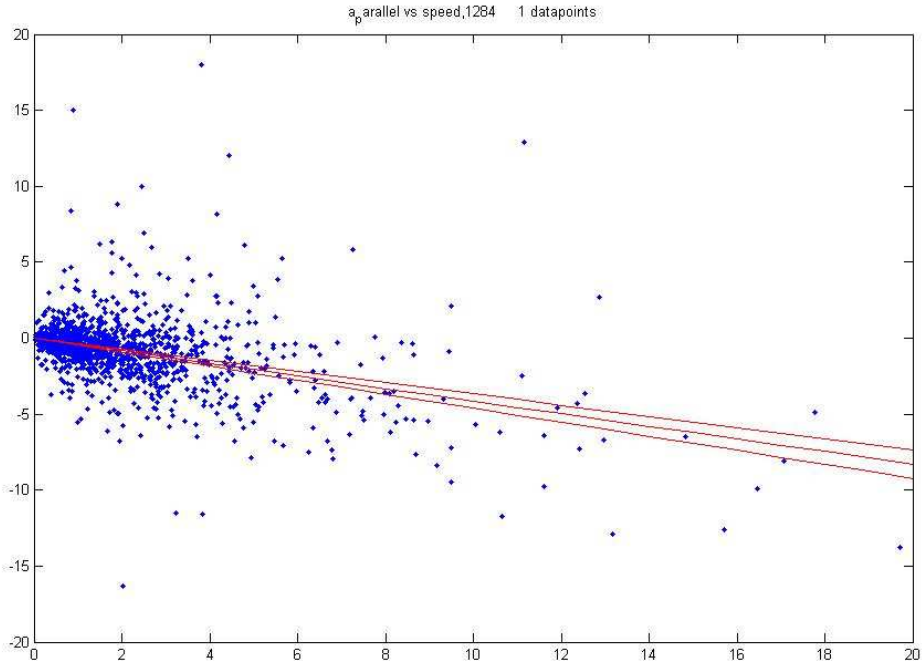

Cell acceleration parallel to cell velocity as a function of cell velocity. Units are µm/frame (x axis) and µm^2/frame (y axis). 1 pixel = 0.977 µm and 1 frame = 4 min.

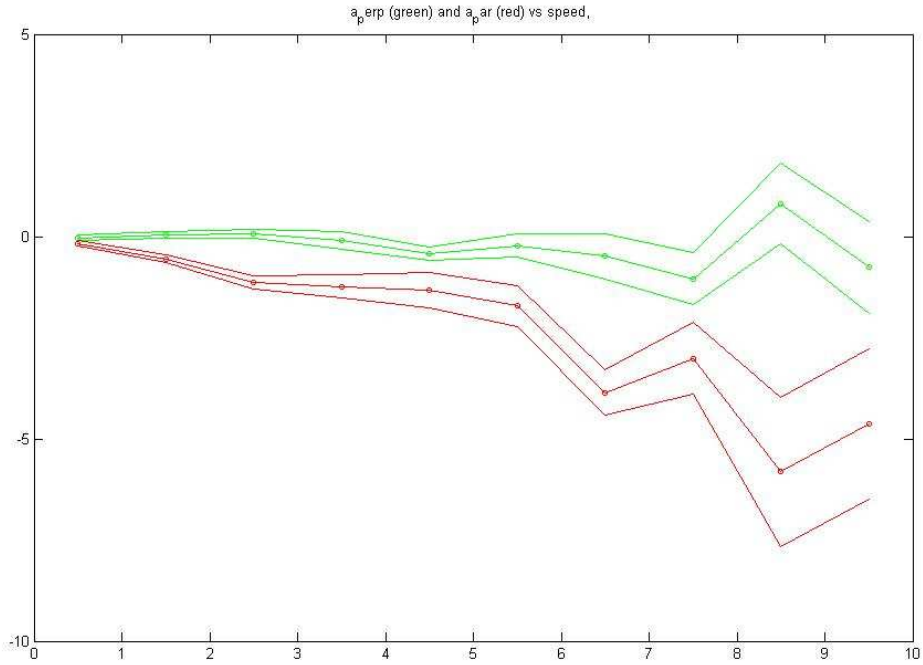

Cell acceleration perpendicular (green, top) and parallel (red, bottom) to cell velocity as a function of cell velocity. Units are µm/frame (x axis) and µm^2/frame (y axis). 1 pixel = 0.977 µm and 1 frame = 4 min.

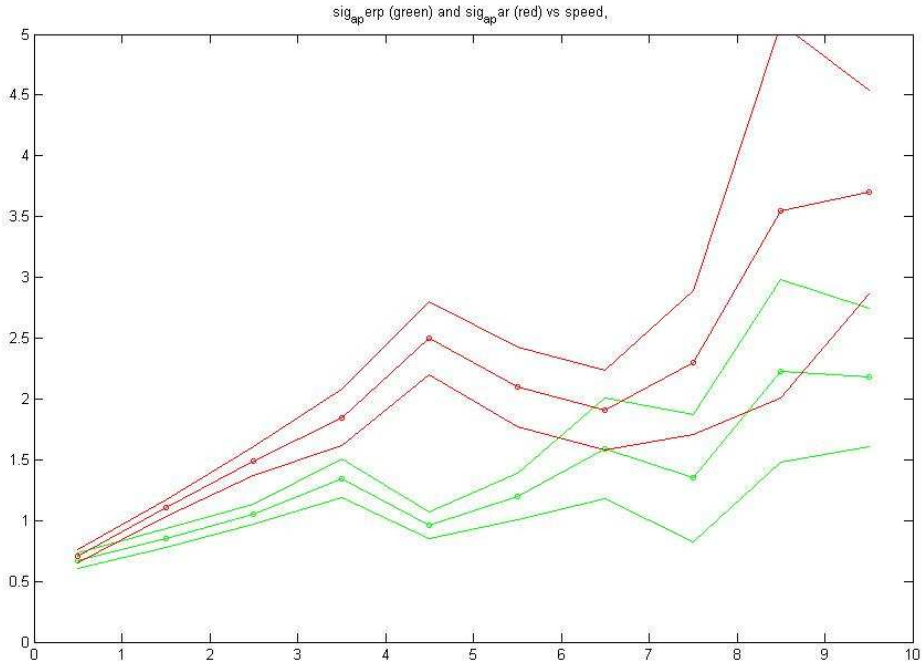

Standard deviation of cell acceleration perpendicular (green, bottom) and parallel (red, top) to cell velocity as a function of cell velocity. Units are µm/frame (x axis) and µm^2/frame (y axis). 1 pixel = 0.977 µm and 1 frame = 4 min.

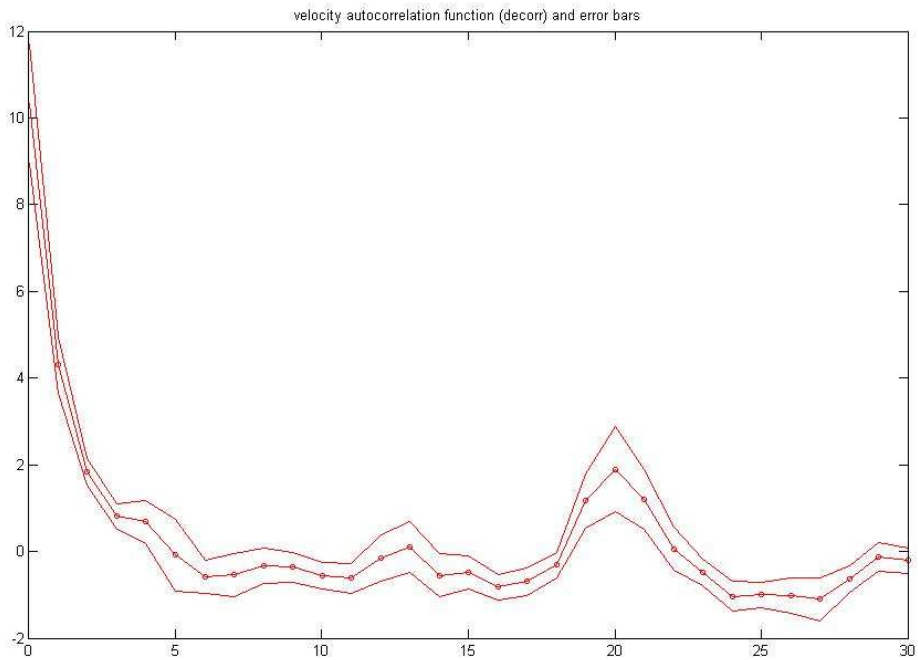

Autocorrelation of the cell velocities as a function of time. Units are frames (x axis) and µm^2/frame^2 (y axis). 1 pixel = 0.977 µm and 1 frame = 4 min.

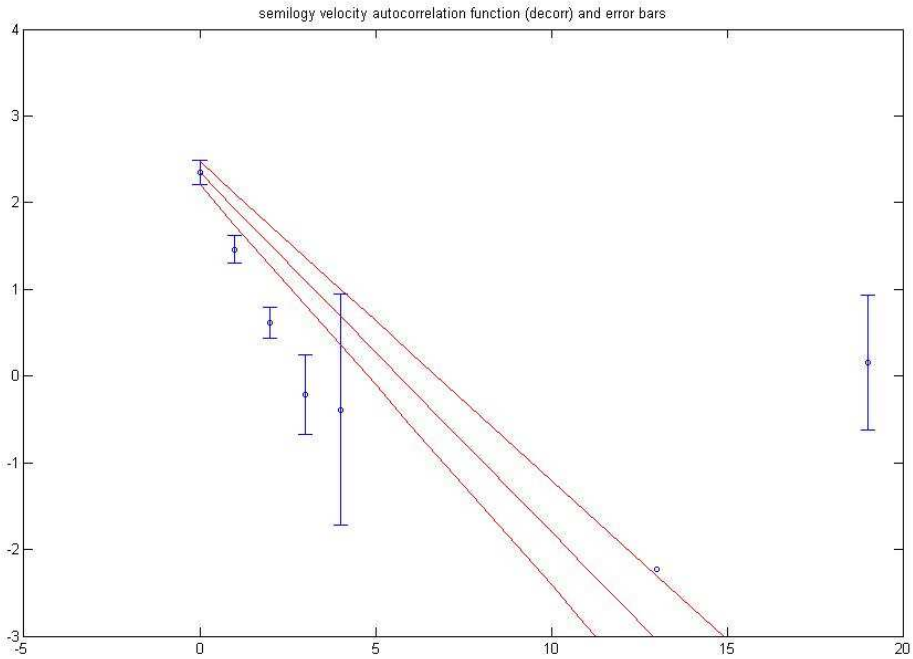

Semi-log plot of the atocorrelation of the cell velocities as a function of time. Units are frames (x axis) and ln(µm^2/frame^2) (y axis). 1 pixel = 0.977 µm and 1 frame = 4 min.

16-05 Black Si (21092009), 4026 data points

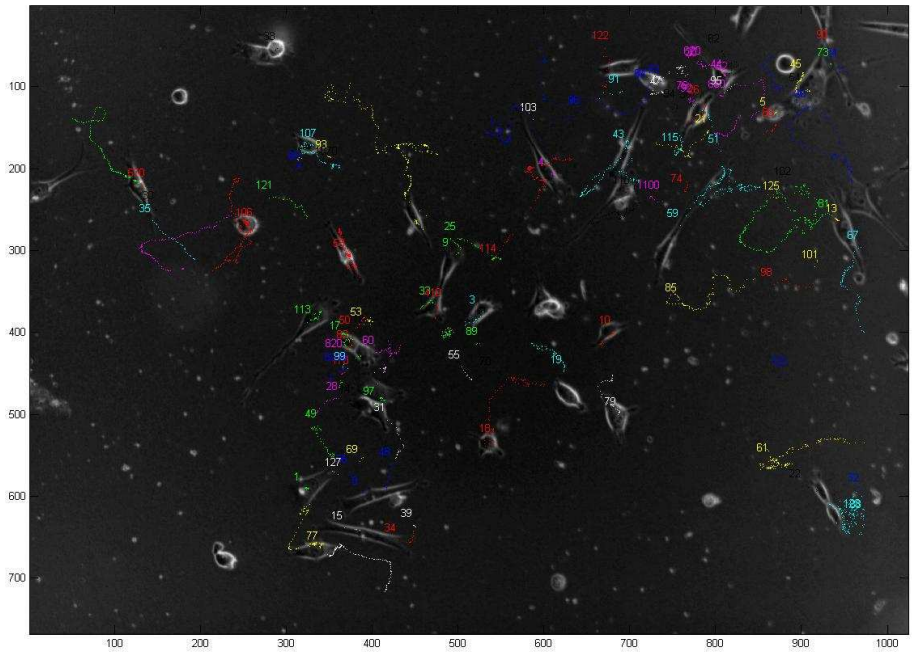

Cell trajectories. Units on both axes are pixels. 1 pixel = 0.977 µm.

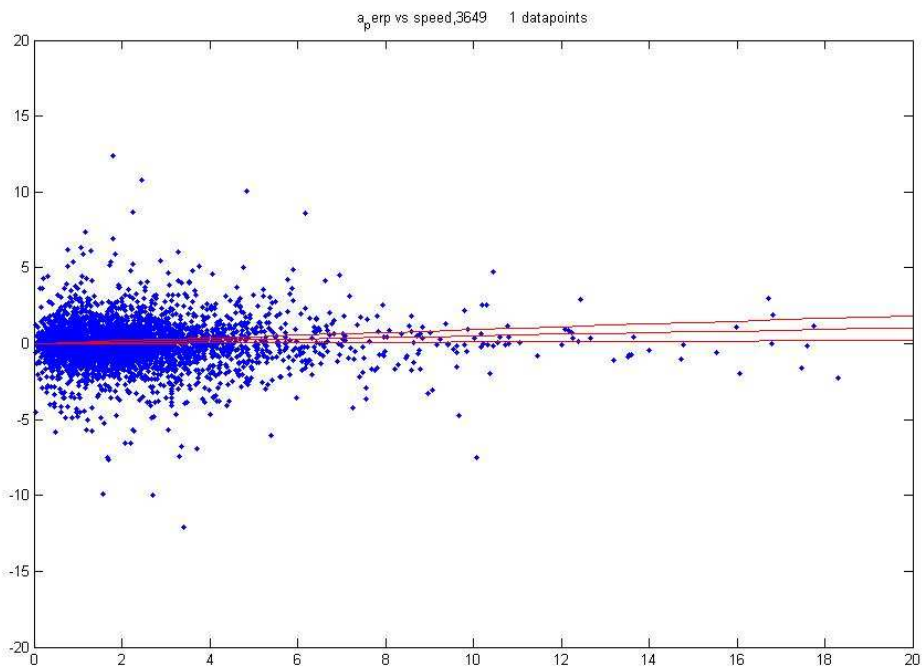

Cell acceleration perpendicular to cell velocity as a function of cell velocity. Units are µm/frame (x axis) and µm^2/frame (y axis). 1 pixel = 0.977 µm and 1 frame = 4 min.

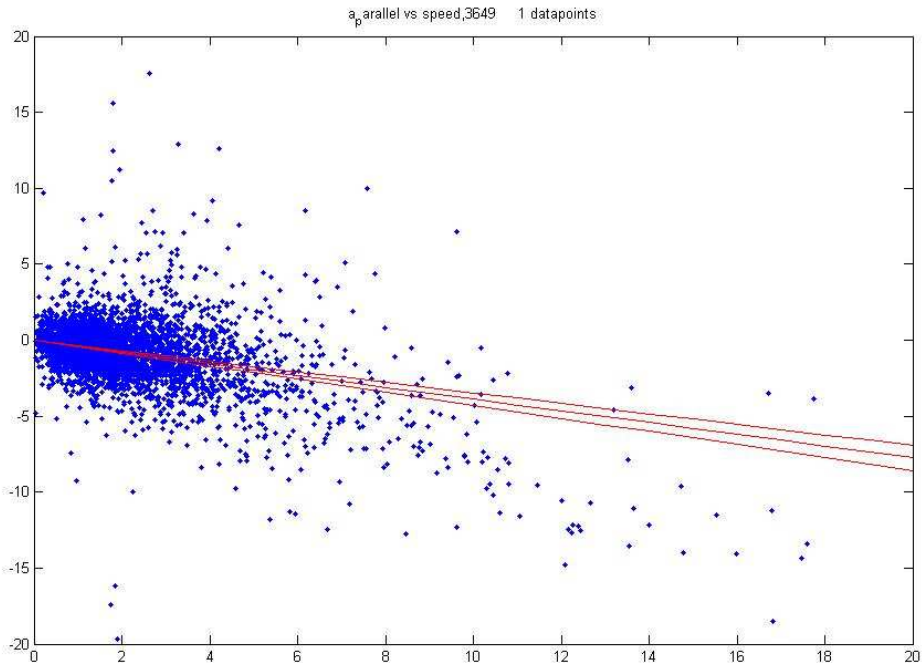

Cell acceleration parallel to cell velocity as a function of cell velocity. Units are µm/frame (x axis) and µm^2/frame (y axis). 1 pixel = 0.977 µm and 1 frame = 4 min.

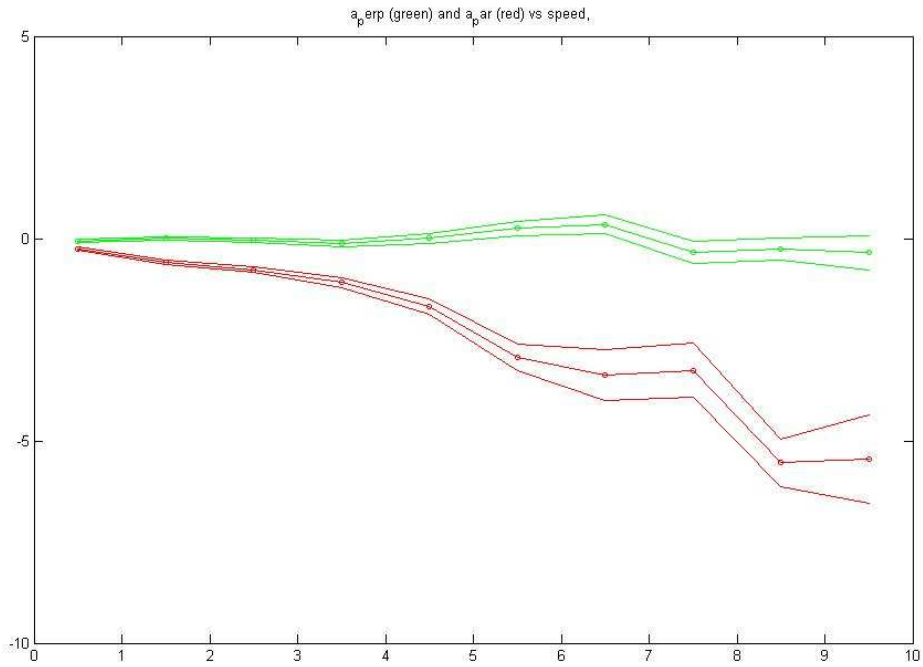

Cell acceleration perpendicular (green, top) and parallel (red, bottom) to cell velocity as a function of cell velocity. Units are µm/frame (x axis) and µm^2/frame (y axis). 1 pixel = 0.977 µm and 1 frame = 4 min.

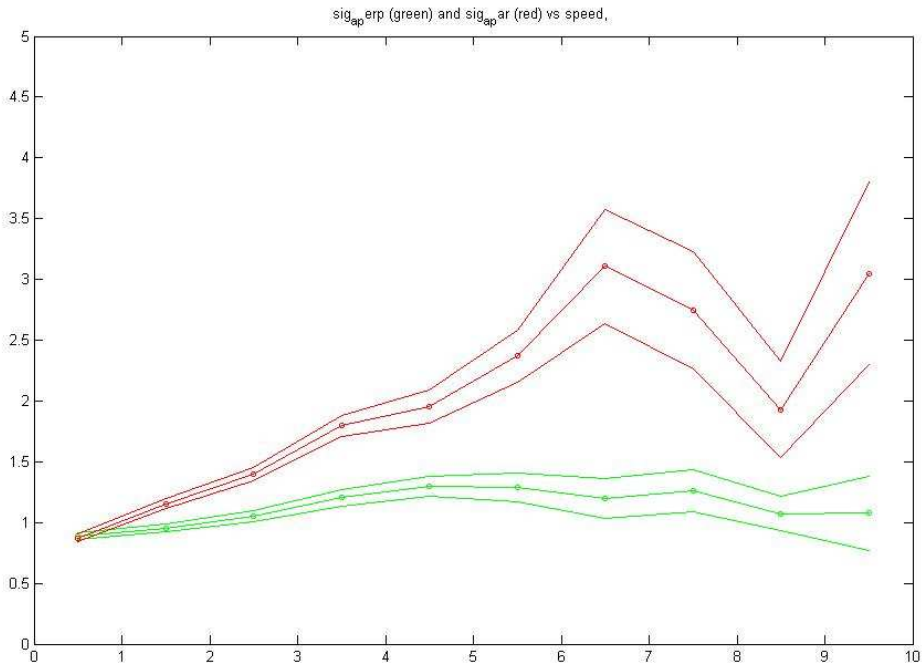

Standard deviation of cell acceleration perpendicular (green, bottom) and parallel (red, top) to cell velocity as a function of cell velocity. Units are µm/frame (x axis) and µm^2/frame (y axis). 1 pixel = 0.977 µm and 1 frame = 4 min.

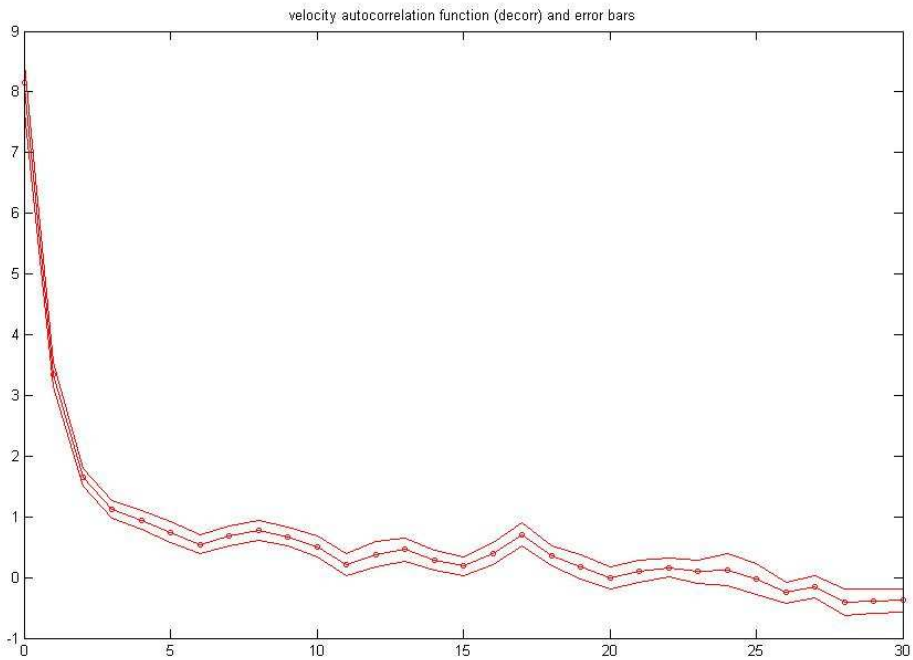

Autocorrelation of the cell velocities as a function of time. Units are frames (x axis) and µm^2/frame^2 (y axis). 1 pixel = 0.977 µm and 1 frame = 4 min.

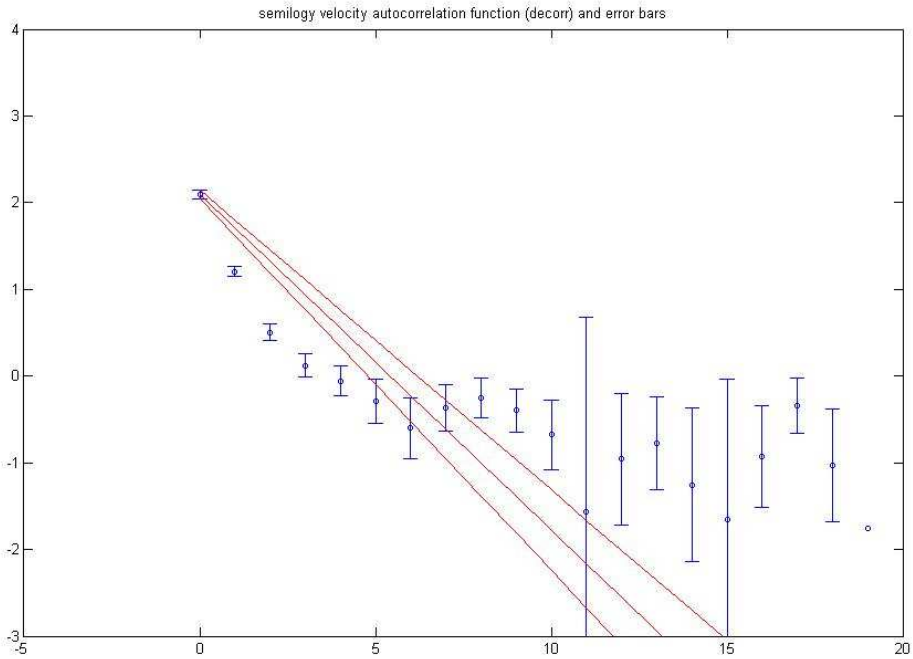

Semi-log plot of the atocorrelation of the cell velocities as a function of time. Units are frames (x axis) and ln(μm^2/frame^2) (y axis). 1 pixel = 0.977 μm and 1 frame = 4 min.

Bs17c Black Si (21092009), 2330 data points

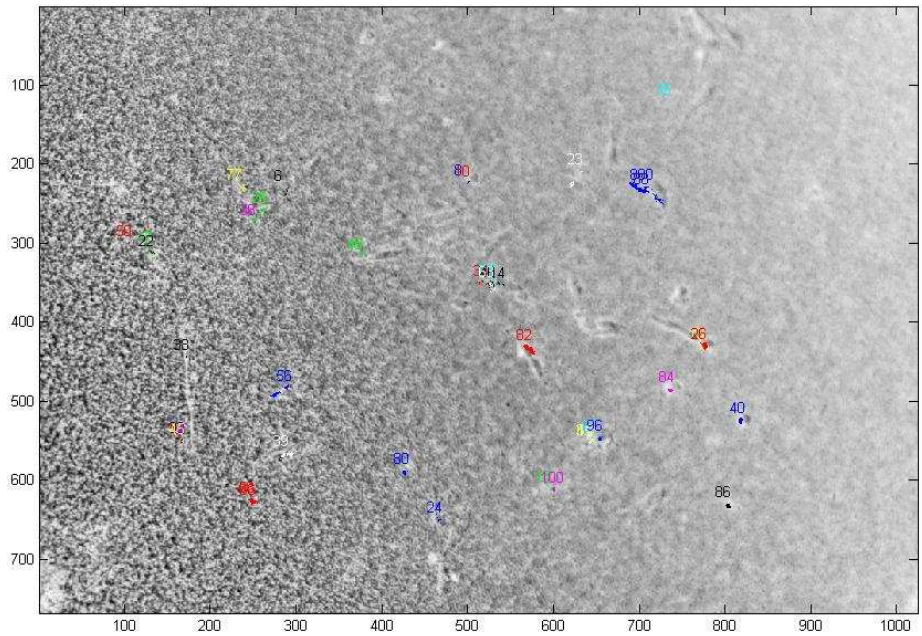

Cell trajectories. Units on both axes are pixels. 1 pixel = 0.977 µm.

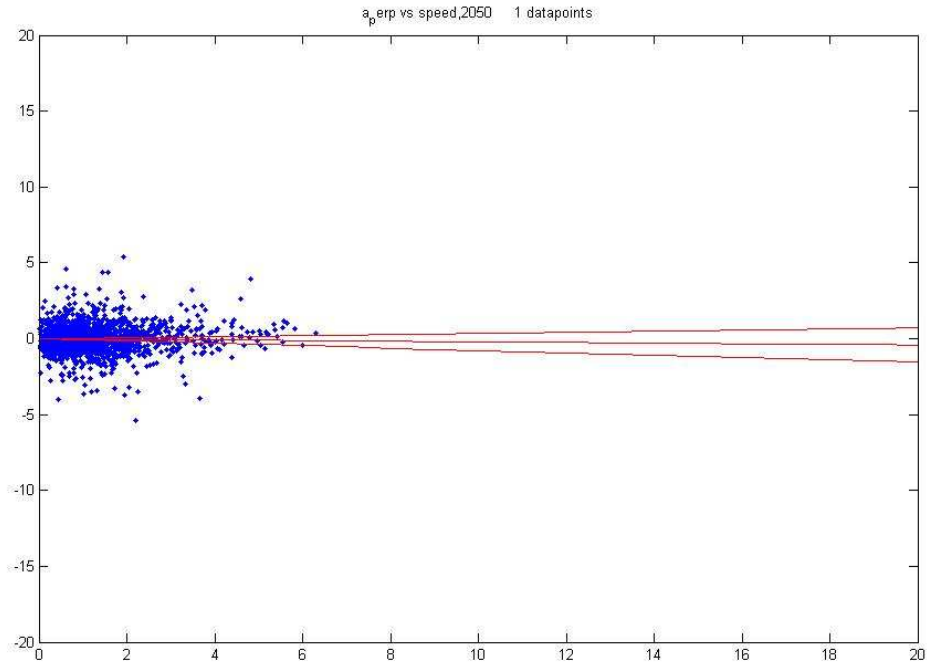

Cell acceleration perpendicular to cell velocity as a function of cell velocity. Units are µm/frame (x axis) and µm^2/frame (y axis). 1 pixel = 0.977 µm and 1 frame = 4 min.

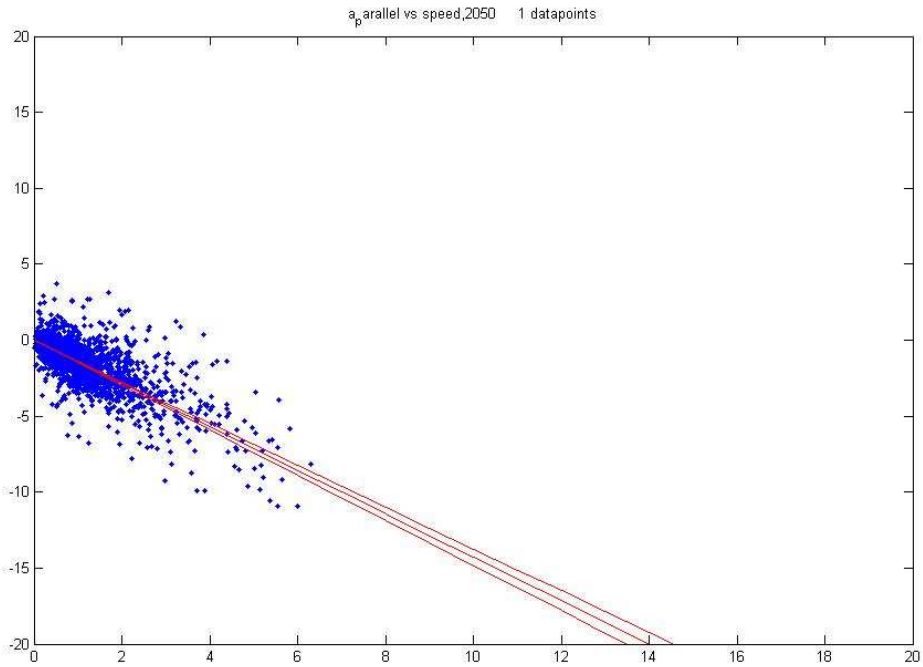

Cell acceleration parallel to cell velocity as a function of cell velocity. Units are µm/frame (x axis) and µm^2/frame (y axis). 1 pixel = 0.977 µm and 1 frame = 4 min.

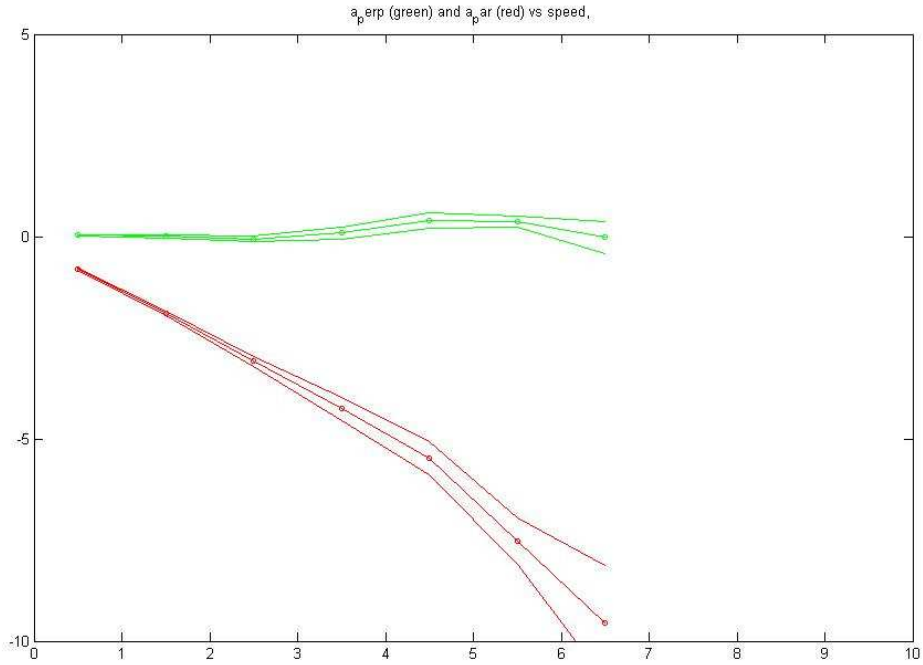

Cell acceleration perpendicular (green, top) and parallel (red, bottom) to cell velocity as a function of cell velocity. Units are µm/frame (x axis) and µm^2/frame (y axis). 1 pixel = 0.977 µm and 1 frame = 4 min.

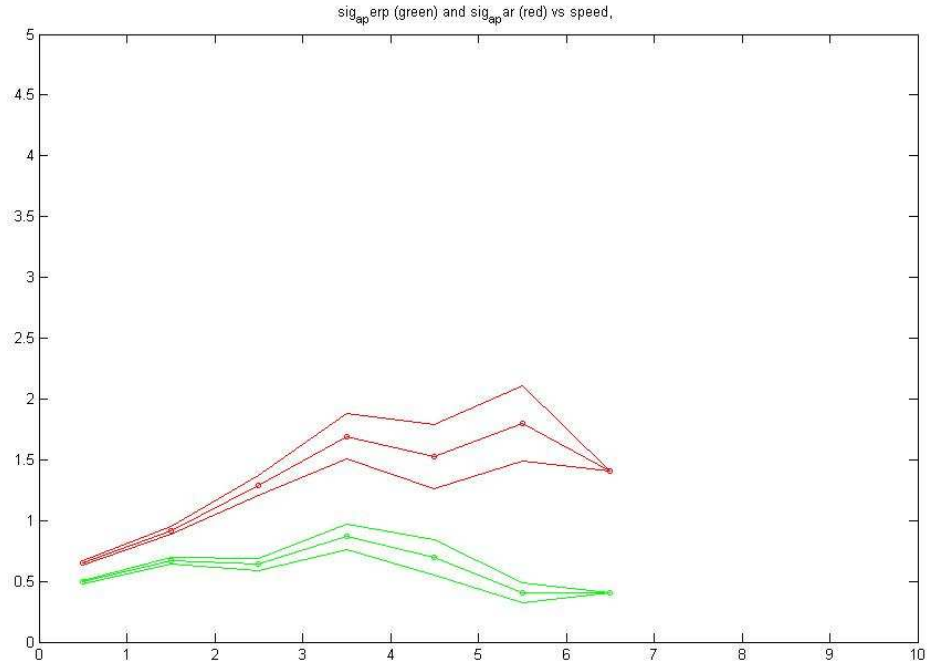

Standard deviation of cell acceleration perpendicular (green, bottom) and parallel (red, top) to cell velocity as a function of cell velocity. Units are µm/frame (x axis) and µm^2/frame (y axis). 1 pixel = 0.977 µm and 1 frame = 4 min.

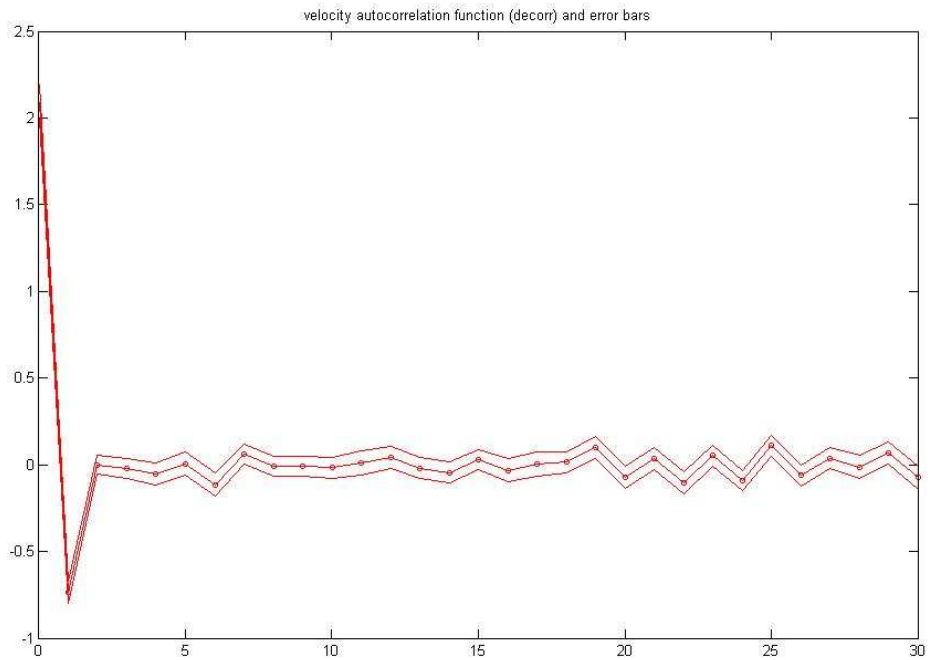

Autocorrelation of the cell velocities as a function of time. Units are frames (x axis) and µm^2/frame^2 (y axis). 1 pixel = 0.977 µm and 1 frame = 4 min.

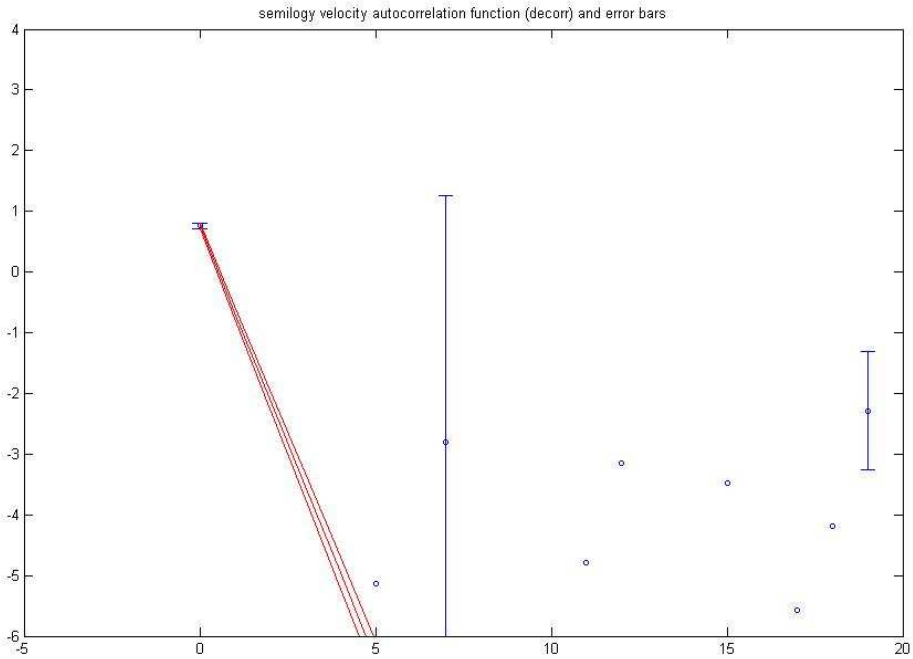

Semi-log plot of the atocorrelation of the cell velocities as a function of time. Units are frames (x axis) and ln(μm^2/frame^2) (y axis). 1 pixel = 0.977 μm and 1 frame = 4 min.

Bs17m Black Si (07092009), 1632 data points

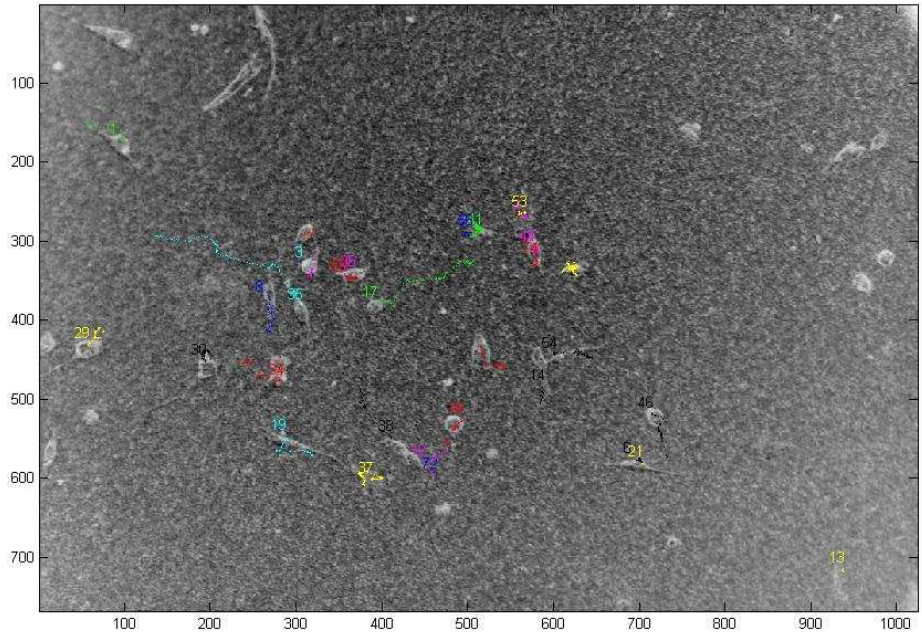

Cell trajectories. Units on both axes are pixels. 1 pixel = 0.977 µm.

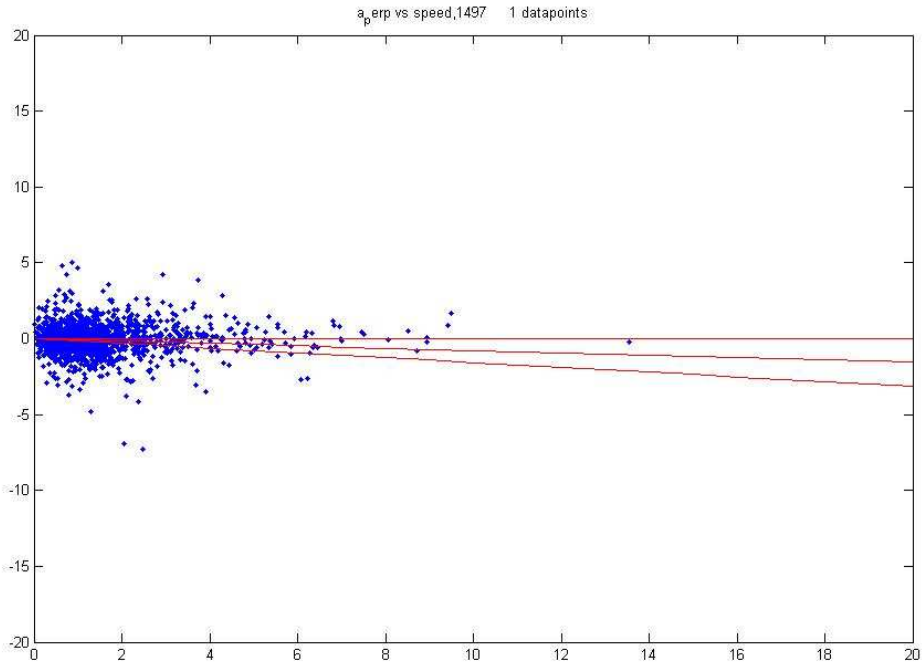

Cell acceleration perpendicular to cell velocity as a function of cell velocity. Units are µm/frame (x axis) and µm^2/frame (y axis). 1 pixel = 0.977 µm and 1 frame = 4 min.

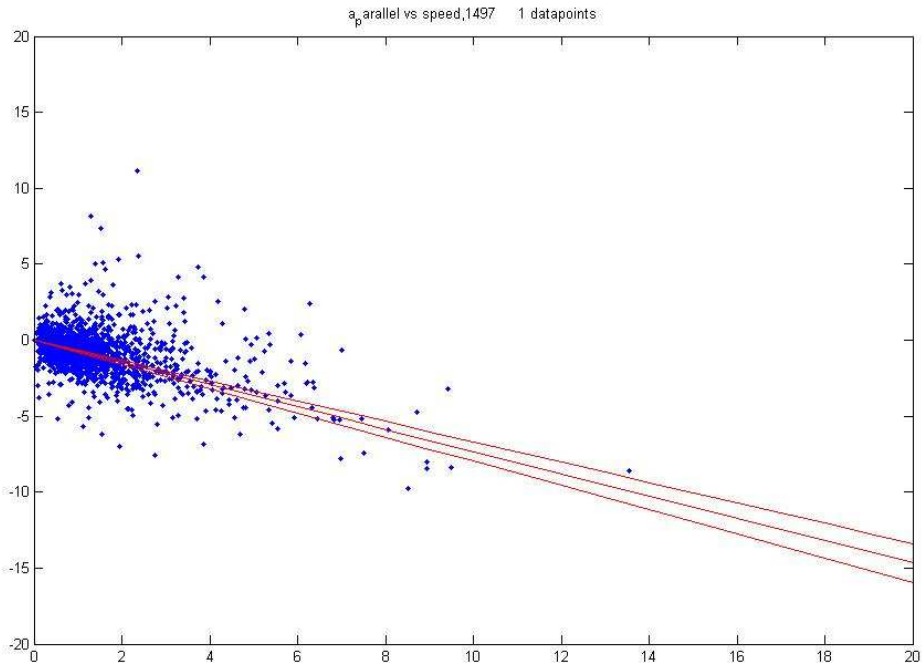

Cell acceleration parallel to cell velocity as a function of cell velocity. Units are µm/frame (x axis) and µm^2/frame (y axis). 1 pixel = 0.977 µm and 1 frame = 4 min.

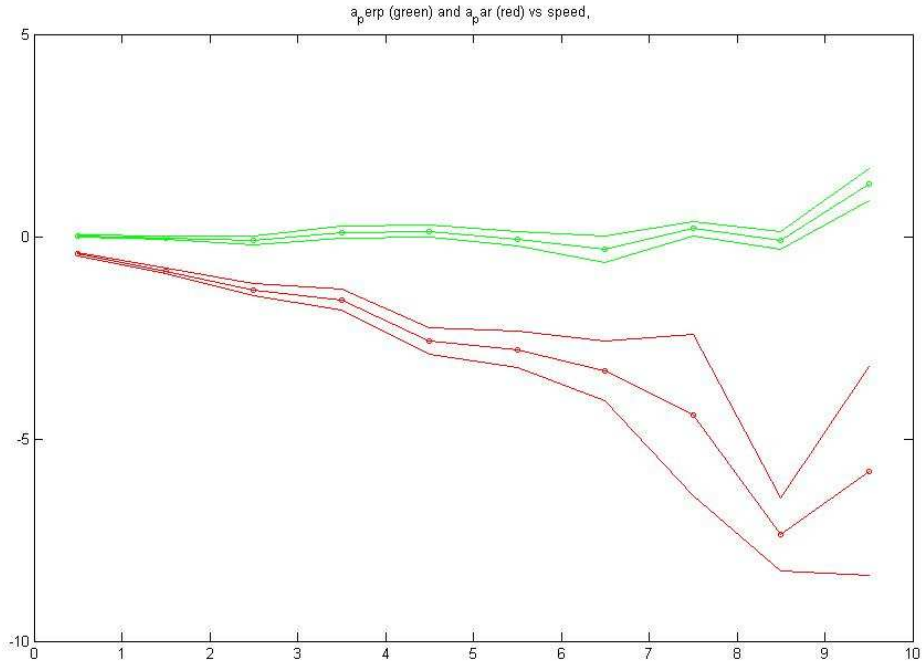

Cell acceleration perpendicular (green, top) and parallel (red, bottom) to cell velocity as a function of cell velocity. Units are µm/frame (x axis) and µm^2/frame (y axis). 1 pixel = 0.977 µm and 1 frame = 4 min.

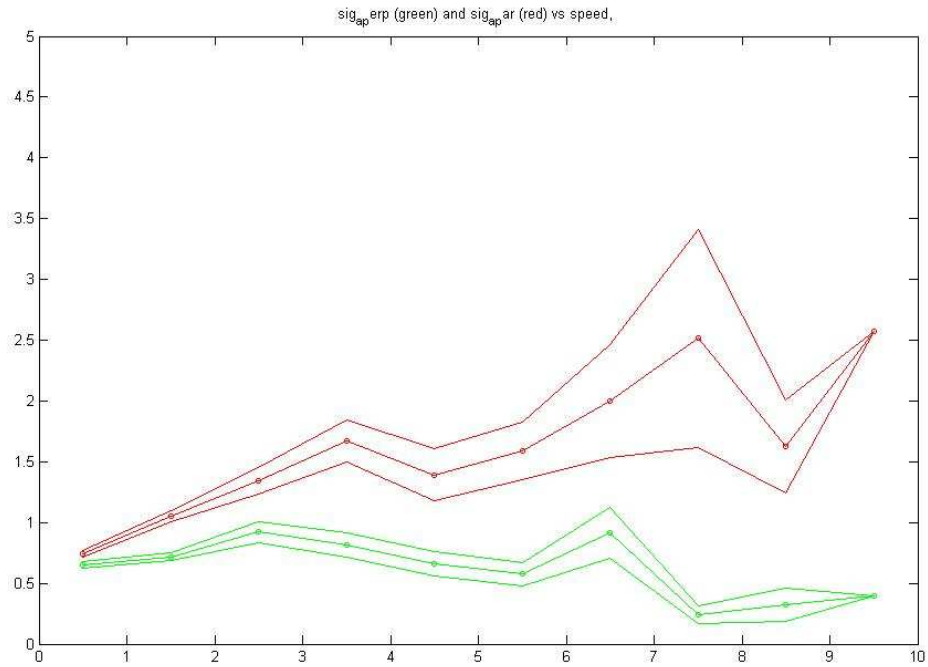

Standard deviation of cell acceleration perpendicular (green, bottom) and parallel (red, top) to cell velocity as a function of cell velocity. Units are µm/frame (x axis) and µm^2/frame (y axis). 1 pixel = 0.977 µm and 1 frame = 4 min.

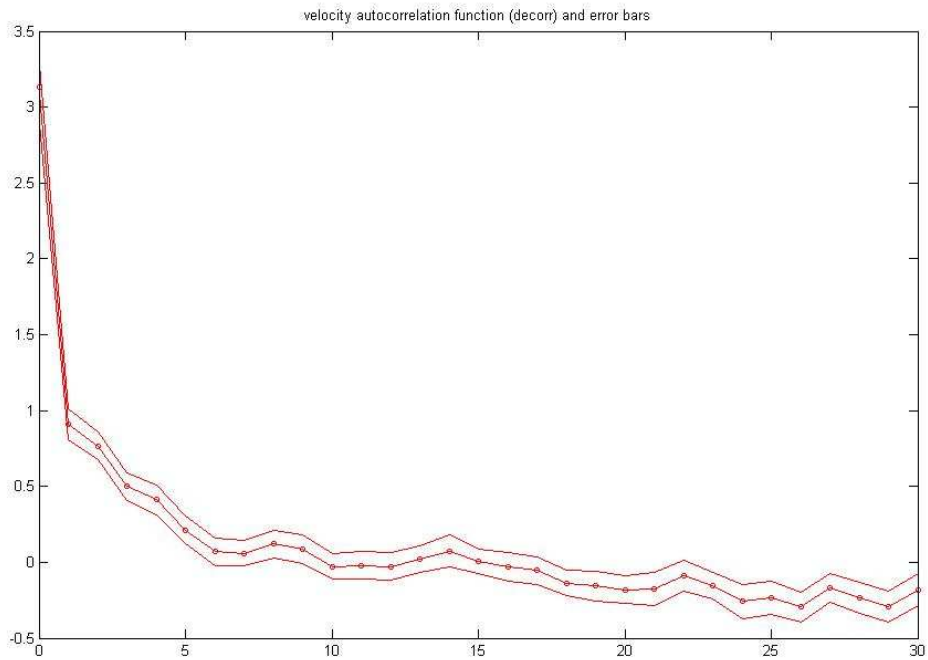

Autocorrelation of the cell velocities as a function of time. Units are frames (x axis) and µm^2/frame^2 (y axis). 1 pixel = 0.977 µm and 1 frame = 4 min.

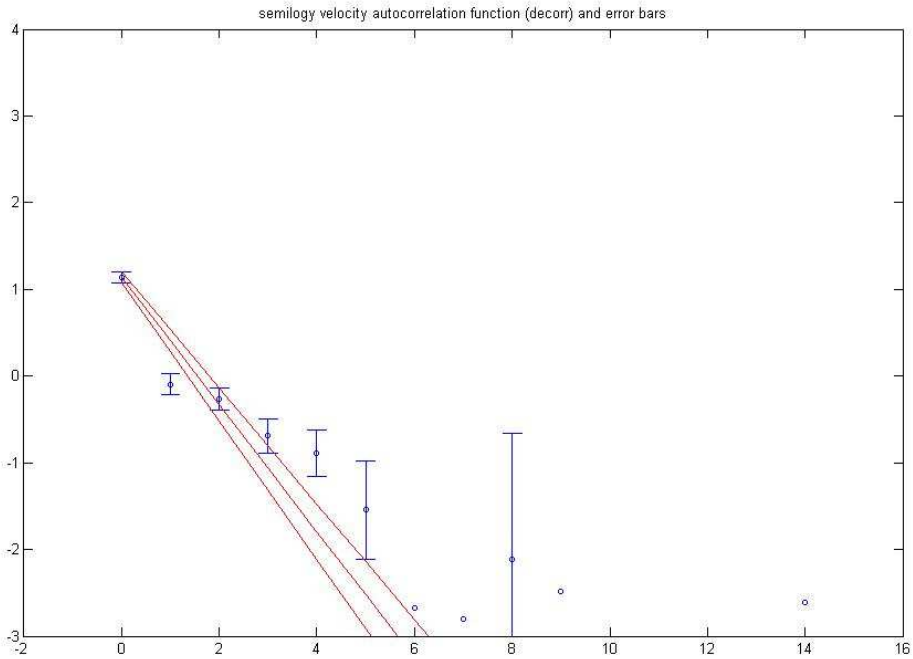

Semi-log plot of the atocorrelation of the cell velocities as a function of time. Units are frames (x axis) and ln(µm^2/frame^2) (y axis). 1 pixel = 0.977 µm and 1 frame = 4 min.

PMMA (10102009), 2078 data points

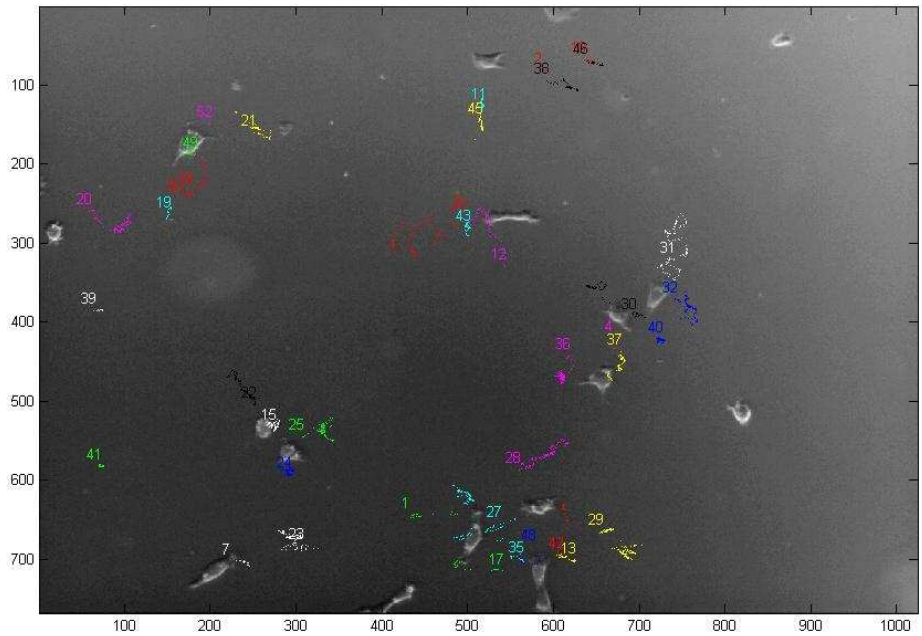

Cell trajectories. Units on both axes are pixels. 1 pixel = 0.977 µm.

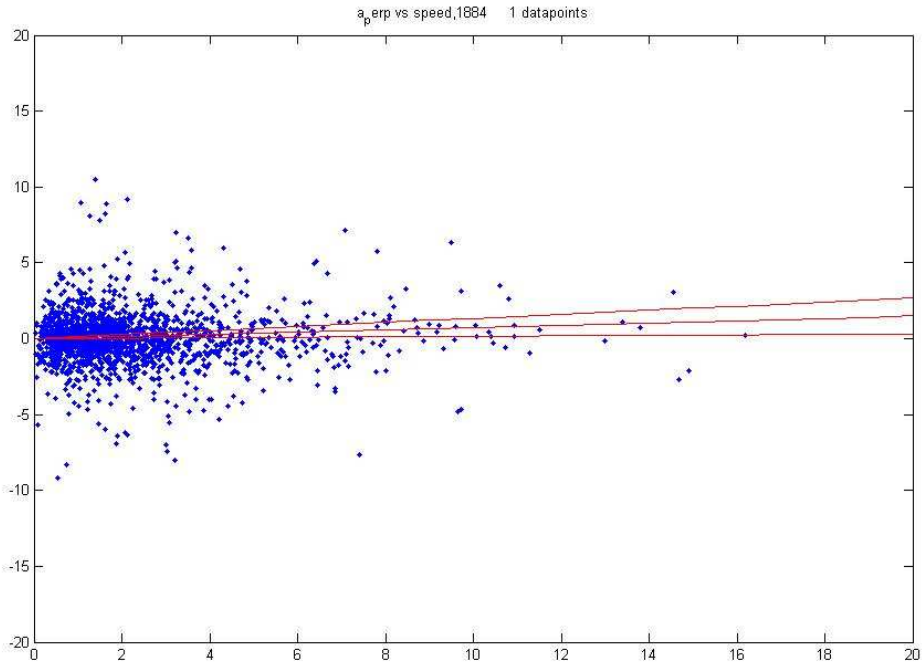

Cell acceleration perpendicular to cell velocity as a function of cell velocity. Units are µm/frame (x axis) and µm^2/frame (y axis). 1 pixel = 0.977 µm and 1 frame = 4 min.

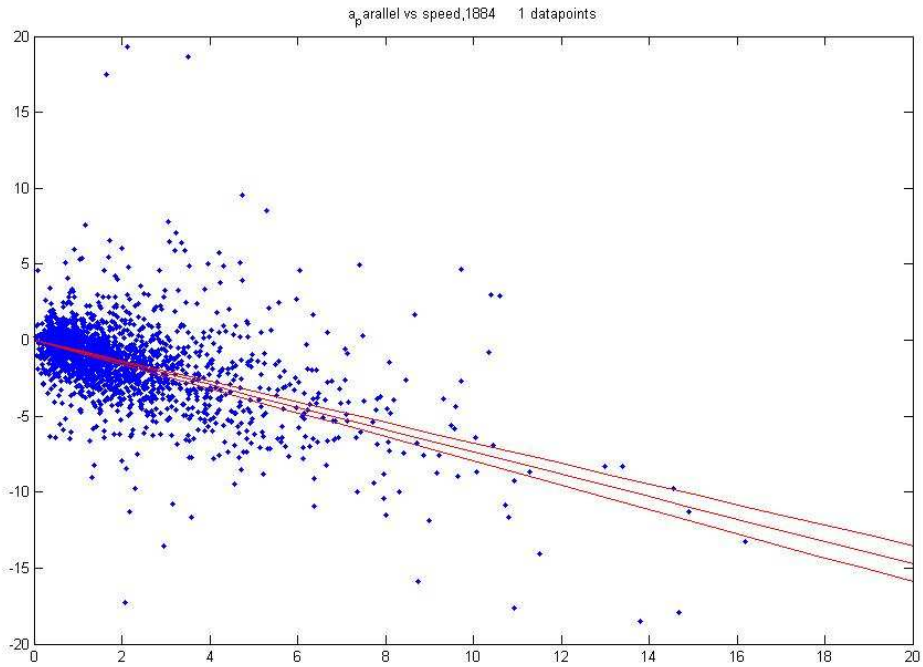

Cell acceleration parallel to cell velocity as a function of cell velocity. Units are µm/frame (x axis) and µm^2/frame (y axis). 1 pixel = 0.977 µm and 1 frame = 4 min.

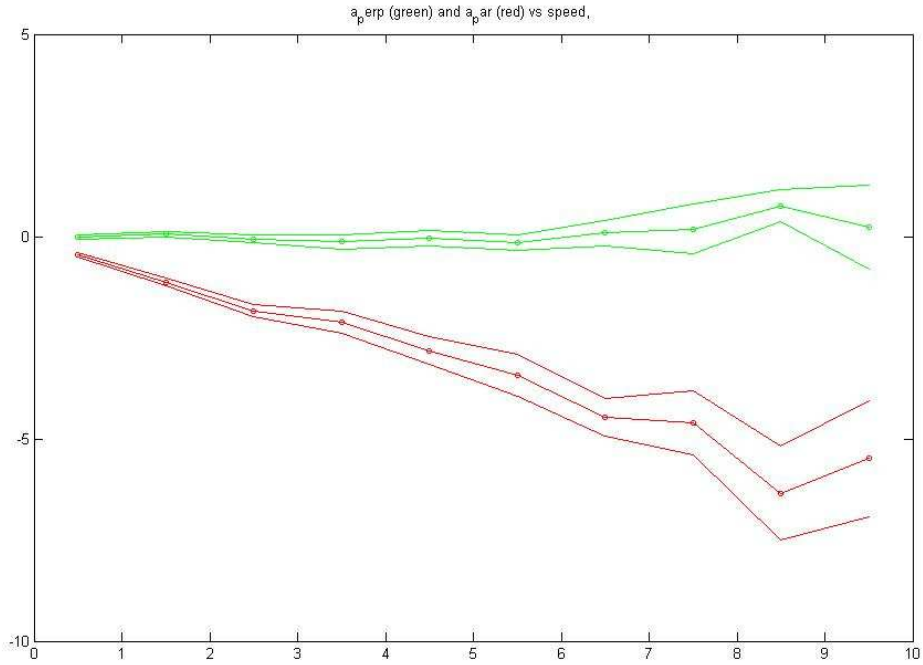

Cell acceleration perpendicular (green, top) and parallel (red, bottom) to cell velocity as a function of cell velocity. Units are µm/frame (x axis) and µm^2/frame (y axis). 1 pixel = 0.977 µm and 1 frame = 4 min.

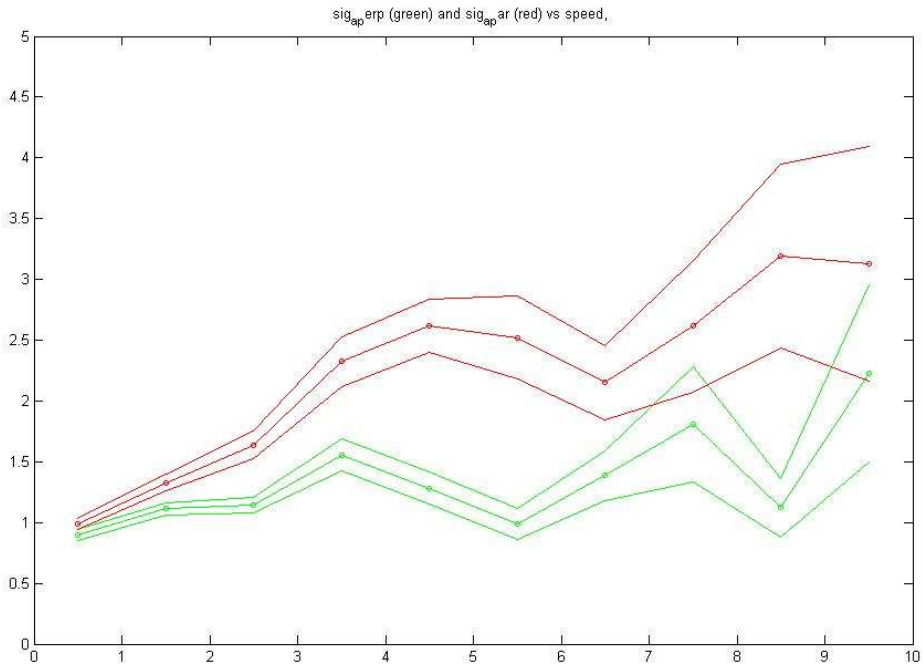

Standard deviation of cell acceleration perpendicular (green, bottom) and parallel (red, top) to cell velocity as a function of cell velocity. Units are µm/frame (x axis) and µm^2/frame (y axis). 1 pixel = 0.977 µm and 1 frame = 4 min.

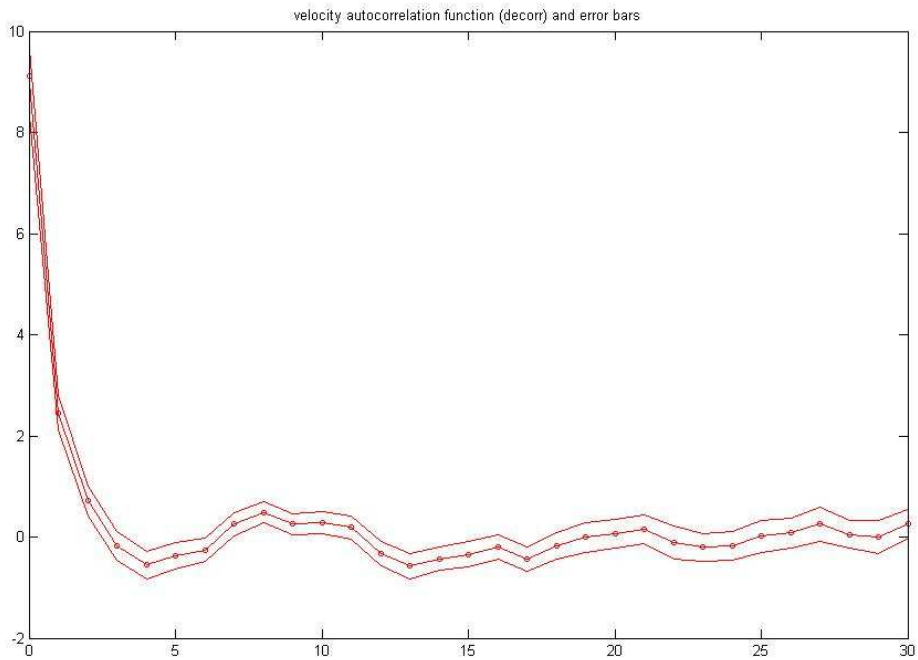

Autocorrelation of the cell velocities as a function of time. Units are frames (x axis) and µm^2/frame^2 (y axis). 1 pixel = 0.977 µm and 1 frame = 4 min.

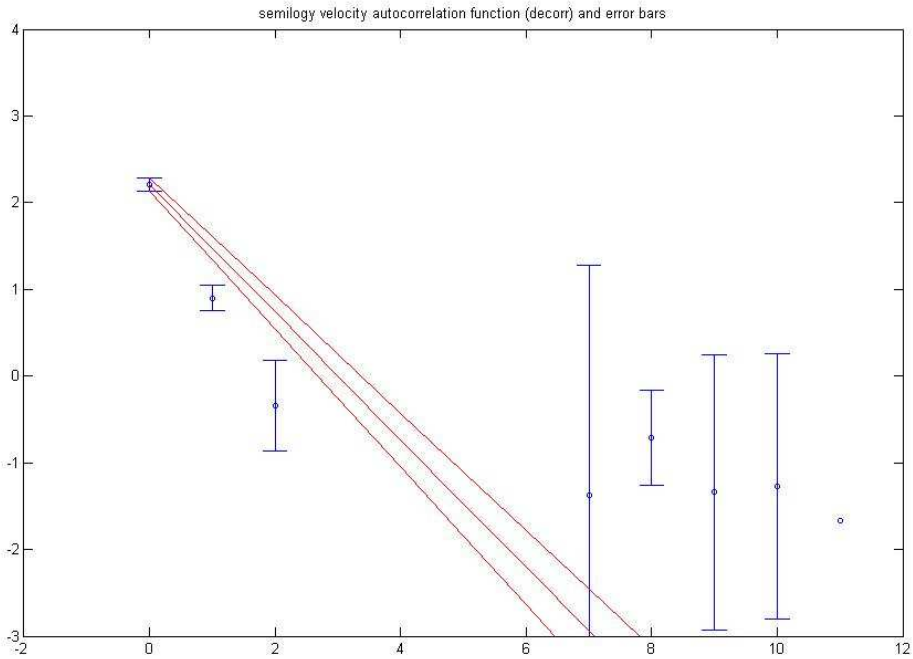

Semi-log plot of the atocorrelation of the cell velocities as a function of time. Units are frames (x axis) and ln(µm^2/frame^2) (y axis). 1 pixel = 0.977 µm and 1 frame = 4 min.

EBL2 (10102009), 2133 data points

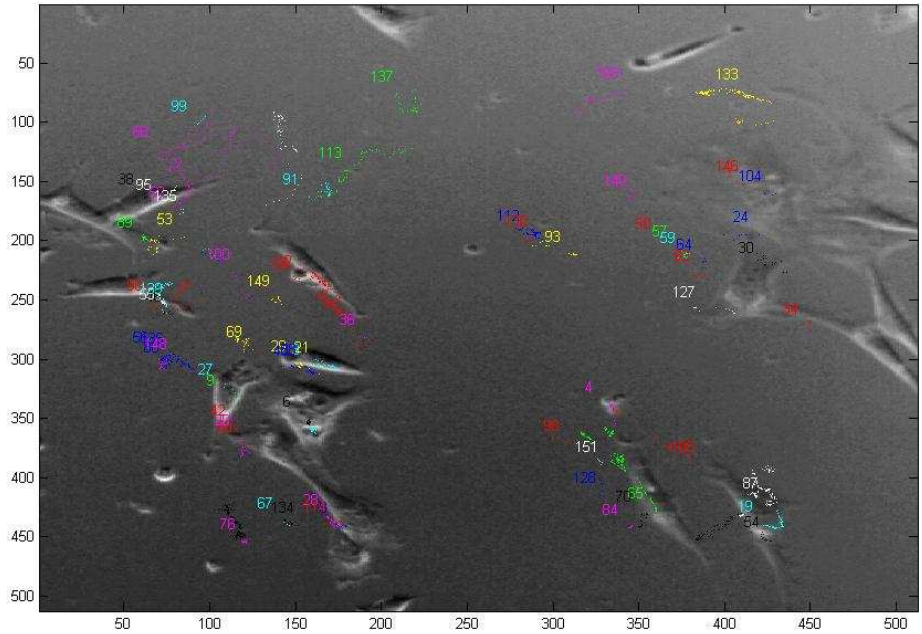

Cell trajectories. Units on both axes are pixels. 1 pixel = 0.977 µm.

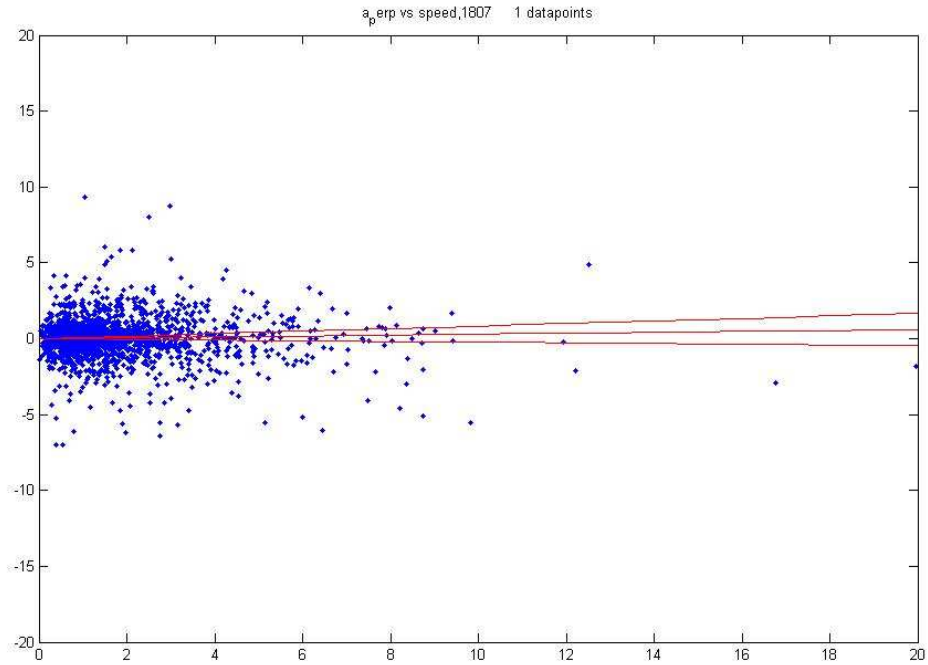

Cell acceleration perpendicular to cell velocity as a function of cell velocity. Units are µm/frame (x axis) and µm^2/frame (y axis). 1 pixel = 0.977 µm and 1 frame = 4 min.

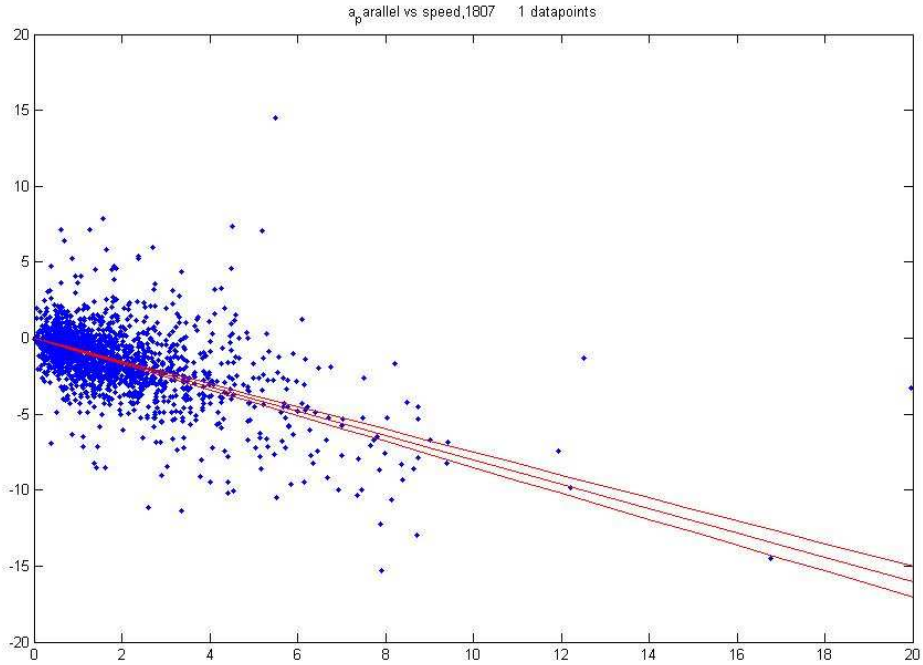

Cell acceleration parallel to cell velocity as a function of cell velocity. Units are µm/frame (x axis) and µm^2/frame (y axis). 1 pixel = 0.977 µm and 1 frame = 4 min.

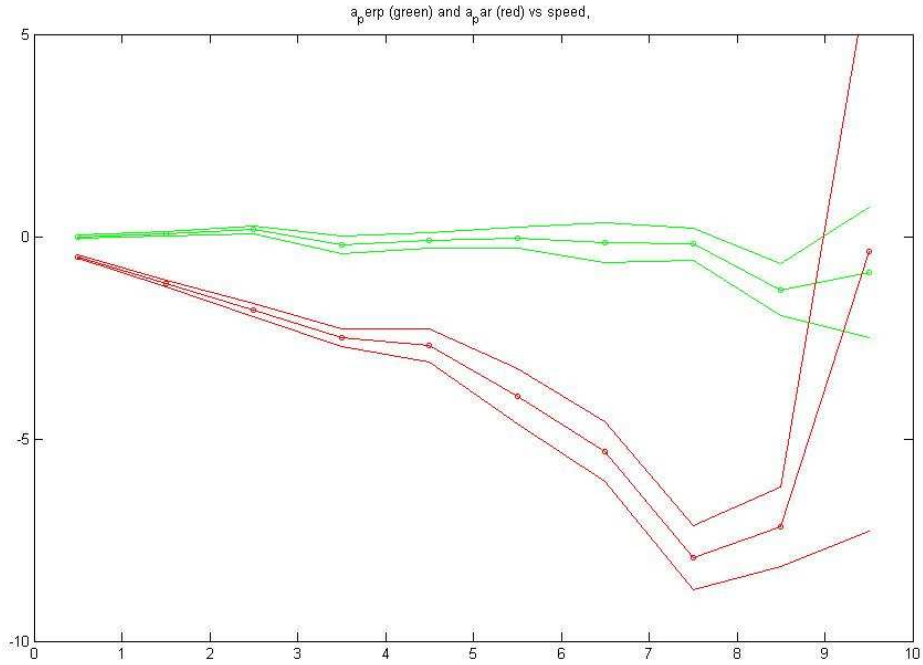

Cell acceleration perpendicular (green, top) and parallel (red, bottom) to cell velocity as a function of cell velocity. Units are µm/frame (x axis) and µm^2/frame (y axis). 1 pixel = 0.977 µm and 1 frame = 4 min.

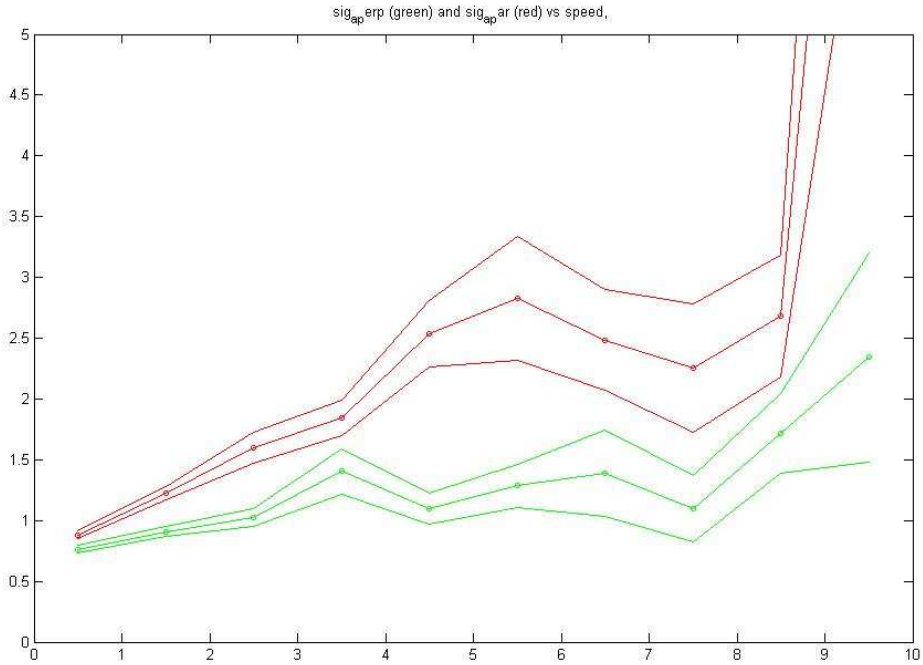

Standard deviation of cell acceleration perpendicular (green, bottom) and parallel (red, top) to cell velocity as a function of cell velocity. Units are µm/frame (x axis) and µm^2/frame (y axis). 1 pixel = 0.977 µm and 1 frame = 4 min.

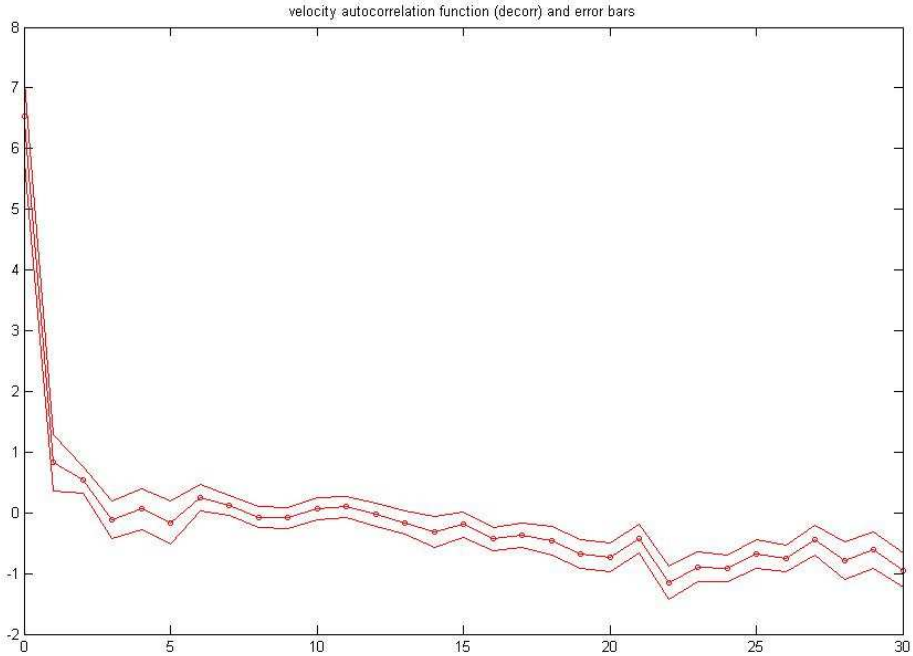

Autocorrelation of the cell velocities as a function of time. Units are frames (x axis) and µm^2/frame^2 (y axis). 1 pixel = 0.977 µm and 1 frame = 4 min.

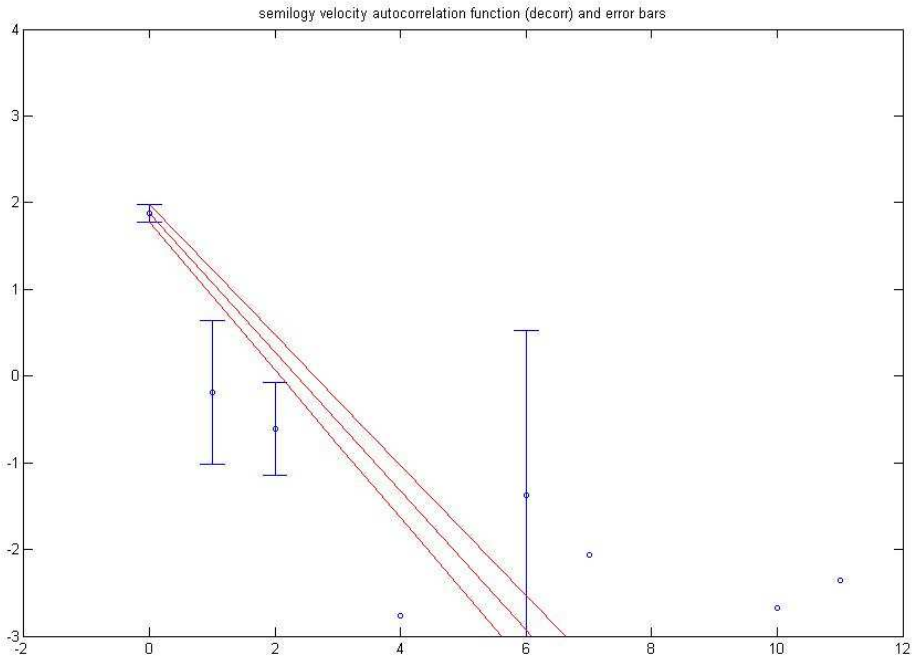

Semi-log plot of the atocorrelation of the cell velocities as a function of time. Units are frames (x axis) and ln(µm^2/frame^2) (y axis). 1 pixel = 0.977 µm and 1 frame = 4 min.

Appendix D - Step-by-Step Guide for Time-Lapse Microscopy of Cells

1) Autoclave Fomblin grease.

2) Turn on the computer connected to the microscope and the computer controlling the temperature stage and then close and pre-heat the temperature stage (just put the two thermistors somewhere inside the stage).

3) Sterile everything (Al block, cell culture chamber, Al lid, microscope slide, PDMS gasket , substrates, bottom glass piece, tubings (which also have to be flushed), screws, Allen key) with 70% ethanol or 0.5M NaOH (only NaOH for PMMA parts, only ethanol for polycarbonate parts) using gloves and sterile tissues.

4) Put everything under sterile laminar flow.

5) Screw cell culture chamber onto the middle of the Al block.

6) Place substrates on the bottom glass piece using the sterile Fomblin grease.

7) Place the glass piece with the substrates on in the cell culture chamber using the sterile Fomblin grease - avoid getting air bubbles and too much grease beneath it as a uniform background is strongly preferred for imaging cells on transparent substrates.

8) Connect tubings to the inlet and the outlet - make sure the screw connectors are tight.

9) Flush with PBS or Hank's buffer to get rid of ethanol or NaOH residues.

10) Put 50,000 cells (in 1-2 mL medium) onto the substrate in the chamber.

11) Put on and align the PDSM gasket, then carefully put on the microscope glass slide.

12) Carefully screw on the Al lid tightening first all the screws a little, than start over and tighten all the screws a little more, and so forth to avoid breaking the microscope slide because of uneven pressure. It needs to be tight in order not to leak.

13) Carefully and slowly (preferably with a syringe with small diameter) fill the cell culture chamber with medium, keeping an eye on any leaking at the PDMS gasket or at the inlet or outlet. To reduce the amount of air (bubbles) in the chamber, tilt the cell culture chamber so that the outlet is at the highest position letting the air escape.

14) Let the syringe be connected to the end of the inlet tubing to avoid contamination.

15) Put a syringe with a needle in the outlet tubing to avoid contamination.

16) Take the assembled cell culture chamber and the Allen key to the lab with the microscope.

17) Stop the heating of the temperature stage.

18) Open the temperature stage and mount the cell culture chamber inside it.

19) Place NTC1 (the one with white wires) inside the Al block and NTC2 (the one with blue wires) inside the small hole in the side of the cell culture chamber.

20) Close the temperature stage - if possible use at least two screws to make sure the top of the temperature stage will not move during the experiment.

21) Start to heat the stage again.

22) Make sure the microscope stage is at the lowest z position and pay attention to the microscope objective, then mount the temperature stage in the microscope - use at least two screws to tighten the temperature stage to the microscope stage to reduce drift during the experiment.

23) Start the time-lapse program on the computer and adjust the focus and settings on the microscope to get a good image.

24) Start obtaining time-lapse movies of the cells.

25) Approximately one day after seeding the cells check that they have adhered to the substrates.

26) When cells have adhered to the substrates apply medium flow (5 µL/min) with a syringe pump.